Year : 2015

CHARACTERIZATION OF A MAF1 KNOCKOUT MOUSE MODEL

Bonhoure Nicolas

UNIL | Université de Lausanne
Faculté de biologie et de médecine

Centre Intégratif de Génomique

CHARACTERIZATION OF A MAF1 KNOCKOUT MOUSE MODEL

Thèse de doctorat ès sciences de la vie (PhD)

présentée à la

Faculté de biologie et de médecine
de l'Université de Lausanne

par

Nicolas Bonhoure

Master de l'Université de la Méditerranée Aix- Marseille II

Jury

Prof. Alexandre Roulin Président
Prof. Nouria Hernandez, Directrice de thèse
Prof. Béatrice Desvergne, expert
Prof. Dominique Langin, expert

Lausanne 2015

UNIL | Université de Lausanne
Faculté de biologie
et de médecine

Ecole Doctorale

Doctorat ès sciences de la vie

Imprimatur

Vu le rapport présenté par le jury d'examen, composé de

Président · e	Monsieur Prof. Alexandre **Roulin**
Directeur · rice de thèse	Madame Prof. Nouria **Hernandez**
Experts · es	Monsieur Prof. Dominique **Langin**
	Madame Prof. Béatrice **Desvergne**

le Conseil de Faculté autorise l'impression de la thèse de

Monsieur Nicolas Bonhoure

Master de l' Université de la Méditerranée Aix-Marseille II, France

intitulée

CHARACTERIZATION OF A MAF1 KNOCKOUT MOUSE MODEL

Lausanne, le 11 décembre 2015

pour le Doyen
de la Faculté de biologie et de médecine

Prof. Alexandre Roulin

Résumé

L'ARN polymérase 3 transcrit un petit groupe de gènes fortement exprimés et impliqués dans plusieurs mécanismes moléculaires. Les ARNs de transfert ou ARNt représentent plus ou moins la moitié du transcriptome de l'ARN polymérase 3. Ils sont directement impliqués dans la traduction des protéines en agissant comme transporteurs d'acides aminés qui sont incorporés à la chaîne naissante de polypeptides. Chez des levures cultivées dans un milieu jusqu'à épuisement des nutriments, Maf1 réprime la transcription par l'ARN polymérase 3, favorisant ainsi l'économie énergétique cellulaire. Dans un modèle de cellules de mammifères, MAF1 réprime aussi la transcription de l'ARN polymérase 3 dans des conditions de stress, cependant il n'existe aucune donnée quant à son rôle chez un mammifère vivant. Pendant mon doctorat, j'ai utilisé une souris délétée pour le gène Maf1 afin de connaître les effets de ce gène chez un mammifère. Etonnamment, la souris Maf1$^{-/-}$ est résistante à l'obésité même si celle-ci est nourrie avec une nourriture riche en matières grasses. Des études moléculaires et de métabolomiques ont montré qu'il existe des cycles futiles de production et dégradation des lipides et des ARNt, ce qui entraîne une augmentation de la dépense énergique et favorise la résistance à l'obésité. En plus de la caractérisation de la souris Maf1$^{-/-}$, pendant ma thèse j'ai également développé une méthode afin de normaliser les données de ChIP-sequencing. Cette méthode est fondée sur l'utilisation d'un contrôle interne, représenté ici par l'ajout d'une quantité fixe de chromatine provenant d'un organisme différent de celui étudié. La méthode a amélioré considérablement la reproductibilité des valeurs entre réplicas biologiques. Elle a aussi révélé des différences entre échantillons issus de conditions différentes. Une occupation supérieure de l'ARN polymérase 3 sur les gènes Pol 3 chez les souris Maf1 KO entraîne une augmentation du niveau de précurseurs d'ARNt, ayant pour effet probable la saturation de la machinerie de maturation des ARNt. En effet, chez les souris Maf1 KO, le pourcentage d'ARNt modifiés est plus faible que chez les souris type sauvage. Ce déséquilibre entre le niveau de précurseurs et d'ARNt matures entraîne une diminution de la traduction protéique. Ces résultats ont permis d'identifier de nouvelles fonctions pour la protéine MAF1, comme étant une protéine régulatrice à la fois de la transcription mais aussi de la traduction et en étant un cible potentielle au traitement à l'obésité.

Abstract

RNA polymerase III (Pol 3) transcribes a small set of highly expressed genes involved in different molecular mechanisms. tRNAs account for almost half of the Pol 3 transcriptome and are involved in translation, bringing a new amino into the nascent polypeptide chain. In yeast, under nutrient deprivation, Maf1 acts for cell energetic economy by repressing Pol 3 transcription. In mammalian cells, MAF1 also represses Pol 3 activity under conditions of serum deprivation or DNA damages but nothing is known about its role in a mammalian organism. During my thesis studies, I used a Maf1 KO mouse model to characterize the effects of Maf1 deletion in a living animal. Surprisingly, the MAF1 KO mouse developed an unexpected phenotype, being resistant to high fat diet-induced obesity and displaying an extended lifespan. Molecular and metabolomics characterizations revealed futile cycles of lipids and tRNAs, which are produced and immediately degraded, which increases energy consumption in the Maf1 KO mouse and probably explains in part the protection to obesity. Additionally to the mouse characterization, I also developed a method to normalize ChIP-seq data, based on the addition of a foreign chromatin to be used as an internal control. The method improved reproducibility between replicates and revealed differences of Pol 3 occupancy between WT and Maf1 KO samples that were not seen without normalization to the internal control. I then established that increased Pol 3 occupancy in the Maf1 KO mouse liver was associated with increased levels of tRNA precursor but not of mature tRNAs, the effective molecules involved in translation. The overproduction of precursor tRNAs associated with the deletion of Maf1 apparently overwhelms the tRNA processing machinery as the Maf1 KO mice have lower levels of fully modified tRNAs. This maturation defect directly impacts on translation efficiency as polysomic fractions and newly synthetized protein levels were reduced in the liver of the Maf1 KO mouse. Altogether, these results indicate new functions for MAF1, a regulator of both transcription and translation as well as a potential target for obesity treatment.

Remerciements

Je voudrais tout d'abord remercier ma directrice de thèse, Nouria Hernandez, de m'avoir accueilli, encadré, financé et conseillé tout au long de ma thèse. J'ai le sentiment d'avoir énormément grandi professionnellement en travaillant avec elle. Avoir rejoint son laboratoire pour ces 5 formidables années de collaboration est la meilleure décision professionnelle que j'ai prise au cours de ma jeune carrière. Bonne chance pour ta nouvelle aventure à la tête de l'Université.

Je voudrais également remercier les Professeurs Béatrice Desvergne et Dominique Langin d'avoir accepté de participer à mon jury de thèse. Leurs conseils avisés pendant mon examen de demi-thèse auront permis de donner une nouvelle dimension au projet.

Les résultats obtenus pendant cette thèse sont le fruit d'étroites collaborations avec plusieurs groupes de recherche. Merci à Ian Willis pour tous les échanges téléphoniques qui auront été extrêmement constructifs et auront permis la réussite du projet « souris Maf1 », à Mauro Delorenzi, Gergana Bounova et David Bernasconi pour leurs conseils en statistique ainsi qu'à Johan Auwerx et Norman Moullan pour m'avoir accueilli et aidé.

Bien sûr, mes plus grands remerciements vont au groupe Hernandez. Sans eux, rien de tout cela n'aurait été possible. Merci à Viviane qui a été la pièce maîtresse de la réussite des analyses de tous mes projets. Plus que professionnellement, je voudrais aussi la remercier pour m'avoir initié à toutes les « bonnes choses » que la Suisse regorge. Mes plus grandes pensées vont à François qui aura égaillé toutes les journées passées ensemble au labo ou ailleurs. En joignant le laboratoire de Nouria, je ne m'attendais pas à me découvrir un petit frère! Mes pensées vont également à Marianne qui a été la colocataire de labo parfaite ainsi qu'à Andrea avec qui j'ai partagé de très bons moments. Merci à Gabriel, Pascal, Donatella, Eugenia, Gilles, Angela, Nicole, Annemieke, Michael, Sasha, Meghdad et Philippe qui auront tous participé de plus ou moins loin à la réussite de cette thèse. Un énorme merci

également à Nathalie et Corinne, nos deux super secrétaires qui auront permis de m'alléger pour toutes les tâches administratives.

Je voudrais également remercier les plateformes du GTF, de la MEF et du SIB présentes au CIG. J'ai la chance d'avoir travaillé dans un confort exceptionnel grâce à leurs compétences. Egalement un grand merci à Catherine qui est l'experte de la microscopie et qui m'a énormément soulagé dans ma charge de travail.

Un petit mot également pour tous les amis que je me suis fait au CIG et avec qui j'ai passé des moments formidables à l'extérieur des labos.

Une énorme pensée à mes parents qui m'ont donné un cadre de vie idéal et m'ont toujours soutenu et encouragé dans les choix que j'ai entrepris depuis tout petit. Mes départs successifs à Marseille et en Ecosse furent des petits chocs pour eux mais leur soutien a toujours été présent. Vous êtes les meilleurs!

Pour finir, je voudrais remercier Muriel qui a toujours été à mes cotés, en voulant bien me suivre que ce soit en Ecosse ou en Suisse et avec qui je m'apprête à vivre la plus belle des aventures en devenant père. Son soutien, ses encouragements et son amour sont les fondations à la réussite de cette thèse.

Table of content

Chapter I - Introduction

Nuclear transcription in eukaryotes is performed by three different multisubunit RNA polymerases (Pol), each one transcribing a different set of genes. The three RNA polymerases contain five common subunits, and Pol 1 and Pol 3 share 2 common subunits. In addition, each polymerase contains specific subunits, although these can be related in sequence: for example, the two largest catalytic subunits are highly related among Pol 1, 2, and 3 and E. coli RNA polymerase. Pol 1, a 14 subunit enzyme, transcribes the ribosomal RNA (or rRNA) genes, which code for RNA components of the ribosome and thus are involved in translation, and Pol 2, a 12 subunit enzyme, transcribes the protein coding genes, the micro RNA genes and some small nuclear RNA genes. Pol 3 is the largest of the RNA polymerases with 17 subunits (see Figure 1A) and its structure has been resolved recently (see figure 1B). Pol 3 transcribes a small set of highly active genes, usually shorter than 400 base pairs (bp) and coding for RNA molecules involved in diverse biological functions such as protein translation, ribosomal biogenesis, RNA maturation, and chromatin regulation (Dieci et al., 2007) (Table 1). During my thesis I used a KO mouse model lacking the Maf1 gene, encoding an important repressor of Pol 3 transcription, to characterize the effects of lack of Maf1 on mouse metabolism, Pol 3 transcription, and protein translation levels.

RNA polymerase III genes

The most abundant Pol 3 genes are the tRNA genes, which constitute 64% (433 out 672) of the Pol 3-occupied loci (Canella et al., 2012) and account for 15% of the total RNA in HeLa cells (Lodish et al., 2008). tRNAs were discovered in the mid 50s (Hoagland et al., 1957), after which their main function, to bring the correct new amino acid specific for each mRNA codon into the nascent polypeptidic chain, was rapidly identified. This main function is, however, probably not the only function of tRNAs. Recently they have been implicated in the regulation of translation during a stress response. In response to a stress condition such as heat shock or UV radiation,

tRNAs are digested by a nuclease (angiogenin in mammals and Rny1p in yeast) to produce tRNA-derived stress-induced fragments (tiRNAs), which accumulate and repress translation as shown both in U2OS osteosarcoma cells (Ivanov et al., 2011; Yamasaki et al., 2009) and in yeast (Thompson and Parker, 2009). Angiogenin also cleaves tRNAs in half when bases of the anticodon loop are lacking methylation modifications, leading to translation reduction and severe neuro-developmental defects in mouse (Blanco et al., 2014). The second most abundant Pol 3 genes are the 5S rRNAs, which are associated with the ribosomal protein L5 (Perederina et al., 2002) as part of the large subunit of the ribosome. The 5S RNAs are key for ribosome stability and translation efficiency, as a deletion of some of the 5S rRNA genes leads to a severe decrease in translation in yeast (Ammons et al., 1999). The BC1 gene, transcribed only in brain, also controls protein translation initiation by interaction of its RNA with the eukaryotic initiation factor 4A (eIF4A) and the poly(a) binding protein (PABP) which inhibits the formation of the 48S pre-initiation complex (Wang et al., 2002, 2005).

In addition to RNA molecules involved in translation, Pol 3 also synthesizes RNAs involved in other processes. U6 snRNA, first discovered in Xenopus and part of the spliceosome (Krol et al., 1987), is involved in pre-mRNA splicing; 7SK RNA represses transcription elongation by Pol II (Barboric et al., 2005); and 7SL RNA is a constituent of the signal recognition particle (Gundelfinger et al., 1983), which is involved in translocation of nascent polypeptides through the reticulum endoplasmic membrane. RNase P RNA (Nash and Robertson, 1981) and RNase MRP RNA (Chu et al., 1994) are also synthesized by Pol 3 and are implicated, respectively, in pre-tRNA and pre-rRNA processing. Other Pol 3 products have less clearly defined functions: Y RNAs interacting with Ro60 and La proteins form the Ro ribonucleoprotein complex, which has been reported to be required for DNA replication (Christov et al., 2006) as well to resistance to radiation (Chen et al., 2000) although its mechanism of action is still unclear. Vault RNAs are part of vault particles, involved in drug resistance (Izquierdo et al., 1996). Finally, the genome contains a large number of short interspersed nuclear elements (SINEs), which derived during evolution from Pol 3 transcription units by retrotransposition. These elements have been classified into several families, for example the B1 elements derived from the 7SL RNA gene and the B2 elements

derived from the tRNA genes. Most of them are transcriptionally silent, nevertheless some are still active and produce RNA molecules whose functions are presently unknown (Barski et al., 2010; Canella et al., 2010, 2012; Kutter et al., 2011; Moqtaderi et al., 2010; Oler et al., 2010)

Class of Pol 3 genes	Types of promoter	Main biological function
5S rRNA	1	Translation
tRNA	2	Translation
SINE RNA	2	?
7SK RNA	3	Pol 2 elongation
7SL RNA	2	Signal recognition particle
RNase P	3	tRNA maturation
RNase MRP	3	rRNA maturation
Y RNA	3	DNA replication
BC1	3	Translation
Vault RNA	3	Drug resistance
U6 snRNA	3	Splicing
$tRNA^{SeC}$	3	Translation
U6 ATAC snRNA	3	Splicing

Table 1. Different classes of Pol 3 genes with their type of promoters and biological functions.

RNA polymerase III transcription

Pol 3 genes can be classified into three categories according to their promoter structure (see Figure 1C) (Schramm and Hernandez, 2002). Briefly, type 1 promoters are intragenic and are composed of three elements, an A box, an intermediate element, and a C box, which together form the internal control region. Type 2 promoters are also intragenic and composed of an A and a B box. Type 3 promoters are extragenic and are constituted of a distal sequence element (DSE), a proximal sequence element (PSE) and a TATA box. The type of promoter determines which transcription factors are recruited together with the RNA polymerase to start

transcription. Figure 1.1 illustrates these various promoters and corresponding transcription factors. The first transcription factor recruited at the type 1 promoters of 5S rRNA genes is TFIIIA, which binds to the internal control region (Lassar et al., 1983). Then TFIIIC is recruited, followed by TFIIIB (Setzer and Brown, 1985), which is composed of 3 proteins: BDP1, TBP, and BRF1. Once this complex is formed, RNA polymerase III is recruited and starts transcription. Type 2 promoters of tRNA and other genes recruit RNA polymerase III by a similar mechanism except that they do not need TFIIIA. Instead, TFIIIC is directly recruited to the A and B boxes followed by TFIIIB and RNA polymerase III. Transcription from type 3 promoters such as the *U6* and *7SK* promoters is more complex. $SNAP_c$ binds to the PSE whereas STAF and OCT1 proteins bind to the DSE (Kleinert et al., 1990) and so stabilize binding of $SNAP_c$ to the PSE. A specialized form of TFIIIB, in which BRF2 replaces BRF1, is recruited through binding of its TBP component to the TATA box and through protein-protein contacts with $SNAP_c$. This complex then recruits RNA polymerase III.

Regulation of RNA polymerase III transcription

Global gene expression in the cell is regulated according to the different stimuli or stresses the cell is facing to produce the appropriate proteins that are key elements for cellular health. Pol 3 products involved in translation can conceivably control cell growth and proliferation by controlling the level of proteins. An upregulation of Pol 3 transcription is important in cancer development (White, 2004) indicating that a tight regulation of Pol 3 transcription is crucial to maintain cell fitness.

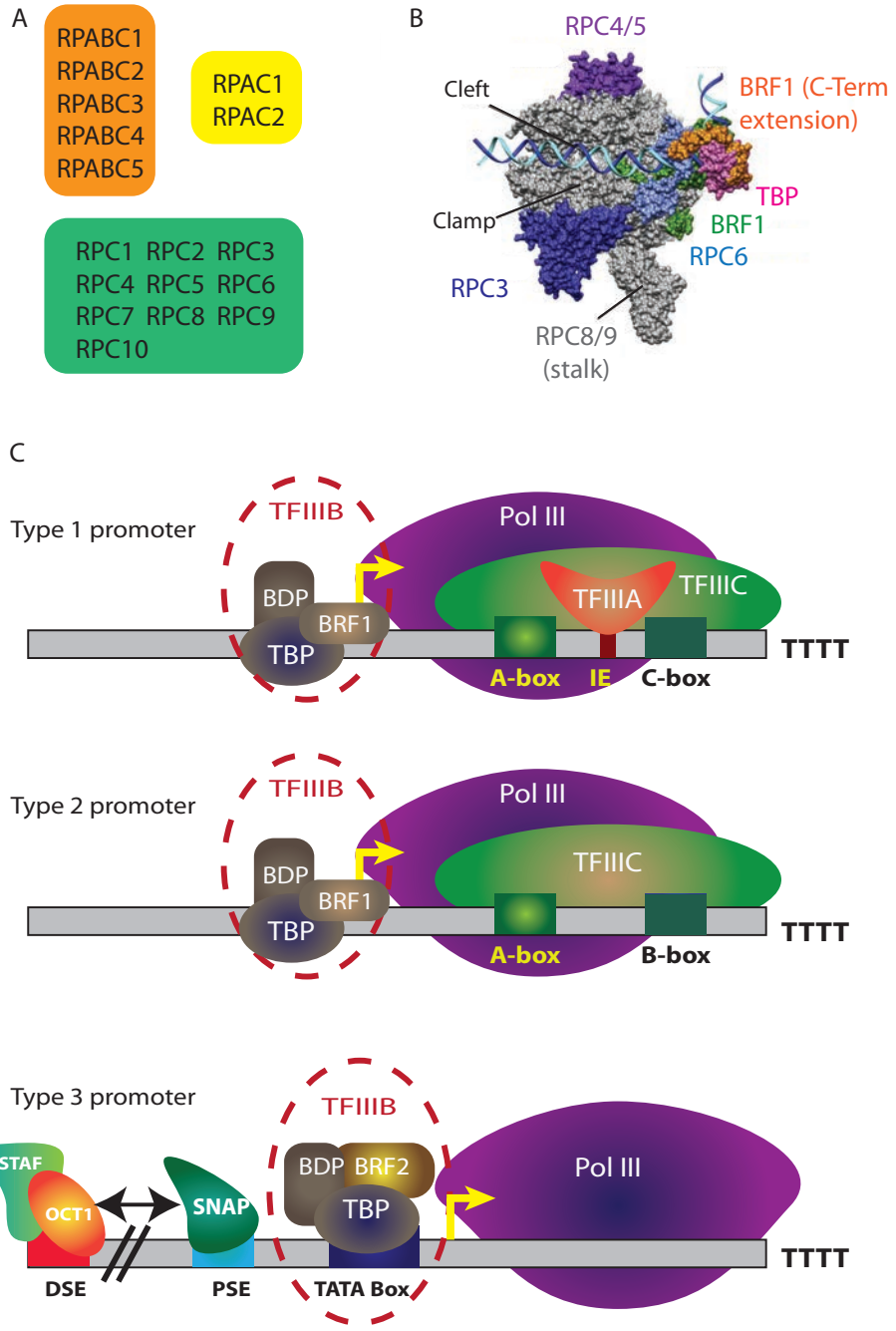

Figure 1.1: RNA polymerase III gene promoters. A. List of the Pol 3 subunits. In orange are the subunits shared by Pol 1, 2 and 3, in yellow the subunits shared by Pol 1 and Pol 3 and in green the subunits specific to Pol 3. B. RNA polymerase 3 structure adapted from (Vannini et al. 2012) C. Type 1 promoters are present in 5S rRNA genes. Types 2 promoters characterize mainly tRNA genes. Types 3 promoters are present in U6, 7SK, RNAse P and others genes.

Activation of Pol 3 transcription

Pol 3 transcription is tightly regulated by the levels of transcription factors present in the cell. For example, cell infection by the adenovirus E1A increases Pol 3 transcription (Hoeffler and Roeder, 1985) by increasing the level of TFIIIC proteins (Hoeffler et al., 1988). More recently, similar results were obtained with infection by Epstein-Barr viruses inducing transcription of the viral Pol 3 EBER gene via overexpression of the TFIIIC components (Felton-Edkins et al., 2006). Component levels of the other members of the TFIIIB complex are also critical for Pol 3 transcription. BDP1 expression was induced after infection by Epstein-Barr virus (Felton-Edkins et al., 2006), and TBP levels were up-regulated following infection by hepatitis B virus (Wang et al., 1995), which like Epstein-Barr viral infection leads to increased Pol 3 transcription. The expression of the third component of the TFIIIB complex, BRF1, was found to be induced in breast cancer lines after ethanol treatment, via overexpression of ERα (Zhang et al., 2013).

The activity of Pol 3 transcription factors is not only controlled by variations of their cellular levels, but also by association with other factors and by post-translational modifications. The oncogene c-Myc, recently shown to be an activator of the majority of the Pol 2 genes (Lin et al., 2012; Lovén et al., 2012), enhances Pol 3 transcription by binding to BRF1 (Felton-Edkins et al., 2003a; White, 2003). The phosphorylation status of Pol 3 transcription factors plays a critical role, and in particular the activity of BRF1 is controlled by several kinases. For example Polo-like kinase 1 (PLK1) has dual effects on Pol 3 transcription: it can associate with and phosphorylate BRF1 on serine 450, thus promoting Pol 3 transcription during late G1, S, and G2 phase, but during mitosis it phosphorylates BRF1 on threonine 270, which decreases Pol 3 transcription during cell division (Fairley et al., 2012). The MAPK (mitogen-activated protein kinase) ERK (extra cellular signal regulated kinase) can phosphorylate BRF1 hence mediating increased Pol 3 activity and thus increased levels of tRNAs (Felton-Edkins et al., 2003b). Casein kinase 2 (CK2) is an important mediator of Pol 3 transcription. The use of CK2 inhibitors decreases Pol 3 transcription and CK2 was shown to directly phosphorylate BRF1, thereby facilitating the recruitment of TFIIIB to TFIIIC (Johnston et al., 2002). In addition to BRF1, the other subunit of TFIIIB are also controlled by phosphorylation: BDP1 is phosphorylated by CK2 as well as by PKA

and Sch9 in yeast under normal growth condition to promote Pol 3 transcription (Lee et al., 2015); and TBP is directly phosphorylated by CK2, which reduces its binding affinity to DNA (Ghavidel and Schultz, 1997; Maldonado and Allende, 1999). Pol 3 transcription is also upregulated by phosphorylation of the transcription factor TFIIIC (Hoeffler et al., 1988).

Inhibition of Pol 3 transcription

Pol 3 transcription can be repressed by tumour suppressors that reduce Pol 3 binding to its transcription factors and so inhibit the formation of pre-initiation complexes. For example, the retinoblastoma tumour suppressor protein (pRB) was shown to repress Pol 3 transcription through its interaction with TFIIIB (Chu et al., 1997; Gjidoda. and Henry., 2012; White et al., 1996). Once bound to TFIIIB, pRB prevents association with TFIIIC and Pol 3, hence blocking transcription at all types of Pol 3 promoters. Furthermore, RB-knockout mice show clear increase in levels of tRNAs and 5S rRNAs (White et al., 1996). Like RB, the p107 and p130 pocket proteins play a role in Pol 3 regulation. Overexpression of either protein results in down-regulation of Pol 3 activity as both proteins directly bind and inhibit BRF1. P53 represses Pol 3 transcription by a somewhat similar mechanism. It targets TBP and so prevents the recruitment of TFIIIB at Pol 3 promoters by blocking its interaction with TFIIIC (Cairns and White, 1998; Chesnokov et al., 1996; Crighton et al., 2003). Consistent with this, P53 KO fibroblasts have elevated levels of tRNAs and 5S rRNAs (Cairns and White, 1998). Finally, MAF1 is a major repressor of Pol 3 transcription. It was first discovered in yeast (Boguta et al., 1997) and can inhibit Pol 3 transcription by binding directly to the Pol 3 subunit C160 and to BRF1. Crystallography studies suggest that binding of MAF1 to Pol 3 causes a rearrangement of Pol 3 subunits C31, C34 and C82, which prevent the recruitment of Pol 3 to the promoter-bound TFIIIB (Vannini et al., 2010). How MAF1 activity is regulated and how it can impact on cell physiology is discussed in the next sections.

MAF1, a major repressor of Pol 3 transcription

MAF1 protein is very conserved through evolution and its activity is regulated via its phosphorylation status. In yeast, it is known that under normal growth conditions Maf1 is phosphorylated by several kinases and stays in the cytoplasm (Lee et al., 2009; Michels et al., 2010; Moir et al., 2006). Under stress conditions, such as nutrient deprivation or DNA damage, Maf1 gets dephosphorylated, goes into the nucleus, and represses transcription by Pol 3 (Oficjalska-Pham et al., 2006; Reina et al., 2006). Yeast cells lacking Maf1 do not repress Pol 3 transcription upon several cellular stresses (Upadhya et al., 2002) suggesting that Maf1 is absolutely necessary for Pol 3 repression, at least under the conditions tested. This mechanism is well characterized in the yeast system but less is known about the mechanism involved in mammals.

MAF1 regulation via its phosphorylation status

Levels of Pol 3 products are diminished after nutrient deprivation via activation of MAF1. The TOR pathway is one the major nutrient regulatory pathways that control growth and metabolism both in yeast (Heitman et al., 1991) and mammals (Sabatini et al., 1994). Its central kinase TORC1 is very specifically inhibited by rapamycin (TOR stands for Target Of Rapamycin) and treatment decreases Pol 3 activity (Michels et al., 2010; Zaragoza et al., 1998), suggesting a direct effect of TORC1 on Pol 3 transcription. One of the TOR targets is S6 kinase (S6K) in mammals or its homologs Sch9 in yeast, which gets activated after phosphorylation and promotes translation initiation by phosphorylating the ribosomal protein S6.

In yeast, Maf1 was shown to be phosphorylated and inactivated by Sch9, which provokes its retention in the cytoplasm (Cai and Wei, 2015; Lee et al., 2009). Other researchers have reported direct phosphorylation of yeast Maf1 by TORC1 (Wei et al., 2009). Conversely, the phosphatase PP2A has been reported to activate Maf1 and Pol 3 repression under unfavourable growth conditions (Oficjalska-Pham et al., 2006) but more recent results suggest that Maf1 is in fact dephosphorylated by PP4 (Oler and Cairns, 2012). Glucose levels also regulate Maf1 activity, via the PKA kinase: glucose induces activation of the Ras pathway, which activates PKA leading to direct phosphorylation and inactivation of Maf1 (Moir et al., 2006). CK2 was also identified as a direct kinase of Maf1. CK2 interacts with, and directly phosphorylates, Maf1 on Pol 3 genes to stop Maf1 repression under favourable growth condition (Graczyk et

al., 2011). Much less is known about MAF1 regulation in mammalian cells. MAF1 was shown to be phosphorylated when cells are cultured in presence of serum (Goodfellow et al., 2008) and became dephosphorylated after rapamycin or MMS treatment (Reina et al., 2006). MAF1 was identified as a direct target of TORC1, which phosphorylates it on three residues (S60, S68 and S75) (Michels et al., 2010), and its phosphorylation state was shown to be unaffected in cells KO for both S6K1 and S6K2, suggesting that these kinases are not essential for MAF1 phosphorylation in mammalian cells. Another study which used specific inhibitors of the mTOR kinase in human tumorigenic lines showed that upon treatment with inhibitors, MAF1 was dephosphorylated, retained in the nucleus, and levels of pre-tRNAs were diminished(Shor et al., 2010). Recently PI3K was found to regulate levels of MAF1 in a PTEN dependant manner (Palian et al., 2014), and sumoylation of MAF1 was shown to promote Pol 3 transcription inhibition without interfering with MAF1 location (Rohira et al., 2013).

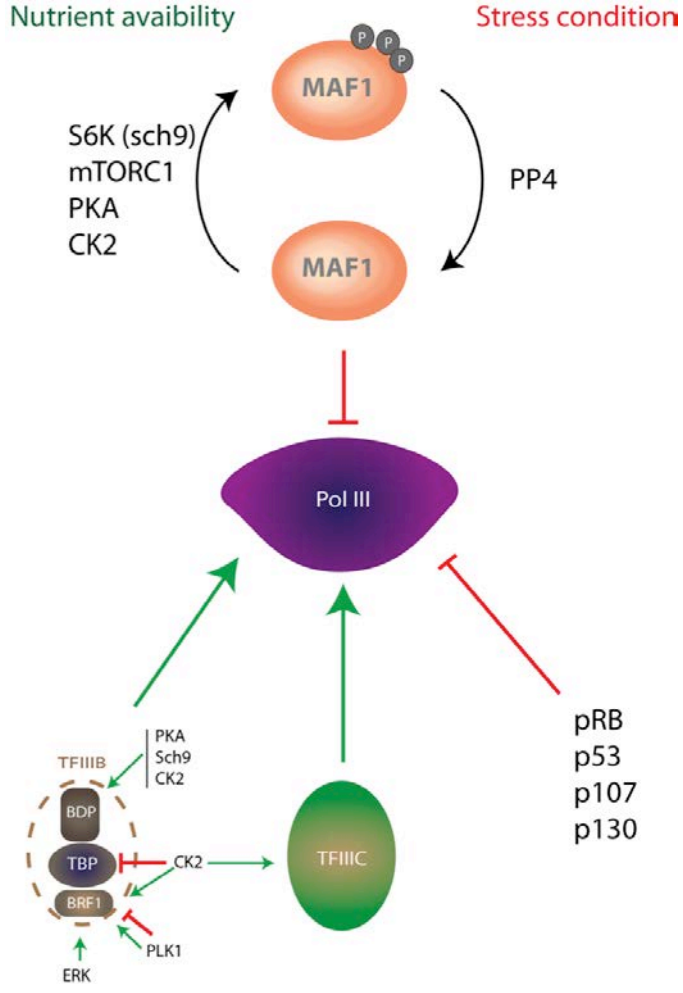

Figure 1.2: Regulation of RNA polymerase 3 transcription.
Pol 3 transcription is upregulated by increased levels of certain modifications of the transcription factors TFIIIB and TFIIIC, and downregulated by the retinoblastoma protein pRB, the pocket proteins p107 and 130, and p53. MAF1 is a major inhibitor of Pol 3 transcription and is regulated by phosphorylation. Under favorable conditions, MAF1 is phosphorylated by several kinases and inactivated; under stress conditions, MAF1 is dephosphorylated by PP4 and prevents transcription by Pol 3.

MAF1 impact on cell physiology and organism phenotypes

MAF1 is well characterized as a repressor of Pol 3 transcription, however in the last few years new functions of MAF1 in regulating metabolism, aging and reproduction were discovered. The first evidence of a link between MAF1 and metabolism was obtained in flies. The Grewal's group observed that knocking-down Drosophila Maf1 (dMaf1) with RNAi (Rideout et al., 2012) increased larvae volume and accelerated development. In the same study, the authors observed that increasing expression from just the initiator tRNA methionine gene induced an increase in protein translation leading to the same phenotypic effects as down regulation of Maf1. In another experiment, they showed that specific deletion of Maf1 in fat body of fly larvae promoted protein translation via enhanced level of $tRNAi^{Met}$, and induced the production of two proteins in the brain, dILP2 and dILP5, which stimulate the peripheral insulin pathway and tissue growth. The connection between enhanced protein levels in the fat tissue and an increased production of the dILPs proteins in the brain is still unclear and will need further investigations. At around the same time, a second publication suggested a link between Pol 3 transcription and drosophila larvae growth (Marshall et al., 2012). In this case, the loss of Brf (an homolog of mammalian BRF1), a core component of the fly TFIIIB, reduced dramatically the larvae size. The authors further showed that combining drugs (or starvation) to inhibit TORC1 with down-regulation of Maf1 by RNAi did not result in significant changes in tRNA levels, consistent with the idea that TORC1 controls Pol3 transcripts through MAF1.

In *Saccharomyces cerevisae*, Maf1 was linked to gluconeogenesis (Morawiec et al., 2013). Microarray studies of WT and Maf1 mutant yeast grown on a non-fermentable carbon source (glycerol) identified two key genes involved in yeast gluconeogenesis regulation that were down-regulated in the Maf1 mutant. One was FBP1, which is required to metabolise fructose 6-phosphate from fructose 1,6-biphosphate; its down-regulation stopped the Maf1 mutant yeast growth under restrictive conditions. The FBP1 gene being located next to a $tRNA^{lys}$ gene, a possibility was that expression of FBP1 was linked to expression of the adjacent Pol 3 gene, and an increase in Pol 3 recruitment to the $tRNA^{lys}$ gene in Maf1-depleted conditions could negatively impact on Pol 2 recruitment at the FBP1 gene. However, mutations in the $tRNA^{Lys}$ promoter

did not result in significant changes in FBP1 expression, arguing against the tRNA gene mediated silencing hypothesis, and keeping unclear the mechanism how Maf1 controls FPB1 expression. The second gene down-regulated was PCK1, which is required for the production of phosphoenolpyruvate from oxaloacetate, the rate-controlling step of gluconeogenesis (Rognstad, 1979). How Maf1 is linked to expression of PCK1 is also unclear.

Maf1 has been associated with metabolism regulation in worms. A recent study indicated that an increase of Maf1 levels leads to a decrease in FASN and ACC1 mRNA levels, and thus decreased *de novo* lipogenesis (Khanna et al., 2014). Maf1 also controls lipid transport in worms, as vitellogenin transcript levels were upregulated upon over-expression of Maf1 and inversely downregulated after RNAi mediated Maf1 knockdown. This effect on lipid transport directly influenced the fecundity of the worms. Last year, Deborah Johnson's group reported that decreasing MAF1 levels by siRNA induces an up-regulation of FASN and ACC in hepatocytes (Palian et al., 2014). They further found that Maf1 expression is controlled by the oncogene PTEN and that MAF1 represses FASN by binding directly to its promoter. Using different cell types they showed that high MAF1 levels lead to low lipid content and vice-versa. All together, these results suggested that Maf1 is a repressor of obesity in a mouse model. As described in the results part of this thesis, our own results seem, however, contradictory to these observations, at least at first sight.

MAF1 role on RNA polymerase II transcription

In yeast, genome-wide localization of MAF1 after stress has shown that MAF1 binds only to Pol 3 transcription units. In mammalian cells, however, several studies have implicated MAF1 as a direct repressor of transcription by RNA Pol 2. MAF1 was first reported to bind directly to the TBP promoter on Elk1 binding sites to repress its expression (Johnson et al., 2007). Similar binding was found at the Egr-1 promoter, which also contains an Elk1 binding site. As mentioned above, a subsequent study reported MAF1 binding on the Fasn and Acc1 promoters in the mouse (Palian et al., 2014), and more recently, at the CDKN1A promoter in human mammary tumor cell (Cai and Wei, 2015). However, in all cases, the evidence for MAF1 binding on protein

coding gene promoters is a ChIP-qPCR experiment. In genome-wide ChIP-sequencing experiments, I have been unable to identify any regions of binding (results shown in discussion). This negative result could be due to a poor affinity of the anti-Maf1 antibody to the endogenous protein, however I obtained similar negative results using a cell line expressing a tagged version of the protein (HA tag) and an anti-HA antibody. The ability of MAF1 to bind directly, and so regulate, Pol 2 promoters remains to be confirmed.

tRNAs physiology and translation control

MAF1 controls tRNA processing and degradation

tRNAs are the most abundant products of Pol 3 transcription and are involved in translation. tRNAs are synthetized as longer precursors and to be fully functional they need to be processed correctly. First the tRNAs are cleaved at the 5' end and 3' end, respectively by RNase P and RNase Z, and then modified by the addition of CCA nucleotides at the 3' end by tRNA nucleotidyl transferase (Lodish et al., 2000). Once the ends are processed, the tRNAs are exported into the cytoplasm and intron containing tRNAs (24 out 433 tRNAs in the mouse) are spliced (Figure 1.3). The processed tRNAs can then exert their function, i.e. bring a new amino acid into the elongating nascent chain.

The main repressor of Pol 3 transcription, Maf1, was shown to affect, indirectly, tRNA processing in yeast (Karkusiewicz et al., 2011). In its absence, precursor tRNAs (pre-tRNAs) accumulated in the nucleus. Accumulation of the pre-tRNAs was caused by the saturation of the exportin LOS1, which is responsible for the transfer of tRNAs between the nucleus and the cytoplasm (Murthi et al., 2010; Sarkar and Hopper, 1998). Overexpression of enzymes involved in processing (RNAse P or splicing endonucleases) did not counterbalance the nuclear accumulation of tRNA precursors (Karkusiewicz et al., 2011). Interestingly, nuclear tRNA accumulation was followed by an increase in the levels of GCN4 (ATF4 in mammals) (Figure 1.4), a transcriptional activator of genes involved in amino acid synthesis and the unfolded protein response (UPR) (Han et al., 2013). Another yeast study also linked tRNA processing and GCN4 expression in a manner independent of the translation initiation factor eiF2a,

indicating that unlike in the classical GCN4 activation pathway, which is triggered by low amino acid levels and proceeds through activation of the kinase GCN2, which then phosphorylates and thus represses eiF2a (see below), this regulation is independent of the amino-acid levels in the cell (Qiu et al., 2000).

To be fully functional, tRNAs also undergo a series of chemical modifications on many of their bases, and a defect in these nucleotide modifications leads to a rapid degradation of the tRNAs. Maf1 overexpression has the ability to protect the tRNAs against degradation by limiting Pol 3 transcription (Turowski et al., 2012). Thus, a fully functional tRNAs undergoes a number of maturation steps, which in principle could all be targets for regulation. Indeed, as described in the following sections, several of these steps have already been shown to be regulated, and this in turn regulates translation.

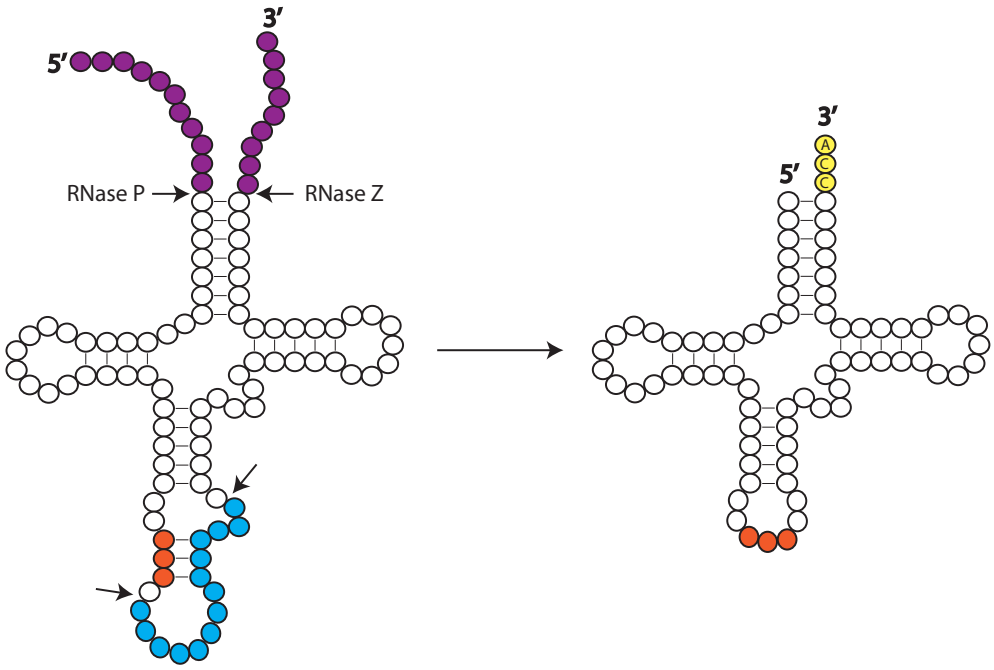

Figure 1.3: tRNA maturation process. tRNAs are generated as longer transcripts and undergo several steps of maturation to become fully functional. First, the 5' and the 3' ends (in purple) of the precursor tRNA are cleaved, respectively by RNase P and RNase Z, then the three nucleotides CCA are added at the 3' end (in yellow). The tRNAs are then exported from the nucleus into the cytoplasm, the intron (in blue) located downstream the anticodon of the tRNA (in orange) is spliced out, and some of the tRNA bases are modified. The appropriately processed tRNAs can then exert their function, namely bring new amino acids during translation, with full efficiency.

tRNAs shuttling between the nucleus and the cytoplasm

Before splicing, the 5' and 3' tRNAs are exported into the cytoplasm via the tRNA export receptor Exportin-t in mammals (or Los1 in yeast) (Kutay et al., 1998). In a *Los1* KO yeast, enzymes involved in CCA addition and amino-acylation could replace Los1 function for tRNA export, indicating that alternatives routes exist. It is clear that tRNAs need to be exported from the nucleus to play their role in protein translation, but an unexpected backward import was later discovered (Takano et al., 2005). Further investigations showed that the backward tRNA import acts as a quality control to ensure the delivery of fully functional tRNAs to the cell. Thus, aberrant tRNAs with extended 5' and 3' end or hypomodified tRNAs were shown to be reimported from the cytoplasm into the nucleus for a second round of maturation (Kramer and Hopper, 2013). Another yeast study using a *Los1* KO and *Msn5* KO (a second protein involved in yeast tRNA trafficking) yeast system indicates that the retrograde tRNA pathway is involved in the regulation of protein translation, and more particularly in the translation of proteins involved in amino acids biosynthesis (Chu and Hopper, 2013). (Feng and Hopper, 2002). tRNA localization is controlled by the physiological state, as under nutrient deprived conditions mature tRNAs are re-imported into the nucleus (Karkusiewicz et al., 2011; Shaheen et al., 2007). These observations suggest that tRNAs are not only exported from the nucleus after synthesis, but can actually shuttle back and forth between the cytoplasmic and nuclear compartment. This shuttling not only allows complete maturation of precursors exported prematurely into the cytoplasm, but also serves to regulate translation.

tRNAs amino-acylation and translation regulation

Translation is a very complex biological process that requires an mRNA, ribosomes, tRNAs, amino acids, and many other factors to produce the appropriate proteins to maintain cell fitness. One of the first steps of the translation reaction is the binding of amino acids to their corresponding tRNAs by several aminoacyl tRNA synthetases. This reaction is tightly regulated according to environmental changes. Amino acid deprivation leads to an increase of uncharged tRNAs in the cell, and such elevation activates GCN2 (Figure 1.4), the primary responder to amino acids deprivation and a kinase of the protein eIF2-α, as mentioned above (Wek et al., 1995; Zaborske et al.,

2009). Genome wide studies in yeast have revealed that deprivation of specific amino acids leads to increase of uncharged levels of both cognate and non-cognate tRNAs, indicating that amino-acylation can be a globally regulated process (Zaborske et al., 2009). However the observed changes in charging levels were different from starvation of one amino acid to starvation of another. The mechanism by which uncharged tRNAs activate GCN2 involves direct binding to a GCN2 region homologous to the enzyme histidyl-tRNA synthetase; the binding of an uncharged tRNA changes the conformation of GCN2, resulting in autophosphorylation and activation of the enzyme (Dong et al., 2000; Hinnebusch, 2005). Once activated, GCN2 phosphorylates eIF2-α at serine 52, leading to a general decrease of protein translation but also preferential translation of some specific stress-related proteins including ATF4, the mammal homolog of the yeast GCN4 protein. Phosphorylation of eIF2-α at serine 52 blocks the recycling of the ternary complex eIF2-α-GTP-tRNAi^{met}, hence repressing the initiation step of translation (Krishnamoorthy et al., 2001). eIF2-α phosphorylation was also linked to lipid metabolism. *Gcn2*-/- mice fed with a leucine-free diet, which should induce general translation repression, develop liver steatosis as expression of key lipogenic genes is not properly repressed (Guo and Cavener, 2007).

tRNA modifications also control translation

The tRNA modification reactions are a key step to yield fully mature tRNAs capable of converting efficiently the genetic code into proteins. So far over 90 modifications have been discovered (Machnicka et al., 2013) in tRNAs in the three domains of life, eukaryotes, archaea and bacteria, but the functions of many of them are still unclear. In general, chemical modifications maintain tRNA structure and stability (Torres et al., 2014). Among all the modifications, methylation on specific bases seems to play a key role regulating translation (Figure 1.4). Cytosine C^5-tRNA methylation is catalysed by the RNA methyltransferases DNMT2 on 3 tRNA isotypes (Asp, Gly and Val) and by NSUN2 on several others (Khoddami and Cairns, 2013). A specific KO of either enzyme in mice leads to viable animals, but each knockout shows very specific tRNA methylation defects, making it possible to attribute modification to either DNMT2 or NSUN2. For example for the tRNA^{Gly}, methylation of the cytosine at position C38 is carried out by DNMT2 whereas methylation of the cytosines at

positions C34, C40, C48, C49 and C50 is carried out by NSUN2 (Blanco et al., 2011; Goll et al., 2006; Hussain et al., 2013; Khoddami and Cairns, 2013). Mice with a KO of both enzymes display severe differentiation defects and reduced protein translation, indicating a role for the tRNA modifications in translation regulation (Tuorto et al., 2012). One of the mechanisms by which methylation on cytosine C^5 controls translation in both flies and mice is by protecting the tRNA against angiogenin-induced cleavage, thus keeping tRNA levels and, as a result, protein translation levels, high (Schaefer et al., 2010; Tuorto et al., 2012). The main donor of methyl group for most of the methyltransferases is S-Adenosyl Methionine (SAM) (Cantoni, 1953), indicating that lowered SAM levels could impact on tRNA methylation levels and thus could reduce translation.

Methylation is not the only modification that has been shown to regulate translation. Reduced translation was also observed in yeast lacking tRNA thiolation (Damon et al., 2015) or tRNA isopentenyl-A37 modifications (Lamichhane et al., 2013), and flies missing N^6-threonylcarbamoyl-adenosine (t^6A) showed reduced developmental growth and translation (Rojas-Benitez et al., 2015).

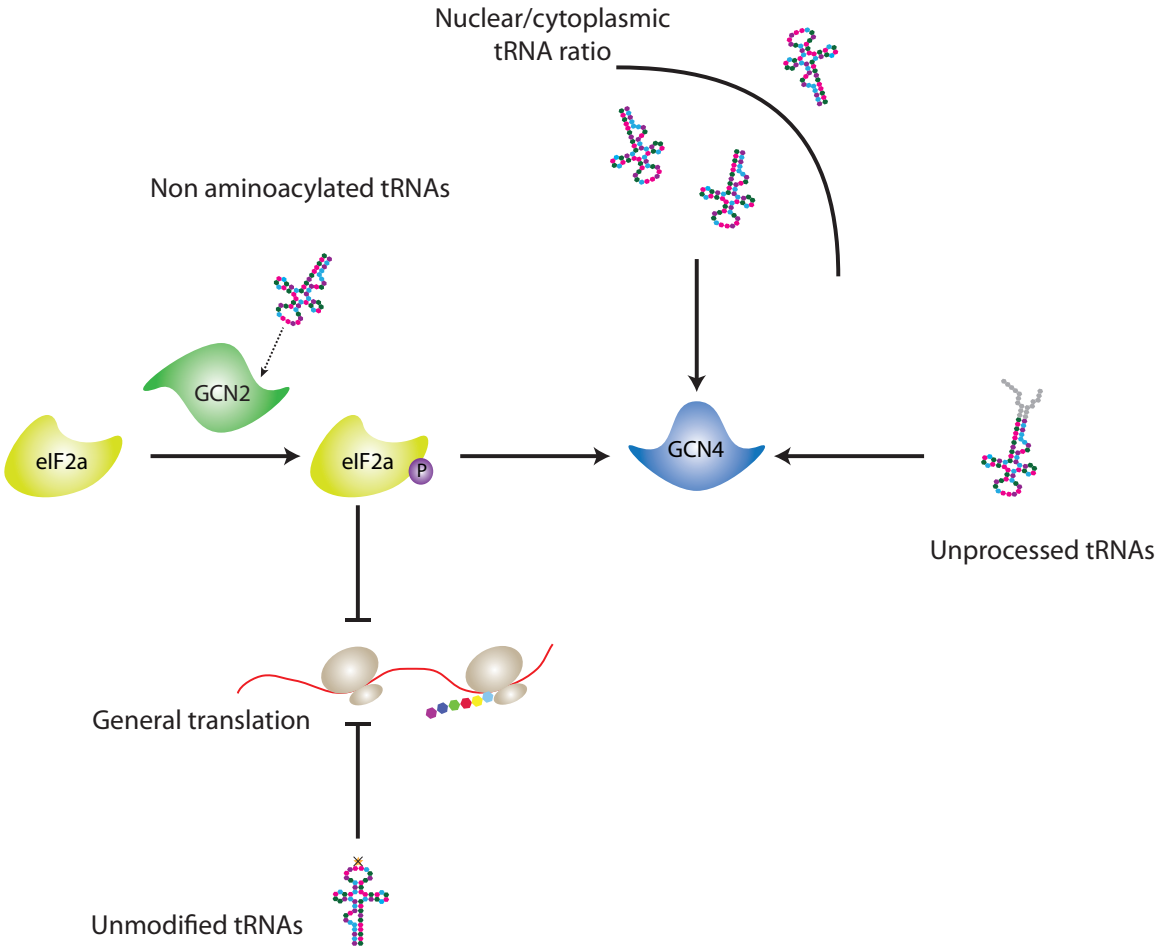

Figure 1.4 tRNA biology and translation control. Translation is inhibited by increased levels of non-aminoacylated (uncharged) tRNAs, by incorrectly modified tRNAs, by changes in ratios of nuclear/cytoplasmic tRNAs, and by improperly processed tRNAs. Several of these conditions also induce translation of specific transcription factors, notably GCN4, which controls expression of genes involved in amino acid synthesis and stress response.

tRNAs and human diseases

As summarized above, alterations in tRNA biology lead to variations in diverse molecular mechanisms, which could in principle lead to severe diseases. Indeed, tRNA modification defects have been identified as a cause of several diseases. For example, important neuro-developmental problems were found in Nsun2-/- mice lacking tRNA methylation at the C^5 position (Blanco et al., 2014). The lack of methylation induces cellular stress, leading to tRNA fragmentation by the endonuclease angiogenin and reduced brain size. tRNA modifications are also implicated in cancer and type 2

diabetes development. Overexpression of the gene Trmt12 coding for a tRNA methyltransferase implicated in wybutosine formation at position 37, 3'-adjacent to the anticodon of the tRNA phenylalanine, was observed in 26 out of 30 screened breast cancer tumours (Rodriguez et al., 2007), and abnormal proinsulin secretion leading to glucose intolerance was linked with altered expression of the tRNA modifying enzyme CDKAL1 (Wei et al., 2011). Interestingly, so far, there is no evidence showing a direct link between mutations in cytoplasmic tRNA and diseases, but several mutations in mitochondrial tRNAs have been associated with severe syndromes (For the full list, see reviews Abbott et al., 2014; Torres et al., 2014).

In addition to defects in tRNA modifications, defects in tRNA processing have been linked to disorders. Thus, the RNA kinase CLP1 is thought to participate in pre-tRNA splicing in mammals as it binds to the tRNA splicing endonuclease complex (TSEN) (Paushkin et al., 2004) responsible for intron removal. Clp1 mutated mice accumulate new tRNA fragments, and this is associated with embryonic loss of motor neuron. In humans, mutated Clp1 is associated with an increase in precursor tRNAs, which leads to brain atrophy and neurological syndrome (Karaca et al., 2014; Schaffer et al., 2014). Altogether these examples show an important role for tRNAs in regulating cell fitness. tRNAs were discovered more than 60 years ago, but we are just beginning to understand their numerous roles in cell biology, and further investigations will undoubtedly identify new functions.

Mouse adipose tissue and liver lipid metabolism

During my PhD studies I analysed a Maf1$^{-/-}$ mouse model. We rapidly realized that the Maf1 KO mice were resistant to diet-induced obesity, indicating a role of MAF1 in regulating mouse weight via white adipose tissue size. In the next sections I will discuss how white adipose tissues are formed and give a simplify view of the role of the adipose tissue and liver on metabolism during fed and fasting periods.

Adipose tissues formation

We often associate adipose tissue with just obesity and its metabolic complications, but adipose tissues are also important for stocking excess energy, controlling body temperature, and protecting the major organs against abnormal fat storage. It has long been thought that only two major adipose tissues exist, the white adipose tissue (WAT) and the brown adipose tissues (BAT), but recently a beige adipose tissue has also been characterized. WAT is the main adipose tissue found in adult humans and is mainly composed of adipocytes, although it also contains fibroblasts, endothelial and smooth muscle cells, and macrophages. WAT's main function is to store excess energy in the form of triglycerides stored in lipid droplets, which can then be released in the form of free fatty acids during periods of energy demand. In addition, adipocytes play a role in several processes such as systemic insulin sensitivity and satiety via leptin production (Zhang et al., 1996). On the other hand, BAT is the key site of heat production in mammals, necessary for survival in cold environment. Beige adipose tissue correspond to a new distinct cell population of BAT derived from the WAT via a browning process (Seale et al., 2008).

WAT and BAT are both derived from mesenchymal stem cells (MSCs), which differentiate into adipocytes during adipogenesis. Adipogenesis is divided into two steps: commitment, when pre-adipocytes are formed, and terminal differentiation, when pre-adipocytes acquire the features of functional, mature adipocytes. In the first step, MSCs receive a series of signals from different transcription factors and proteins to differentiate into pre-adipocytes during commitment. For example, *in vitro* experiments showed that the zinc-finger protein 423 (ZFP423) was enriched in pre-adipose versus non-pre-adipose fibroblasts and was essential for non-preadipose fibroblasts to activate PPARg and to undergo adipocyte differentiation (Gupta et al., 2010). A second important transcription factor for pre-adipocytes formation is the transcription factor 7-like 1 (TCF7L1), as its depletion is blocking adipogenesis (Cristancho et al., 2011). WNT glycoproteins also play a key role during commitment of MSCs into preadipocytes as they repress this process. Thus, down-regulation of Wnt-5a abolished the ability of MSCs to undergo osteogenesis and favors adipogenesis (Bilkovski et al., 2010), and 3T3-L1 cells infected by a retrovirus containing the gene Wnt-1 were maintained in an undifferentiated state and thus

unable to differentiate into adipocytes. This phenotype could be rescued by overexpression of CCATT/enhancer-binding protein α (C/EBPα) and PPARγ (Ross et al., 2000).

Terminal differentiation is better understood and is also controlled by transcription factors, which activate the expression of the key metabolic genes characteristic of adipocytes such as leptin, fatty acid binding protein 4 or glucose transporter type 4. Four transcription factors play key roles in terminal adipocyte differentiation: C/EBPα, C/EBPβ, C/EBPδ and PPARγ (Farmer, 2006; Rosen and MacDougald, 2006). C/EBPβ and C/EBPδ are expressed early in terminal differentiation and promote the expression of C/EBPα and PPARγ, the last one being essential for terminal differentiation (Rosen et al., 1999).

Liver and adipose tissue metabolism in the fed state

The liver plays a main role in regulating metabolic homeostasis by being a site of storage, synthesis, oxidation, and redistribution of carbohydrates and lipids, and its metabolism is tightly regulated by insulin. After a meal (Figure 1.5, top panel), the food is digested and absorbed into enterocytes of the small intestine where fatty acids are re-esterified with glycerol-3-phosphate to form triglycerides. Triglycerides are coated by several proteins to form chylomicrons, which are released into the blood stream via the lymphatic system. When the chylomicrons reach the vicinity of the major consumer organs, they are digested by lipoprotein lipase (LPL) and chylomicron remnants are absorbed by the liver. Absorption is mediated either by several fatty acid transport proteins and fatty acid translocase/CD36, or by direct diffusion (Bonen et al., 2004; Falcon et al., 2010). Absorbed fatty acids are used to form triglycerides by diacylglycerol acyltransferases (DGAT) (Yen et al., 2008), which catalyses the addition of a fatty acyl chain to diaglycerol. Most of these triglycerides are then integrated into very low-density lipoproteins (VLDL) to be transported to extra-hepatic tissues where they are stored (adipose tissue) or oxidized (skeletal and cardiac muscles).

Liver uses the carbohydrates released from food to produce glycogen, an energy reserve for fasting periods. Glucose enters the liver via the transporter Glut2, is

phosphorylated by glucokinases into glucose-1-P, which is used by glycogen synthase to produce glycogen. The liver also uses glucose excess to produce fatty acids by *de novo* lipogenesis, a reaction catalysed by two main enzymes: acetyl-CoA carboxylase (ACC) and fatty acid synthase (FAS). Briefly, a high carbohydrate diet will increase, via glycolysis, the level of pyruvate, which is then converted to acetyl-CoA. The first step of *de novo* lipogenesis is the carboxylation of acetyl-CoA into malonyl-CoA by ACC1 and ACC2. FAS can then use malonyl-CoA together with the reducing agent NADPH to produce palmitic acid, a precursor of other fatty acids (Ameer et al., 2014; Rui, 2014). DGATs enzymes then convert the fatty acid into triglycerides, which will be incorporated into VLDL. The expression of the FAS and ACCs genes is regulated by several transcription factors. For example, carbohydrate-responsive element-binding protein (ChREBP) and the sterol regulatory element-binding protein 1c (SREBP1c) are directly regulated by, respectively, glucose and insulin levels (Dentin et al., 2005), and promote expression of the FAS and ACCs genes (Denechaud et al., 2008; Shimano, 2001).

Adipose tissue is the main triglyceride storage tissue. As for the liver, chylomicrons are lysed (Figure 1.5 top panel) in the vicinity of the organ, by the LPL present in adipose blood capillaries, and chylomicron remnants are absorbed into adipose tissue. VLDL produced in the liver are also digested by LPL, fatty acids are taken up by adipocytes and esterified to form triglycerides by the DGATs enzymes. Glucose is also used by adipose tissue to form triglycerides via *de novo* lipogenesis (Chascione et al., 1987), however this process is less efficient compared to *de novo* lipogenesis in liver (Lodhi et al., 2011). The newly formed triglycerides are incorporated into lipid droplets for storage and ulterior usage.

A. Fed state

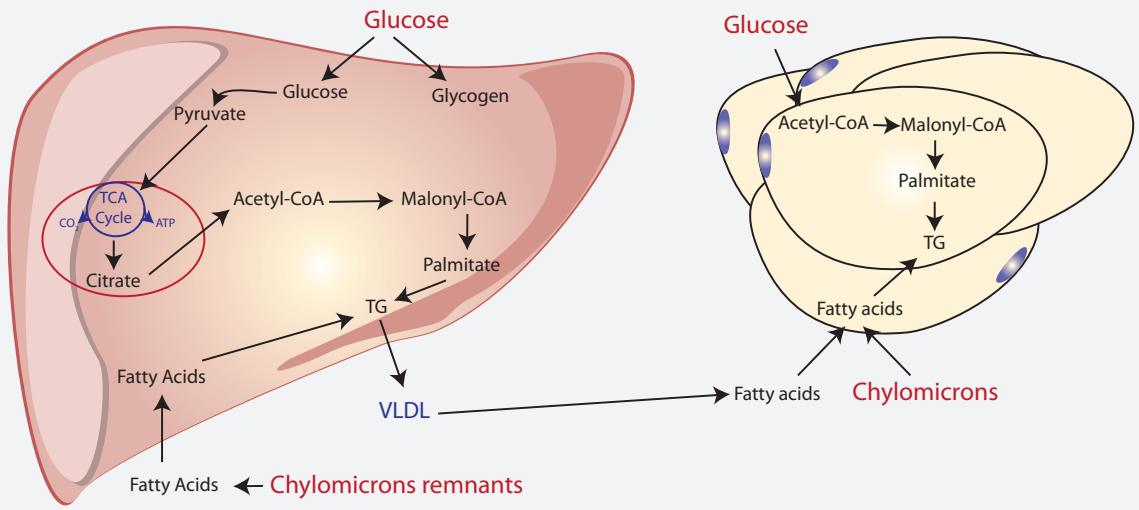

B. Fasted state

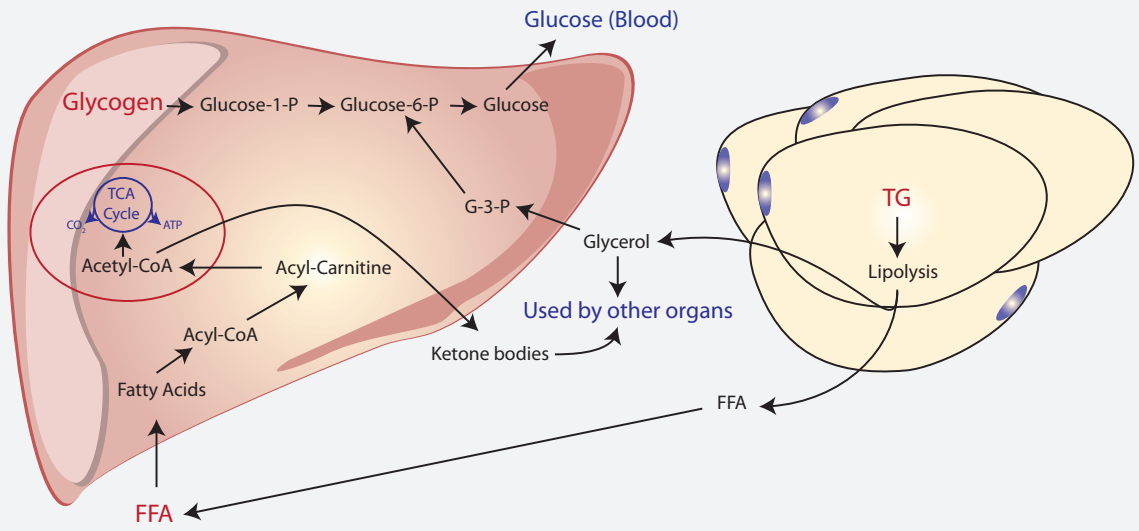

Figure 1.5. Simplified view of carbohydrate and lipid metabolism in adipose tissue and liver in fasted and fed states. Panel A. After a meal, circulating chylomicrons are lysed in the vicinity of the liver and adipose tissue to allow for fatty acids to be incorporated into these tissues, and chylomicrons remnants are lysed and incorporated into the liver. Both organs use the released fatty acids to produce once again triglycerides (TGs). Excess glucose is also used by both tissues to produce TGs. Liver-produced TGs are exported as VLDL that can be used by the adipose tissue for storage. Panel B. During fasting, TGs present in adipocytes are lysed and free fatty acids (FFAs) and glycerol are released. FFAs are oxidised by the liver for energy and the by-products, ketone bodies, are used as another source of energy by other organs. Liver also produces glucose via its glycogen stock or released glycerol.
In both panels, the sources of energy are represented in red and the produced compounds in blue.

Liver and adipose tissues metabolism during fasting

White adipose tissue is the main energy reserve of the body. During nutrient deprivation or physical exercise, the triglycerides present inside the adipocytes are lysed and fatty acids and glycerol are released into the vascular system as free fatty acids bound to albumin to be used by other organs as an energy source (Figure 1.5 lower panel). The main enzyme responsible for triglycerides digestion is hormone-sensitive lipase (HSL) (Jungas and Schwartz, 1970), but other lipases are also involved as HSL null mice show impaired, but not total lack of, triglycerides hydrolysis (Osuga et al., 2000). The activity of HSL is regulated by catecholamines via increased cAMP levels, which activate protein kinase A (PKA) (Carmen and Víctor, 2006; Langin, 2006). PKA then phosphorylates and activates HSL by facilitating its translocation from the cytosol into lipid droplets (Brasaemle et al., 2000; Egan et al., 1992). Glucagon can also stimulate lipolysis in adipocytes via upregulation of cAMP levels (Perea et al., 1995). In contrast, during re-feeding, insulin inhibits lipolysis by two mechanisms. It will activate, via the PI3K/PKA pathway, phosphodiesterase 3B, which degrades cAMP and so inhibits lipolysis (Wijkander et al., 1998). It will also stimulates the production of protein phosphatase 1, which dephosphorylates and inactivates HSL (Olsson and Belfrage, 1987; Ragolia and Begum, 1998).

The fatty acids released via adipose tissue lipolysis can be oxidized in the liver during fasting periods. Hepatic β-oxidation of fatty acids occurs in the mitochondria and

peroxisome. Carnitine palmitoyltransferase I (CPT1) catalyses the production of acyl-carnitine by transferring an acyl group of a long chain fatty acid to carnitine. Acyl-carnitine is next transferred into the mitochondria for subsequent oxidation and acetyl-CoA production by CPT2. Acetyl-CoA is used by the TCA cycle to produce energy, but excess acetyl-CoA is transformed into ketone bodies that are transported to extra-hepatic tissues as an alternative source of energy. During fasting periods, the liver also produces glucose to be used as an energy source by other organs. Glycogen produced during fed period is used during fasting to produce glucose through glycogenolysis, which is then released into the vascular system. During a fasting period, when glycogen stocks become depleted, hepatocytes produce glucose via gluconeogenesis using lactate, pyruvate, glycerol, and amino acids. Released glycerol from adipocytes lipolysis enters hepatocytes through aquaporin 9 (Jelen et al., 2011) and is transformed into glycerate-3-phosphate which is used to produce glucose.

References

Abbott, J. a, Francklyn, C.S., and Robey-Bond, S.M. (2014). Transfer RNA and human disease. Front. Genet. *5*, 158.

Ameer, F., Scandiuzzi, L., Hasnain, S., Kalbacher, H., and Zaidi, N. (2014). De novo lipogenesis in health and disease. Metabolism. *63*, 895–902.

Ammons, D., Rampersad, J., and Fox, G.E. (1999). 5S rRNA gene deletions cause an unexpectedly high fitness loss in Escherichia coli. Nucleic Acids Res. *27*, 637–642.

Barboric, M., Kohoutek, J., Price, J.P., Blazek, D., Price, D.H., and Peterlin, B.M. (2005). Interplay between 7SK snRNA and oppositely charged regions in HEXIM1 direct the inhibition of P-TEFb. EMBO J. *24*, 4291–4303.

Barski, A., Chepelev, I., Liko, D., Cuddapah, S., Fleming, A.B., Birch, J., Cui, K., White, R.J., and Zhao, K. (2010). Pol II and its associated epigenetic marks are present at Pol III-transcribed noncoding RNA genes. Nat. Struct. Mol. Biol. *17*, 629–634.

Bilkovski, R., Schulte, D.M., Oberhauser, F., Gomolka, M., Udelhoven, M., Hettich, M.M., Roth, B., Heidenreich, A., Gutschow, C., Krone, W., et al. (2010). Role of Wnt-5a in the determination of human mesenchymal stem cells into preadipocytes. J. Biol. Chem. *285*, 6170–6178.

Blanco, S., Kurowski, A., Nichols, J., Watt, F.M., Benitah, S.A., and Frye, M. (2011). The RNA-methyltransferase misu (NSun2) poises epidermal stem cells to differentiate. PLoS Genet. *7*.

Blanco, S., Dietmann, S., Flores, J. V, Hussain, S., Kutter, C., Humphreys, P., Lukk, M., Lombard, P., Treps, L., Popis, M., et al. (2014). Aberrant methylation of tRNAs links cellular stress to neuro-developmental disorders. *33*, 2020–2040.

Boguta, M., Czerska, K., and Zoładek, T. (1997). Mutation in a new gene MAF1 affects tRNA suppressor efficiency in Saccharomyces cerevisiae. Gene *185*, 291–296.

Bonen, A., Campbell, S.E., Benton, C.R., Chabowski, A., Coort, S.L.M., Han, X.-X., Koonen, D.P.Y., Glatz, J.F.C., and Luiken, J.J.F.P. (2004). Regulation of fatty acid transport by fatty acid translocase/CD36. Proc. Nutr. Soc. *63*, 245–249.

Brasaemle, D.L., Levin, D.M., Adler-Wailes, D.C., and Londos, C. (2000). The lipolytic stimulation of 3T3-L1 adipocytes promotes the translocation of hormone-sensitive lipase to the surfaces of lipid storage droplets. Biochim. Biophys. Acta - Mol. Cell Biol. Lipids *1483*, 251–262.

Cai, Y., and Wei, Y.H. (2015). Distinct regulation of Maf1 for lifespan extension by Protein kinase A. *7*, 133–143.

Cairns, C. a., and White, R.J. (1998). p53 is a general repressor of RNA polymerase III transcription. EMBO J. *17*, 3112–3123.

Canella, D., Praz, V., Reina, J.H., Cousin, P., and Hernandez, N. (2010). Defining the RNA polymerase III transcriptome: Genome-wide localization of the RNA polymerase III transcription machinery in human cells. Genome Res. *20*, 710–721.

Canella, D., Bernasconi, D., Gilardi, F., LeMartelot, G., Migliavacca, E., Praz, V., Cousin, P., Delorenzi, M., Hernandez, N., Deplancke, B., et al. (2012). A multiplicity of factors contributes to selective RNA polymerase III occupancy of a subset of RNA polymerase III genes in mouse liver. Genome Res. *22*, 666–680.

Cantoni (1953). S-Adenosylmethionine: a new intermediate formed enzymatically from l-methionine and adenosine triphosphate. J. Cell Biol. 403–416.

Carmen, G.Y., and Víctor, S.M. (2006). Signalling mechanisms regulating lipolysis. Cell. Signal. *18*, 401–408.

Chascione, C., Elwyn, D.H., Davila, M., Gil, K.M., Askanazi, J., and Kinney, J.M. (1987). Effect of carbohydrate intake on de novo lipogenesis in human adipose tissue. Am. J. Physiol. *253*, E664–E669.

Chen, X., Quinn, A.M., and Wolin, S.L. (2000). Ro ribonucleoproteins contribute to the resistance of Deinococcus radiodurans to ultraviolet irradiation Ro ribonucleoproteins contribute to the resistance of Deinococcus radiodurans to ultraviolet irradiation. 777–782.

Chesnokov, I., Chu, W.M., Botchan, M.R., and Schmid, C.W. (1996). p53 inhibits RNA polymerase III-directed transcription in a promoter-dependent manner. Mol. Cell. Biol. *16*, 7084–7088.

Christov, C.P., Gardiner, T.J., Szüts, D., and Krude, T. (2006). Functional requirement of noncoding Y RNAs for human chromosomal DNA replication. Mol. Cell. Biol. *26*, 6993–7004.

Chu, H.-Y., and Hopper, A.K. (2013). Genome-wide investigation of the role of the tRNA nuclear-cytoplasmic trafficking pathway in regulation of the yeast Saccharomyces cerevisiae transcriptome and proteome. Mol. Cell. Biol. *33*, 4241–4254.

Chu, S., Archer, R.H., Zengel, J.M., and Lindahl, L. (1994). The RNA of RNase MRP is required for normal processing of ribosomal RNA. Proc. Natl. Acad. Sci. U. S. A. *91*, 659–663.

Chu, W.M., Wang, Z., Roeder, R.G., and Schmid, C.W. (1997). RNA polymerase III transcription repressed by Rb through its interactions with TFIIIB and TFIIIC2. J. Biol. Chem. *272*, 14755–14761.

Crighton, D., Woiwode, A., Zhang, C., Mandavia, N., Morton, J.P., Warnock, L.J., Milner, J., White, R.J., and Johnson, D.L. (2003). p53 represses RNA polymerase III transcription by targeting TBP and inhibiting promoter occupancy by TFIIIB. EMBO J. *22*, 2810–2820.

Cristancho, a. G., Schupp, M., Lefterova, M.I., Cao, S., Cohen, D.M., Chen, C.S., Steger, D.J., and Lazar, M. a. (2011). Repressor transcription factor 7-like 1 promotes adipogenic competency in precursor cells. Proc. Natl. Acad. Sci. *108*, 16271–16276.

Damon, J.R., Pincus, D., and Ploegh, H.L. (2015). tRNA thiolation links translation to stress responses in Saccharomyces cerevisiae. Mol. Biol. Cell *26*, 270–282.

Denechaud, P.D., Bossard, P., Lobaccaro, J.M.A., Millatt, L., Staels, B., Girard, J., and Postic, C. (2008). ChREBP, but not LXRs, is required for the induction of glucose-regulated genes in mouse liver. J. Clin. Invest. *118*, 956–964.

Dentin, R., Girard, J., and Postic, C. (2005). Carbohydrate responsive element binding protein (ChREBP) and sterol regulatory element binding protein-1c (SREBP-1c): Two key regulators of glucose metabolism and lipid synthesis in liver. Biochimie *87*, 81–86.

Dieci, G., Fiorino, G., Castelnuovo, M., Teichmann, M., and Pagano, A. (2007). The expanding RNA polymerase III transcriptome. Trends Genet. *23*, 614–622.

Dong, J., Qiu, H., Garcia-Barrio, M., Anderson, J., and Hinnebusch, a G. (2000). Uncharged tRNA activates GCN2 by displacing the protein kinase moiety from a bipartite tRNA-binding domain. Mol. Cell *6*, 269–279.

Egan, J.J., Greenberg, a S., Chang, M.K., Wek, S. a, Moos, M.C., and Londos, C. (1992). Mechanism of hormone-stimulated lipolysis in adipocytes: translocation of hormone-sensitive lipase to the lipid storage droplet. Proc. Natl. Acad. Sci. U. S. A. *89*, 8537–8541.

Fairley, J.A., Mitchell, L.E., Berg, T., Kenneth, N.S., von Schubert, C., Silljé, H.H.W., Medema, R.H., Nigg, E.A., and White, R.J. (2012). Direct Regulation of tRNA and 5S rRNA Gene Transcription by Polo-like Kinase 1. Mol. Cell *45*, 541–552.

Falcon, A., Doege, H., Fluitt, A., Tsang, B., Watson, N., Kay, M.A., and Stahl, A. (2010). FATP2 is a hepatic fatty acid transporter and peroxisomal very long-chain acyl-CoA synthetase. Am. J. Physiol. Endocrinol. Metab. *299*, E384–E393.

Farmer, S.R. (2006). Transcriptional control of adipocyte formation. Cell Metab. *4*, 263–273.

Felton-Edkins, Z. a., Kenneth, N.S., Brown, T.R.P., Daly, N.L., Gomez-Roman, N., Grandori, C., Eisenman, R.N., and White, R.J. (2003a). Direct regulation of RNA polymerase III transcription by RB, p53 and c-Myc. Cell Cycle *2*, 181–184.

Felton-Edkins, Z. a., Fairley, J. a., Graham, E.L., Johnston, I.M., White, R.J., and Scott, P.H. (2003b). The mitogen-activated protein (MAP) kinase ERK induces tRNA synthesis by phosphorylating TFIIIB. EMBO J. *22*, 2422–2432.

Felton-Edkins, Z. a., Kondrashov, A., Karali, D., Fairley, J. a., Dawson, C.W., Arrand, J.R., Young, L.S., and White, R.J. (2006). Epstein-Barr virus induces cellular transcription factors to allow active expression of EBER genes by RNA polymerase III. J. Biol. Chem. *281*, 33871–33880.

Feng, W., and Hopper, A.K. (2002). A Los1p-independent pathway for nuclear export of intronless tRNAs in Saccharomycescerevisiae. Proc. Natl. Acad. Sci. U. S. A. *99*, 5412–5417.

Ghavidel, a, and Schultz, M.C. (1997). Casein kinase II regulation of yeast TFIIIB is mediated by the TATA-binding protein. Genes Dev. *11*, 2780–2789.

Gjidoda., A., and Henry., W. (2012). RNA polymerase III repression by the Retinoblastoma tumor suppressor protein. Changes *29*, 997–1003.

Goll, M.G., Kirpekar, F., Maggert, K. a, Yoder, J. a, Hsieh, C.-L., Zhang, X., Golic, K.G., Jacobsen, S.E., and Bestor, T.H. (2006). Methylation of tRNAAsp by the DNA methyltransferase homolog Dnmt2. Science *311*, 395–398.

Goodfellow, S.J., Graham, E.L., Kantidakis, T., Marshall, L., Coppins, B. a., Oficjalska-Pham, D., Gérard, M., Lefebvre, O., and White, R.J. (2008). Regulation of RNA Polymerase III Transcription by Maf1 in Mammalian Cells. J. Mol. Biol. *378*, 481–491.

Graczyk, D., Debski, J., Muszyńska, G., Bretner, M., Lefebvre, O., and Boguta, M. (2011). Casein kinase II-mediated phosphorylation of general repressor Maf1 triggers RNA polymerase III activation. Proc. Natl. Acad. Sci. U. S. A. *108*, 4926–4931.

Gundelfinger, E.D., Krause, E., Melli, M., and Dobberstein, B. (1983). The organization of the 7SL RNA in the signal recognition particle. Nucleic Acids Res. *11*, 7363–7374.

Guo, F., and Cavener, D.R. (2007). The GCN2 eIF2a Kinase Regulates Fatty-Acid Homeostasis in the Liver during Deprivation of an Essential Amino Acid. Cell Metab. *5*, 103–114.

Gupta, R.K., Arany, Z., Seale, P., Mepani, R.J., Ye, L., Conroe, H.M., Roby, Y. a, Kulaga, H., Reed, R.R., and Spiegelman, B.M. (2010). Transcriptional control of preadipocyte determination by Zfp423. Nature *464*, 619–623.

Han, J., Back, S.H., Hur, J., Lin, Y.-H., Gildersleeve, R., Shan, J., Yuan, C.L., Krokowski, D., Wang, S., Hatzoglou, M., et al. (2013). ER-stress-induced transcriptional regulation increases protein synthesis leading to cell death. Nat. Cell Biol. *15*, 481–490.

Heitman, J., Movva, N.R., and Hall, M.N. (1991). Targets for cell cycle arrest by the immunosuppressant rapamycin in yeast. Science *253*, 905–909.

Hinnebusch, A.G. (2005). Translational regulation of GCN4 and the general amino acid control of yeast. Annu. Rev. Microbiol. *59*, 407–450.

Hoagland, M.B., Stephenson, M.L., Scott, J., Hecht, L.I., and Zamecnik, A.P.C. (1957). A soluble ribonucleic acid intermediate in protein synthesis.

Hoeffler, W.K., and Roeder, R.G. (1985). Enhancement of RNA polymerase III transcription by the E1A gene product of adenovirus. Cell *41*, 955–963.

Hoeffler, W.K., Kovelman, R., and Roeder, R.G. (1988). Activation of transcription factor IIIC by the adenovirus E1A protein. Cell *53*, 907–920.

Hussain, S., Sajini, A. a., Blanco, S., Dietmann, S., Lombard, P., Sugimoto, Y., Paramor, M., Gleeson, J.G., Odom, D.T., Ule, J., et al. (2013). NSun2-mediated cytosine-5 methylation of vault noncoding RNA determines its processing into regulatory small RNAs. Cell Rep. *4*, 255–261.

Ivanov, P., Emara, M.M., Villen, J., Gygi, S.P., and Anderson, P. (2011). Angiogenin-Induced tRNA Fragments Inhibit Translation Initiation. Mol. Cell *43*, 613–623.

Izquierdo, M.A., Scheffer, G.L., Flens, M.J., Shoemaker, R.H., Rome, L.H., and Scheper, R.J. (1996). Relationship of LRP-human major vault protein to in vitro and clinical resistance to anticancer drugs. Cytotechnology *19*, 191–197.

Jelen, S., Wacker, S., Aponte-Santamaría, C., Skott, M., Rojek, A., Johanson, U., Kjellbom, P., Nielsen, S., De Groot, B.L., and Rützler, M. (2011). Aquaporin-9 protein is the primary route of hepatocyte glycerol uptake for glycerol gluconeogenesis in mice. J. Biol. Chem. *286*, 44319–44325.

Johnson, S.S., Zhang, C., Fromm, J., Willis, I.M., and Johnson, D.L. (2007). Mammalian Maf1 Is a Negative Regulator of Transcription by All Three Nuclear RNA Polymerases. Mol. Cell *26*, 367–379.

Johnston, I.M., Allison, S.J., Morton, J.P., Schramm, L., Scott, P.H., and White, R.J. (2002). CK2 Forms a Stable Complex with TFIIIB and Activates RNA Polymerase III Transcription in Human Cells CK2 Forms a Stable Complex with TFIIIB and Activates RNA Polymerase III Transcription in Human Cells. *22*, 3757–3768.

Jungas, R.L., and Schwartz, J.P. (1970). Studies on the lipases of adipose tissue. Horm. Metab. Res. *2*, Suppl 2:37–40.

Karaca, E., Weitzer, S., Pehlivan, D., Shiraishi, H., Gogakos, T., Hanada, T., Jhangiani, S.N., Wiszniewski, W., Withers, M., Campbell, I.M., et al. (2014). Human CLP1 mutations alter tRNA biogenesis, affecting both peripheral and central nervous system function. Cell *157*, 636–650.

Karkusiewicz, I., Turowski, T.W., Graczyk, D., Towpik, J., Dhungel, N., Hopper, A.K., and Boguta, M. (2011). Maf1 protein, repressor of RNA polymerase III, indirectly affects tRNA processing. J. Biol. Chem. *286*, 39478–39488.

Khanna, A., Johnson, D.L., and Curran, S.P. (2014). Physiological Roles for mafr-1 in Reproduction and Lipid Homeostasis. Cell Rep. *9*, 2180–2191.

Khoddami, V., and Cairns, B.R. (2013). Identification of direct targets and modified bases of RNA cytosine methyltransferases. Nat. Biotechnol. *31*, 458–464.

Kleinert, H., Bredow, S., and Benecke, B.J. (1990). Expression of a human 7S K RNA gene in vivo requires a novel pol III upstream element. EMBO J. *9*, 711–718.

Kramer, E.B., and Hopper, A.K. (2013). Retrograde transfer RNA nuclear import provides a new level of tRNA quality control in Saccharomyces cerevisiae. Proc. Natl. Acad. Sci. U. S. A. *110*, 21042–21047.

Kraus, D., Yang, Q., Kong, D., Banks, A.S., Zhang, L., Rodgers, J.T., Pirinen, E., Pulinilkunnil, T.C., Gong, F., Wang, Y., et al. (2014). Nicotinamide N-methyltransferase knockdown protects against diet-induced obesity. Nature *508*, 258–262.

Krishnamoorthy, T., Pavitt, G.D., Zhang, F., Dever, T.E., and Hinnebusch, a G. (2001). Tight binding of the phosphorylated alpha subunit of initiation factor 2 (eIF2alpha) to the regulatory subunits of guanine nucleotide exchange factor eIF2B is required for inhibition of translation initiation. Mol. Cell. Biol. *21*, 5018–5030.

Krol, A., Carbon, P., Ebel, J.P., and Appel, B. (1987). Xenopus tropicalis U6 snRNA genes transcribed by pot III contain the upstream promoter elements used by pol II dependent U snRNA genes. Nucleic Acids Res. *15*, 2463–2478.

Kutay, U., Lipowsky, G., Izaurralde, E., Bischoff, F.R., Schwarzmaier, P., Hartmann, E., and Görlich, D. (1998). Identification of a tRNA-specific nuclear export receptor. Mol. Cell *1*, 359–369.

Kutter, C., Brown, G.D., Gonçalves, Â., Wilson, M.D., Watt, S., Brazma, a., White, R.J., and Odom, D.T. (2011). Pol III binding in six mammals shows conservation among amino acid isotypes despite divergence among tRNA genes. *43*.

Lamichhane, T.N., Blewett, N.H., Crawford, A.K., Cherkasova, V. a, Iben, J.R., Begley, T.J., Farabaugh, P.J., and Maraia, R.J. (2013). Lack of tRNA modification isopentenyl-A37 alters mRNA decoding and causes metabolic deficiencies in fission yeast. Mol. Cell. Biol. *33*, 2918–2929.

Langin, D. (2006). Control of fatty acid and glycerol release in adipose tissue lipolysis. Comptes Rendus - Biol. *329*, 598–607.

Lassar, A.B., Martin, P.L., and Roeder, R.G. (1983). Transcription of class III genes: formation of preinitiation complexes. Science *222*, 740–748.

Lee, J., Moir, R.D., and Willis, I.M. (2015). Differential Phosphorylation of RNA Polymerase III and the Initiation Factor TFIIIB in Saccharomyces cerevisiae. PLoS One *10*, e0127225.

Lee, J.H., Moir, R.D., and Willis, I.M. (2009). Regulation of RNA polymerase III transcription involves SCH9-dependent and SCH9-independent branches of the target of rapamycin (TOR) pathway. J. Biol. Chem. *284*, 12604–12608.

Lin, C.Y., Lovén, J., Rahl, P.B., Paranal, R.M., Burge, C.B., Bradner, J.E., Lee, T.I., and Young, R. a. (2012). Transcriptional amplification in tumor cells with elevated c-Myc. Cell *151*, 56–67.

Lodhi, I.J., Wei, X., and Semenkovich, C.F. (2011). Lipoexpediency: De novo lipogenesis as a metabolic signal transmitter. Trends Endocrinol. Metab. *22*, 1–8.

Lodish, H., Berk, A., and Zipursky, S. (2000). Processing of rRNA and tRNA. In Molecular Cell Biology, p. Section 11.6.

Lodish, H.F., Berk, A., Zipursky, S.L., Matsudaira, P., Baltimore, D., and James, D. (2008). Molecular Cell Biology.

Lovén, J., Orlando, D. a., Sigova, A. a., Lin, C.Y., Rahl, P.B., Burge, C.B., Levens, D.L., Lee, T.I., and Young, R. a. (2012). Revisiting global gene expression analysis. Cell *151*, 476–482.

Machnicka, M. a., Milanowska, K., Oglou, O.O., Purta, E., Kurkowska, M., Olchowik, A., Januszewski, W., Kalinowski, S., Dunin-Horkawicz, S., Rother, K.M., et al. (2013). MODOMICS: A database of RNA modification pathways - 2013 update. Nucleic Acids Res. *41*, 262–267.

Maldonado, E., and Allende, J.E. (1999). Phosphorylation of yeast TBP by protein kinase CK2 reduces its specic binding to DNA. *443*, 256–260.

Marshall, L., Rideout, E.J., and Grewal, S.S. (2012). Nutrient/TOR-dependent regulation of RNA polymerase III controls tissue and organismal growth in Drosophila. EMBO J. *31*, 1916–1930.

Michels, A. a, Robitaille, A.M., Buczynski-Ruchonnet, D., Hodroj, W., Reina, J.H., Hall, M.N., and Hernandez, N. (2010). mTORC1 directly phosphorylates and regulates human MAF1. Mol. Cell. Biol. *30*, 3749–3757.

Moir, R.D., Lee, J., Haeusler, R. a, Desai, N., Engelke, D.R., and Willis, I.M. (2006). Protein kinase A regulates RNA polymerase III transcription through the nuclear localization of Maf1. Proc. Natl. Acad. Sci. U. S. A. *103*, 15044–15049.

Moqtaderi, Z., Wang, J., Raha, D., White, R.J., Snyder, M., Weng, Z., and Struhl, K. (2010). Genomic binding profiles of functionally distinct RNA polymerase III transcription complexes in human cells. Nat. Struct. Mol. Biol. *17*, 635–640.

Morawiec, E., Wichtowska, D., Graczyk, D., Conesa, C., Lefebvre, O., and Boguta, M. (2013). Maf1, repressor of tRNA transcription, is involved in the control of gluconeogenetic genes in Saccharomyces cerevisiae. Gene *526*, 16–22.

Murthi, A., Shaheen, H.H., Huang, H.-Y., Preston, M. a, Lai, T.-P., Phizicky, E.M., and Hopper, A.K. (2010). Regulation of tRNA bidirectional nuclear-cytoplasmic trafficking in Saccharomyces cerevisiae. Mol. Biol. Cell *21*, 639–649.

Nash, H.A., and Robertson, C.A. (1981). Purification and properties of the Escherichia coli protein factor required for lambda integrative recombination. J. Biol. Chem. *256*, 9246–9253.

Oficjalska-Pham, D., Harismendy, O., Smagowicz, W.J., Gonzalez de Peredo, A., Boguta, M., Sentenac, A., and Lefebvre, O. (2006). General Repression of RNA Polymerase III Transcription Is Triggered by Protein Phosphatase Type 2A-Mediated Dephosphorylation of Maf1. Mol. Cell *22*, 623–632.

Oler, A.J., and Cairns, B.R. (2012). PP4 dephosphorylates Maf1 to couple multiple stress conditions to RNA polymerase III repression. EMBO J. *31*, 1440–1452.

Oler, A.J., Alla, R.K., Roberts, D.N., Wong, A., Hollenhorst, P.C., Chandler, K.J., Cassiday, P. a, Nelson, C. a, Hagedorn, C.H., Graves, B.J., et al. (2010). Human RNA polymerase III transcriptomes and relationships to Pol II promoter chromatin and enhancer-binding factors. Nat. Struct. Mol. Biol. *17*, 620–628.

Olsson, H., and Belfrage, P. (1987). The regulatory and basal phosphorylation sites of hormone-sensitive lipase are dephosphorylated by protein phosphatase-1, 2A and 2C but not by protein phosphatase-2B. Eur. J. Biochem. *168*, 399–405.

Osuga, J., Ishibashi, S., Oka, T., Yagyu, H., Tozawa, R., Fujimoto, a, Shionoiri, F., Yahagi, N., Kraemer, F.B., Tsutsumi, O., et al. (2000). Targeted disruption of hormone-sensitive lipase results in male sterility and adipocyte hypertrophy, but not in obesity. Proc. Natl. Acad. Sci. U. S. A. *97*, 787–792.

Palian, B.M., Rohira, A.D., Johnson, S. a. S., He, L., Zheng, N., Dubeau, L., Stiles, B.L., and Johnson, D.L. (2014). Maf1 Is a Novel Target of PTEN and PI3K Signaling That Negatively Regulates Oncogenesis and Lipid Metabolism. PLoS Genet. *10*, e1004789.

Paushkin, S. V., Patel, M., Furia, B.S., Peltz, S.W., and Trotta, C.R. (2004). Identification of a human endonuclease complex reveals a link between tRNA splicing and pre-mRNA 3' end formation. Cell *117*, 311–321.

Perea, a, Clemente, F., Martinell, J., Villanueva-Peñacarrillo, M.L., and Valverde, I. (1995). Physiological effect of glucagon in human isolated adipocytes. Horm. Metab. Res. *27*, 372–375.

Perederina, A., Nevskaya, N., Nikonov, O., Nikulin, A., Dumas, P., Yao, M., Tanaka, I., Garber, M., Gongadze, G., and Nikonov, S. (2002). Detailed analysis of RNA-protein interactions within the bacterial ribosomal protein L5/5S rRNA complex. RNA *8*, 1548–1557.

Qiu, H., Hu, C., Anderson, J., Björk, G.R., Sarkar, S., Hopper, a K., and Hinnebusch, a G. (2000). Defects in tRNA processing and nuclear export induce GCN4 translation

independently of phosphorylation of the alpha subunit of eukaryotic translation initiation factor 2. Mol. Cell. Biol. *20*, 2505–2516.

Ragolia, L., and Begum, N. (1998). Protein phosphatase-1 and insulin action. 49–58.

Reina, J.H., Azzouz, T.N., and Hernandez, N. (2006). Maf1, a new player in the regulation of human RNA polymerase III transcription. PLoS One *1*.

Rideout, E.J., Marshall, L., and Grewal, S.S. (2012). Drosophila RNA polymerase III repressor Maf1 controls body size and developmental timing by modulating tRNAiMet synthesis and systemic insulin signaling. Proc. Natl. Acad. Sci. *109*, 1139–1144.

Rodriguez, V., Chen, Y., Elkahloun, A., Dutra, A., Pak, E., and Chandrasekharappa, S. (2007). Chromosome 8 BAC array comparative genomic hybridization and expression analysis identify amplification and overexpression of TRMT12 in breast cancer. Genes Chromosom. Cancer *46*, 694–707.

Rognstad, R. (1979). Rate-limiting steps in metabolic pathways. J. Biol. Chem. *254*, 1875–1878.

Rohira, A.D., Chen, C., Allen, J.R., and Johnson, D.L. (2013). Covalent SUMO modification of Maf1 controls RNA polymerase III-dependent transcription repression. 1–17.

Rojas-Benitez, D., Thiaville, P.C., de Crecy-Lagard, V., and Glavic, A. (2015). The Levels of a Universally Conserved tRNA Modification Regulate Cell Growth. J. Biol. Chem. jbc.M115.665406.

Rosen, E.D., and MacDougald, O. a (2006). Adipocyte differentiation from the inside out. Nat. Rev. Mol. Cell Biol. *7*, 885–896.

Rosen, E.D., Sarraf, P., Troy, A.E., Bradwin, G., Moore, K., Milstone, D.S., Spiegelman, B.M., and Mortensen, R.M. (1999). PPARγ is required for the differentiation of adipose tissue in vivo and in vitro. Mol. Cell *4*, 611–617.

Ross, S.E., Hemati, N., Longo, K. a, Bennett, C.N., Lucas, P.C., Erickson, R.L., and MacDougald, O. a (2000). Inhibition of adipogenesis by Wnt signaling. Science *289*, 950–953.

Rui, L. (2014). Energy metabolism in the liver. Compr. Physiol. *4*, 177–197.

Sabatini, D.M., Erdjument-Bromage, H., Lui, M., Tempst, P., and Snyder, S.H. (1994). RAFT1: A mammalian protein that binds to FKBP12 in a rapamycin-dependent fashion and is homologous to yeast TORs. Cell *78*, 35–43.

Sarkar, S., and Hopper, a K. (1998). tRNA nuclear export in saccharomyces cerevisiae: in situ hybridization analysis. Mol. Biol. Cell *9*, 3041–3055.

Schaefer, M., Pollex, T., Hanna, K., Tuorto, F., Meusburger, M., Helm, M., and Lyko, F. (2010). RNA methylation by Dnmt2 protects transfer RNAs against stress-induced cleavage. Genes Dev. *24*, 1590–1595.

Schaffer, A.E., Eggens, V.R.C., Caglayan, A.O., Reuter, M.S., Scott, E., Coufal, N.G., Silhavy, J.L., Xue, Y., Kayserili, H., Yasuno, K., et al. (2014). CLP1 founder mutation links tRNA splicing and maturation to cerebellar development and neurodegeneration. Cell *157*, 651–663.

Schramm, L., and Hernandez, N. (2002). Recruitment of RNA polymerase III to its target promoters Recruitment of RNA polymerase III to its target promoters. 2593–2620.

Seale, P., Bjork, B., Yang, W., Kajimura, S., Chin, S., Kuang, S., Scimè, A., Devarakonda, S., Conroe, H.M., Erdjument-Bromage, H., et al. (2008). PRDM16 controls a brown fat/skeletal muscle switch. Nature *454*, 961–967.

Setzer, D.R., and Brown, D.D. (1985). Formation and stability of the 5 S RNA transcription complex. J. Biol. Chem. *260*, 2483–2492.

Shaheen, H.H., Horetsky, R.L., Kimball, S.R., Murthi, A., Jefferson, L.S., and Hopper, A.K. (2007). Retrograde nuclear accumulation of cytoplasmic tRNA in rat hepatoma cells in response to amino acid deprivation. Proc. Natl. Acad. Sci. U. S. A. *104*, 8845–8850.

Shimano, H. (2001). Sterol regulatory element-binding proteins (SREBPs): Transcriptional regulators of lipid synthetic genes. Prog. Lipid Res. *40*, 439–452.

Shor, B., Wu, J., Shakey, Q., Toral-Barza, L., Shi, C., Follettie, M., and Yu, K. (2010). Requirement of the mTOR kinase for the regulation of Maf1 phosphorylation and control of RNA polymerase III-dependent transcription in cancer cells. J. Biol. Chem. *285*, 15380–15392.

Takano, A., Endo, T., and Yoshihisa, T. (2005). tRNA actively shuttles between the nucleus and cytosol in yeast. Science *309*, 140–142.

Thompson, D.M., and Parker, R. (2009). The RNase Rny1p cleaves tRNAs and promotes cell death during oxidative stress in Saccharomyces cerevisiae. J. Cell Biol. *185*, 43–50.

Torres, A.G., Batlle, E., and Ribas de Pouplana, L. (2014). Role of tRNA modifications in human diseases. Trends Mol. Med. *20*, 306–314.

Tuorto, F., Liebers, R., Musch, T., Schaefer, M., Hofmann, S., Kellner, S., Frye, M., Helm, M., Stoecklin, G., and Lyko, F. (2012). RNA cytosine methylation by Dnmt2 and NSun2 promotes tRNA stability and protein synthesis. Nat. Struct. Mol. Biol. *19*, 900–905.

Turowski, T.W., Karkusiewicz, I., Kowal, J., and Boguta, M. (2012). Maf1-mediated repression of RNA polymerase III transcription inhibits tRNA degradation via RTD pathway. RNA *18*, 1823–1832.

Upadhya, R., Lee, J., and Willis, I.M. (2002). Maf1 is an essential mediator of diverse signals that repress RNA polymerase III transcription. Mol. Cell *10*, 1489–1494.

Vannini, A., Ringel, R., Kusser, A.G., Berninghausen, O., Kassavetis, G. a., and Cramer, P. (2010). Molecular basis of RNA polymerase III transcription repression by Maf1. Cell *143*, 59–70.

Vannini, A., and Cramer, P. (2012). Conservation between the RNA Polymerase I,II and III transcription initiation machineries. Mol. Cell *45*, 439–446.

Wang, H., Iacoangeli, A., Popp, S., Muslimov, I. a, Imataka, H., Sonenberg, N., Lomakin, I.B., and Tiedge, H. (2002). Dendritic BC1 RNA: functional role in regulation of translation initiation. J. Neurosci. *22*, 10232–10241.

Wang, H., Iacoangeli, A., Lin, D., Williams, K., Denman, R.B., Hellen, C.U.T., and Tiedge, H. (2005). Dendritic BC1 RNA in translational control mechanisms. J. Cell Biol. *171*, 811–821.

Wang, H.D., Yuh, C.H., Dang, C. V, and Johnson, D.L. (1995). The hepatitis B virus X protein increases the cellular level of TATA-binding protein, which mediates transactivation of RNA polymerase III genes. Mol. Cell. Biol. *15*, 6720–6728.

Wei, F., Suzuki, T., Watanabe, S., Kimura, S., Kaitsuka, T., Fujimura, A., Matsui, H., Atta, M., Michiue, H., Fontecave, M., et al. (2011). Deficit of tRNA Lys modification by Cdkal1 causes the development of type 2 diabetes in mice. J. Clin. Invest. *121*, 3598–3608.

Wei, Y., Tsang, C.K., and Zheng, X.F.S. (2009). Mechanisms of regulation of RNA polymerase III-dependent transcription by TORC1. EMBO J. *28*, 2220–2230.

Wek, S. a, Zhu, S., and Wek, R.C. (1995). The histidyl-tRNA synthetase-related sequence in the eIF-2 alpha protein kinase GCN2 interacts with tRNA and is required for activation in response to starvation for different amino acids. Mol. Cell. Biol. *15*, 4497–4506.

White, R.J. (2003). Direct activation of RNA polymerase III transcription by c-Myc. Nature *421*, 1698–1701.

White, R.J. (2004). RNA polymerase III transcription and cancer. Oncogene *23*, 3208–3216.

White, R.J., Trouche, D., Martin, K., Jackson, S.P., and Kouzarides, T. (1996). Repression of RNA polymerase III transcription by the retinoblastoma protein. Nature *382*, 88–90.

Wijkander, J., Landström, T.R., Manganiello, V., Belfrage, P., and Degerman, E. (1998). Insulin-induced phosphorylation and activation of phosphodiesterase 3B in rat adipocytes: possible role for protein kinase B but not mitogen-activated protein kinase or p70 S6 kinase. Endocrinology *139*, 219–227.

Yamasaki, S., Ivanov, P., Hu, G.-F., and Anderson, P. (2009). Angiogenin cleaves tRNA and promotes stress-induced translational repression. J. Cell Biol. *185*, 35–42.

Yen, C.-L.E., Stone, S.J., Koliwad, S., Harris, C., and Farese, R. V (2008). Thematic review series: glycerolipids. DGAT enzymes and triacylglycerol biosynthesis. J. Lipid Res. *49*, 2283–2301.

Zaborske, J.M., Narasimhan, J., Jiang, L., Wek, S. a., Dittmar, K. a., Freimoser, F., Pan, T., and Wek, R.C. (2009). Genome-wide analysis of tRNA charging and activation of the eIF2 kinase Gcn2p. J. Biol. Chem. *284*, 25254–25267.

Zaragoza, D., Ghavidel, a, Heitman, J., and Schultz, M.C. (1998). Rapamycin induces the G0 program of transcriptional repression in yeast by interfering with the TOR signaling pathway. Mol. Cell. Biol. *18*, 4463–4470.

Zhang, B., Graziano, M.P., Doebber, T.W., Leibowitz, M.D., White-Carrington, S., Szalkowski, D.M., Hey, P.J., Wu, M., Cullinan, C. a., Bailey, P., et al. (1996). Down-regulation of the expression of the obese gene by an antidiabetic thiazolidinedione in Zucker diabetic fatty rats and db/db mice. J. Biol. Chem. *271*, 9455–9459.

Zhang, Q., Jin, J., Zhong, Q., Yu, X., Levy, D., and Zhong, S. (2013). ERα mediates alcohol-induced deregulation of Pol III genes in breast cancer cells. Carcinogenesis *34*, 28–37.

Chapter II – Characterization of a Maf1 KO mouse model.

Abstract

MAF1 is thought to be the main repressor of Pol 3 transcription and its inhibition increases the level of Pol 3 products (Oficjalska-Pham et al., 2006; Reina et al., 2006). tRNAs are the main Pol 3 products (Canella et al., 2012) and are essential for translation by their function of bringing successive new amino acids into the nascent polypeptide chain. Other Pol 3 products are required for various cellular processes such as maturation of some RNA molecules and the control of transcription elongation. Upregulated Pol 3 activity is a hallmark of cancer cells, and indeed there are indications that an increase in just the levels of methionine initiator tRNAs can transform mouse cells, presumably by increasing translation. It is conceivable, then, that removing an inhibitor of Pol 3 transcription such as MAF1 might drive cells into a malignant state.

Before my arrival, our group in collaboration with the group of Ian Willis from the Albert Einstein Center in New York had ordered from the Ozgene company a Maf1 KO mouse to check how increased Pol 3 activity could impact on the phenotype of a mammalian organism. Surprisingly, pathology reports of the Maf1 KO mouse did not show any evidence of cancer development (data not shown). On the contrary, the Maf1 KO mouse had a slightly increased life span compared to the WT counterpart. It is however important to note that the Maf1 KO mouse was not challenged by any tumorigenic treatment, which could still reveal a propensity to develop cancer. Nevertheless, it remains that these mice did not show any increase in spontaneous tumor development. Instead, the deletion of the Maf1 gene was accompanied with leanness and a resistance to diet-induced obesity. This was a highly unexpected

result, as at that stage there was no indication linking MAF1 to lipid metabolism.

A previous post-doctoral fellow had noticed that in the Maf1 KO mouse, there was slightly increased expression of the KIAA1875 gene, located just downstream of the Maf1 gene. Given the completely unexpected phenotype of the Maf1 KO mouse, we worried that it might reflect upregulation of KIAA1875 rather than KO of the Maf1 gene. We reasoned that although the upregulation of KIAA1875 might be a direct effect of the loss of Maf1 function, it more likely resulted from transcriptional read-through from the Maf1 promoter into the KIAA1875 sequences as a result of the genomic deletion in the Maf1 KO mouse. Indeed, such read-through transcripts could be observed by RNAseq. When I joined the project, I designed a new Maf1 KO mouse, using the zinc finger nuclease (ZFN) technology, to confirm the phenotype. The ZFN technology uses an engineered nuclease consisting of zinc fingers designed to bind to the sequence of interest fused to the catalytic domain of the restriction enzyme Fok1 (see Figure 2.1A). When injected into fertilized eggs, the nuclease induces a cut at the targeted genomic region, which is then repaired by nonhomologous end joining, leading sometimes to mutations and thus disruption of the coding frame. I obtained two mutations within the Maf1 coding sequence, one introducing a single T residue and the other removing 8 base pairs. Both mutations result in a frame shift and introduction of a stop codon shortly downstream of the mutation. I found that, as expected, mice carrying either of these mutations did not express full-length MAF1, and displayed unchanged expression levels of the downstream KIAA1875 gene. Nevertheless, the two ZFN Maf1 KO mice were resistant to high fat diet-induced obesity, thus confirming that the phenotype is directly linked to the absence of MAF1.

To understand the Maf1 KO mouse phenotype, I performed Affymetrix microarrays to check the changes in Pol 2 gene expression genome-wide in liver and epididymal white adipose tissue. Few genes were differentially expressed in WT and Maf1 KO mice but one of them, Nnmt, particularly interested me. Indeed, knockdown of Nnmt in liver and white adipose tissue had recently been linked to diet-induced obesity protection (Kraus et al., 2014) and its expression was significantly down-regulated in the liver of the Maf1 KO mouse. These results allowed us to link the Maf1 KO mouse reduced body weight under high fat diet and the lifespan expansion to metabolism.

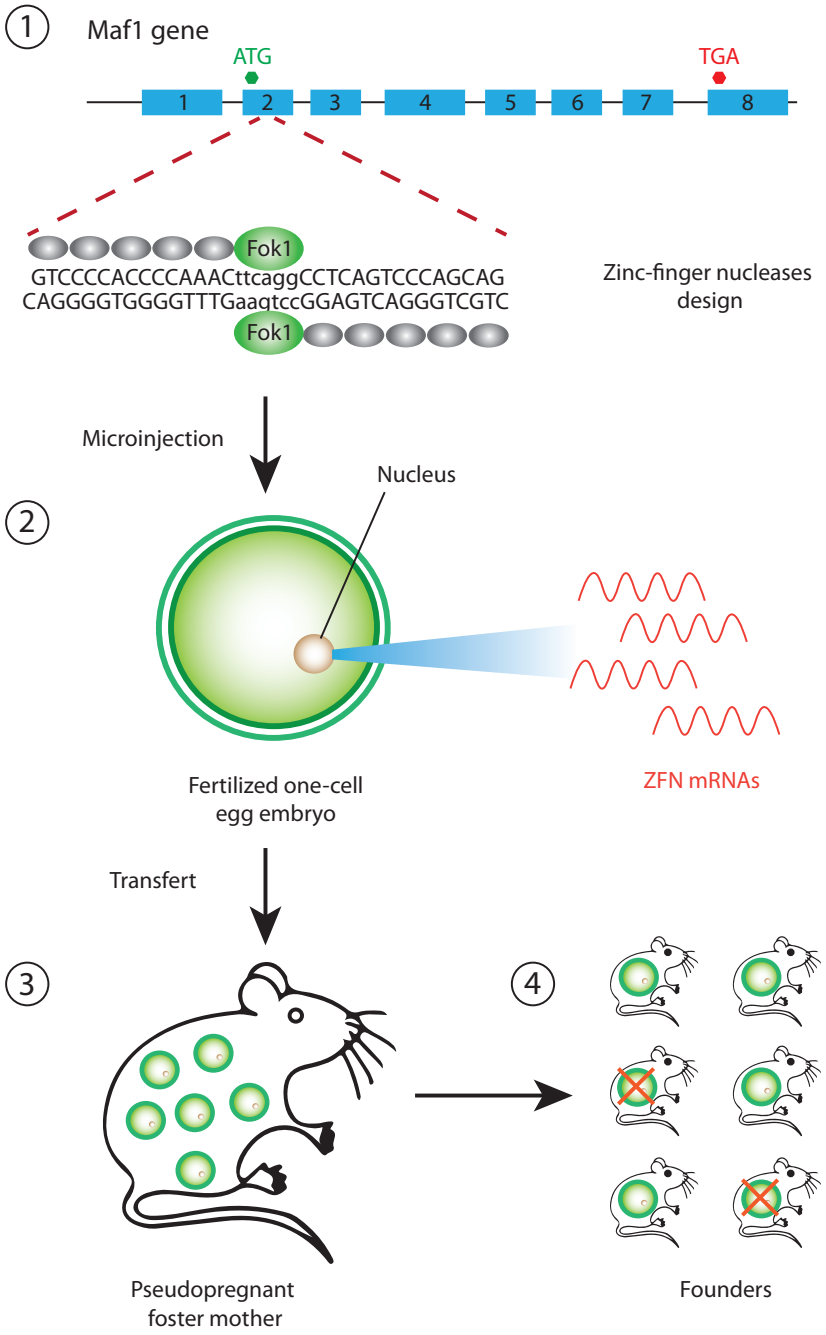

Figure 2.1: ZFN Maf1 KO mouse generation. (1). ZFN are designed to recognize and cleave the second exon of the Maf1 gene. After cleavage, the non-homologous end joining machinery is repairing the damaged DNA including sometimes some errors in the genetic code hence creating mutations. (2). ZFN mRNAs are injected into the nucleus of mouse one-cell egg embryo. (3). Embryos are next transferred into a foster mother and mouse progeny are analysed (4) by Sanger sequencing to identify the animals carrying a mutation.

The same RNAs used for the Affymetrix arrays were also analyzed by RNA-seq by our collaborator, and the results confirmed the lower expression of Nnmt. The RNA-seq analysis also allowed us to check tRNAs expression, which was not possible with the microarrays. Precursor tRNA levels were significantly upregulated in the Maf1 KO liver and white adipose tissue but mature tRNAs levels remained constant. This result lead us to conclude that a futile cycle of production/degradation of tRNAs is source of energy consumption and one of the causes of protection to diet induced obesity.

Finally, I was also interested in comparing mitochondria activity in the WT and Maf1 KO mice. In collaboration with the group of Johan Auwerx at the EPFL, we measured mitochondrial activity and concluded that there was an increase in mitochondria respiration and ATP production in the liver of Maf1 KO mice under high fat diet. These differences were not due to an increase in the numbers of mitochondria in the liver of the Maf1 KO mouse. The Maf1 KO mouse lean phenotype description and how of molecular and metabolic changes are associated with the obesity resistance are described in this chapter.

On the following study which was part of a collaboration with the group of Ian Willis, I generated and analyzed the ZFN Maf1 KO mouse, checked the levels of NNMT in liver and muscle tissues and the levels of expression of the polyamine genes in liver. I also tested the mitochondria activity in liver homogenates, checked the mitochondrial copy number and looked at the stoichiometry of the different complexes of the electron transport chain in liver samples.

Loss of the RNA polymerase III repressor MAF1 confers obesity resistance

Nicolas Bonhoure,[1,8] Ashlee Byrnes,[2,8] Robyn D. Moir,[2,8] Wassim Hodroj,[1] Frédéric Preitner,[3] Viviane Praz,[1,4] Genevieve Marcelin,[5] Streamson C. Chua Jr.,[5,6] Nuria Martinez-Lopez,[5] Rajat Singh,[5,6] Norman Moullan,[7] Johan Auwerx,[7] Gilles Willemin,[1,3] Hardik Shah,[5] Kirsten Hartil,[5] Bhavapriya Vaitheesvaran,[5] Irwin Kurland,[5,6] Nouria Hernandez,[1] and Ian M. Willis[2,6]

[1]Center for Integrative Genomics, Faculty of Biology and Medicine, University of Lausanne, 1015 Lausanne, Switzerland; [2]Department of Biochemistry, Albert Einstein College of Medicine, Bronx, New York 10461, USA; [3]Mouse Metabolic Evaluation Facility, Center for Integrative Genomics, University of Lausanne, 1015 Lausanne, Switzerland; [4]Swiss Institute of Bioinformatics, 1015 Lausanne, Switzerland; [5]Division of Endocrinology, Department of Medicine, Albert Einstein College of Medicine, Bronx, New York 10461, USA; [6]Diabetes Research Center, Albert Einstein College of Medicine, Bronx, New York 10461, USA; [7]Laboratory for Integrative and Systems Physiology, Ecole Polytechnique Fédérale de Lausanne (EPFL), 1015 Lausanne, Switzerland

MAF1 is a global repressor of RNA polymerase III transcription that regulates the expression of highly abundant noncoding RNAs in response to nutrient availability and cellular stress. Thus, MAF1 function is thought to be important for metabolic economy. Here we show that a whole-body knockout of *Maf1* in mice confers resistance to diet-induced obesity and nonalcoholic fatty liver disease by reducing food intake and increasing metabolic inefficiency. Energy expenditure in *Maf1*$^{-/-}$ mice is increased by several mechanisms. Precursor tRNA synthesis was increased in multiple tissues without significant effects on mature tRNA levels, implying increased turnover in a futile tRNA cycle. Elevated futile cycling of hepatic lipids was also observed. Metabolite profiling of the liver and skeletal muscle revealed elevated levels of many amino acids and spermidine, which links the induction of autophagy in *Maf1*$^{-/-}$ mice with their extended life span. The increase in spermidine was accompanied by reduced levels of nicotinamide *N*-methyltransferase, which promotes polyamine synthesis, enables nicotinamide salvage to regenerate NAD$^+$, and is associated with obesity resistance. Consistent with this, NAD$^+$ levels were increased in muscle. The importance of MAF1 for metabolic economy reveals the potential for MAF1 modulators to protect against obesity and its harmful consequences.

[*Keywords*: obesity; RNA polymerase III; metabolic efficiency; MAF1; autophagy; futile cycling; polyamines]

Supplemental material is available for this article.

Received January 7, 2015; revised version accepted April 7, 2015.

In natural populations, metabolic efficiency promotes survival in stressful environments, such as when the quality or quantity of food is limited (Parsons 2007). However, as evidenced by the global obesity epidemic and its associated comorbidities (e.g., insulin resistance, type 2 diabetes, cardiovascular disease, nonalcoholic fatty liver disease, and cancer) (Guh et al. 2009; Flegal et al. 2010; Unger and Scherer 2010), metabolic efficiency has become a liability for a large number of modern day humans. Reducing obesity through diet and exercise produces health benefits, but maintaining weight loss over the long term remains a challenge for most overweight people (Kraschnewski et al. 2010; Maclean et al. 2011), and pharmacological approaches to reduce food intake or absorption have undesirable side effects or safety concerns (Tseng et al. 2010; Clapham and Arch 2011). With the identification of functional brown adipose tissue (BAT) in adult humans and the inducible browning of white adipose tissue (WAT), new strategies to increase energy expenditure have emerged as promising therapies for obesity and metabolic disease (Harms and Seale 2013; Rosen and Spiegelman 2014). These approaches stimulate facultative thermogenic responses that uncouple substrate oxidation from ATP synthesis, dissipate the mitochondrial proton gradient, and release chemical energy as heat. Other possibilities to enhance energy expenditure by decreasing the metabolic efficiency of obligatory cellular processes remain largely unexplored (Alekseev et al. 2010; Anunciado-Koza et al. 2011; Oie et al. 2014).

[8]These authors contributed equally to this work.
Corresponding authors: nouria.hernandez@unil.ch, ian.willis@einstein.yu.edu

Article is online at http://www.genesdev.org/cgi/doi/10.1101/gad.258350.115. Freely available online through the *Genes & Development* Open Access option.

Ribosome biogenesis has long been recognized as a significant consumer of metabolic energy, with ~60% of the nucleotides polymerized in nuclear gene transcription of exponentially growing cells going toward the synthesis of the large ribosomal RNAs (rRNAs) (Warner 1999; Grummt 2013). The energetic cost of this synthesis along with the production of 5S rRNA and tRNAs underlies a biological imperative for tight control of these processes in all organisms. Thus, metabolic economy is ensured when nutrients are limiting and under various stress conditions by regulatory systems that rapidly repress transcription involving the protein synthetic machinery (Warner 1999; Grummt 2013; Moir and Willis 2013). In higher eukaryotes, repression of rDNA transcription in response to nutrient deprivation is mediated in part by the energy-dependent nucleolar silencing complex (eNoSC). eNoSC binding throughout the rDNA repeat is achieved via the nucleolar protein nucleomethylin (NML) and its interaction with histone H3 dimethylated at Lys9. Together with the action of other eNoSC subunits, a repressive chromatin structure is established by the SIRT1 histone deacetylase and the histone H3 methyltransferase Suv39h1, leading to the repression of rDNA transcription (Murayama et al. 2008). The biological importance of the energy conservation provided by this repression is indicated by the resistance of mice with a liver-specific knockout of NML to diet-induced obesity (Oie et al. 2014). In the absence of NML, increased rDNA transcription in high-fat-fed mice promotes hepatic energy expenditure and alters lipid metabolism, leading to reduced fat accumulation and reduced body weight gain. Thus, repression of hepatic rDNA transcription allows excess energy storage as fat.

MAF1 functions to promote metabolic economy by repressing RNA polymerase III (Pol III) transcription of highly abundant cellular RNAs under conditions of nutrient limitation and cellular stress (Upadhya et al. 2002; Reina et al. 2006). In yeast, MAF1 is required universally for this response, and, in its absence, strains exhibit reduced fitness, stress sensitivity, altered respiratory metabolism, and decreased sporulation efficiency (Cherry et al. 2012). These phenotypes can be rationalized by the inappropriate diversion of metabolic resources into the energetically costly synthesis of 5S RNA and tRNAs, which together account for ~15% of total RNA. MAF1 is a terminal node in the target of rapamycin (TOR) signaling network, which drives cell growth, controls metabolism, and contributes to metabolic disease, cancer, and aging (Michels et al. 2010; Zoncu et al. 2011; Moir and Willis 2013). The phospho-regulation of MAF1, its interactions with the RNA Pol III transcription machinery, and its function in transcriptional repression are conserved from yeast to mammals, but the impact of its ablation has not been assessed in metazoans.

Results

Obesity and fatty liver resistance of Maf1$^{-/-}$ *mice*

MAF1 is encoded by a single ubiquitously expressed gene in mice and humans (Wu et al. 2009) and was knocked out in mouse embryonic stem cells by homologous recombination (Supplemental Fig. S1A–C). Crosses of *Maf1*$^{+/-}$ mice generated in the C57Bl/6J background produced *Maf1*$^{-/-}$ progeny in numbers that were not statistically different from Mendelian expectation (Supplemental Fig. S1D). Thus, the whole-body knockout is unconditionally viable. Interbreeding of *Maf1*$^{-/-}$ animals revealed reduced fertility and fecundity compared with wild-type mice (Supplemental Fig. S1E). *Maf1*$^{-/-}$ mice appeared normal at birth but exhibited lower body weight compared with age-matched controls after weaning (Fig. 1A; Supplemental Fig. S1F). These differences were extreme under a high-fat diet (HFD), as wild-type mice rapidly became obese. In contrast, *Maf1*$^{-/-}$ mice maintained essentially the same body weight on HFDs and regular chow diets (Fig. 1A). Body composition analyses showed that chow-fed *Maf1*$^{-/-}$ mice had substantially less fat as a percentage of total body weight compared with wild-type mice, consistent with the reduced size of their epididymal fat pads (Fig. 1B,C). In older animals (>6 mo of age), differences in body length and absolute lean body mass were also apparent, suggesting an overall reduction in the growth rate of the knockout (Fig. 1D,E). *Maf1*$^{-/-}$ mice maintained on a HFD had little omental and subcutaneous adipose tissue compared with controls (Fig. 1F). In contrast, epididymal WAT (eWAT) and BAT were retained in the knockout, yet the adipocytes did not become hypertrophic as seen in wild-type tissue (Fig. 1G). eWAT adipocyte cell volume was markedly reduced in *Maf1*$^{-/-}$ mice on both low-fat diets and HFDs (Fig. 1G,I; Supplemental Fig. S1G). These differences in cell volume (especially for chow-fed mice) predict larger differences in epididymal fat pad size than were observed (Fig. 1C). However, *Maf1*$^{-/-}$ mice had almost twice the number of adipocytes in this fat depot as wild-type mice (Fig. 1J). Wild-type mice fed a HFD for 6 mo and chow-fed mice at 1 yr exhibited severe hepatocellular swelling due to lipid droplet (LD) accumulation in the liver. This defining phenotype of nonalcoholic fatty liver disease was not observed in the knockout (Fig. 1F–H; Supplemental Fig. S1G). To confirm that the body weight phenotype of *Maf1*$^{-/-}$ mice was due to the loss of the MAF1 protein and was not an effect of the deletion on expression of some other gene, *Maf1*-null mice were generated with targeted zinc finger nucleases. Two different C57Bl/6J lines were obtained: one with a single-base-pair insertion and another with an 8-base-pair (bp) deletion. Both mutations change the reading frame after Thr64, resulting in translation termination shortly thereafter (Supplemental Fig. S2A). Under ad libitum high-fat feeding, these *Maf1*-null mice showed a dramatic resistance to weight gain similar to that of mice lacking the entire coding region (Fig. 1A; Supplemental Fig. S2B). We conclude that whole body loss of MAF1 results in mice that are lean and profoundly resistant to diet-induced obesity and fatty liver disease. All subsequent experiments in this study were performed with the complete gene knockout.

Reduced food intake and metabolic inefficiency

To explore possible factors contributing to the reduced weight of *Maf1*$^{-/-}$ mice, we measured the fecal lipid

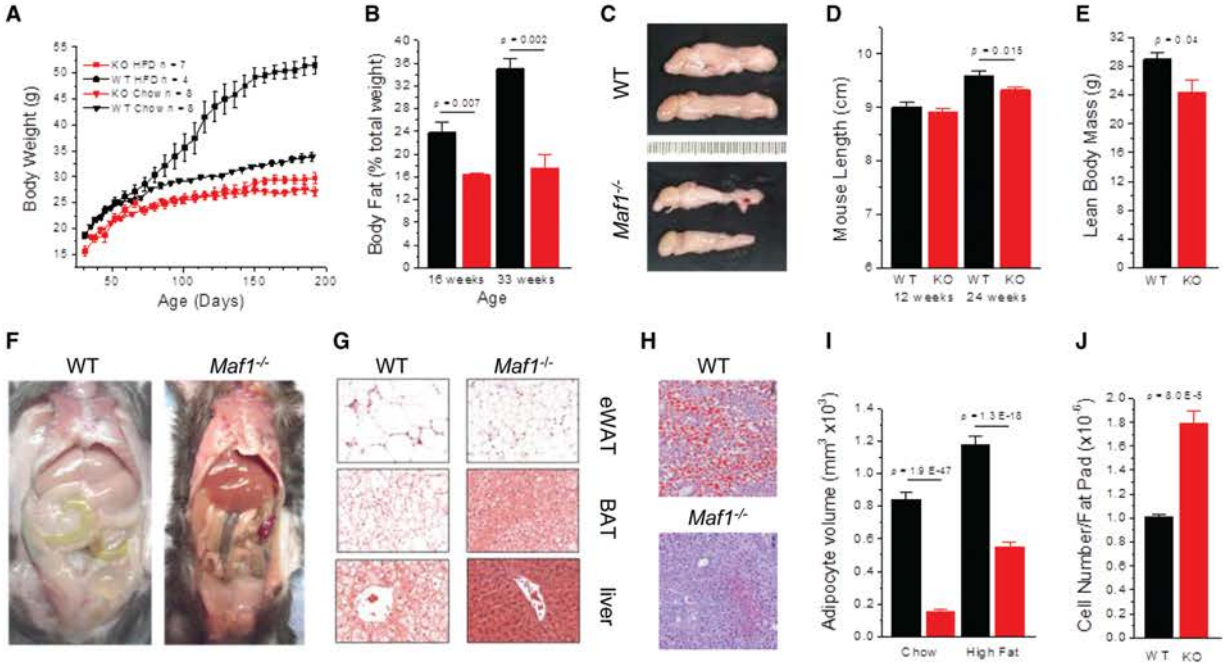

Figure 1. *Maf1*$^{-/-}$ mice exhibit resistance to diet-induced obesity and fatty liver disease. (*A*) Body weight curves of wild-type (WT) and *Maf1*$^{-/-}$ (KO) animals on chow diets and HFDs. (*B*) Fat mass as a percentage body weight for chow-fed mice at 16 and 33 wk ($n = 3$ per group). (*C*) Epididymal fat pads harvested from chow-fed wild-type and *Maf1*$^{-/-}$ mice at 5 mo of age. Images are oriented with the testes to the *left*. (*D*) Nose to anus body length of chow-fed mice ($n = 8$ per group at 3 mo; $n = 19$ per group at 6 mo of age). (*E*) Lean body mass of chow-fed mice at 12 mo of age ($n = 5$ wild type; $n = 4$ knockout). (*F*) Gross pathology of 7-mo-old HFD-fed mice (representative of three animals per group). (*G*) Hematoxylin and eosin (H&E)-stained eWAT, BAT, and livers from the HFD-fed mice in *F*. Images are at the same magnification. (*H*) Oil-Red-O staining of livers from 12-mo-old chow-fed mice. (*I*) Estimation of adipocyte cell volumes for mice on chow-fed diets versus HFDs (see also Supplemental Fig. S1G). (*J*) eWAT fat pad cell counts for 12-mo-old chow-fed mice ($n = 5$ per group). (Black) Wild-type; (red) *Maf1*$^{-/-}$. All values are presented as the mean ± SEM.

content of chow-fed animals and found that malabsorption of dietary fat was not a significant factor in the lean phenotype of the knockout (Fig. 2A). We then performed feeding studies on weight-matched wild-type and *Maf1*$^{-/-}$ animals and observed a reduction in food intake in the knockout mice (Fig. 2B,C). To determine whether this difference in behavior could explain the reduced body weight phenotype, we pair-fed animals on a HFD starting at 10 wk of age, a point at which there was no difference in the weight of the mice. Body weight curves diverged over 8 wk of HFD paired feeding, with *Maf1*$^{-/-}$ mice being significantly lighter than wild-type mice under these conditions (Fig. 2D). The body fat content of *Maf1*$^{-/-}$ mice increased following the switch to a HFD but remained significantly lower than for wild-type mice (Fig. 2E). Thus, while reduced food intake undoubtedly contributes to the lower weight of *Maf1*$^{-/-}$ mice, it does not account entirely for this phenotype or the difference in body fat content. These observations suggested that wild-type and *Maf1*$^{-/-}$ mice might show differences in energy expenditure. Indirect calorimetry studies of HFD pair-fed mice revealed an increase in the energy expenditure of *Maf1*$^{-/-}$ animals, normalized for lean body mass, during both the day and night, with the differences being greater at night during the active period (Fig. 2F). The increase in energy expenditure was not the result of *Maf1*$^{-/-}$ mice being more active, as locomotor activity determined by the number of infrared beam breaks in the metabolic chambers did not reveal any differences (Supplemental Fig. S3A). The respiratory exchange ratio was slightly elevated in *Maf1*$^{-/-}$ mice during both the day and night, suggestive of a marginally enhanced use of glucose as an energy source (Supplemental Fig. S3B). Consistent with the increase in energy expenditure, liver homogenates of high-fat-fed *Maf1*$^{-/-}$ mice showed increased O_2 consumption by mitochrondrial complex 2 compared with wild-type controls (Fig. 2G). This occurred without any increase in mitochondrial DNA or changes in the cellular levels of selected proteins in the electron transport chain (Supplemental Fig. S3C,D). Thus, *Maf1*$^{-/-}$ mice are resistant to obesity as a result of both reduced caloric intake (feeding) and increased energy expenditure. Notably, the diminished ability of *Maf1*$^{-/-}$ mice to transform calories into biomass under pair feeding conditions (Fig. 2D) indicates that the animals are metabolically inefficient.

Altered lipid homeostasis in livers and eWAT

Changes in metabolic efficiency could impact many processes, including glucose or lipid homeostasis. However,

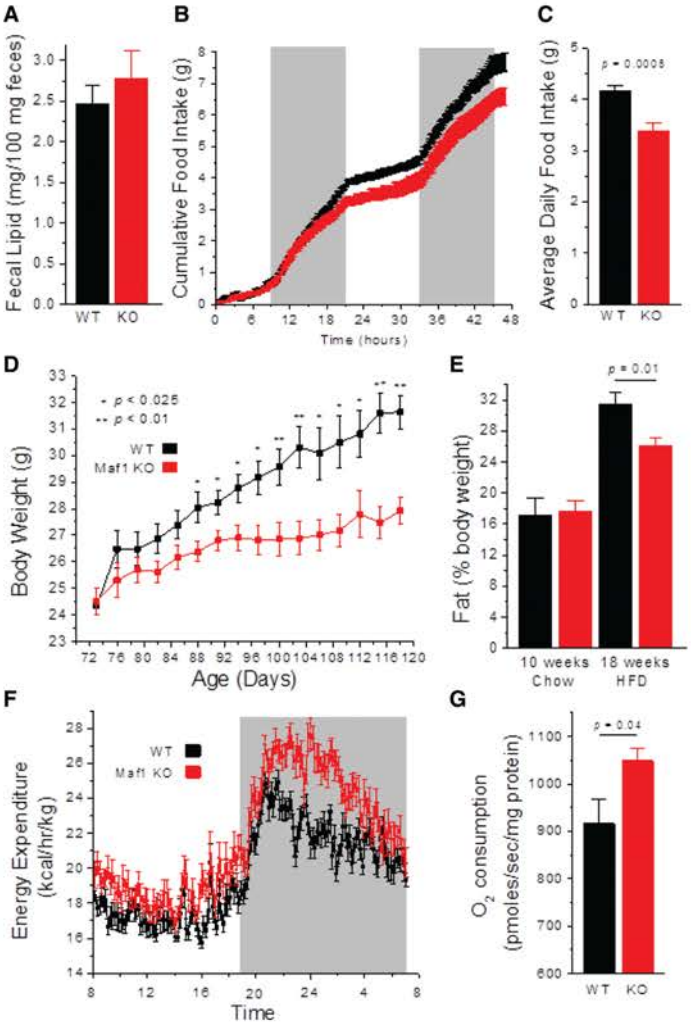

Figure 2. Hypophagia and metabolic inefficiency of *Maf1*$^{-/-}$ mice. (*A*) Fecal lipid content of chow-fed mice ($n = 4$ per group). (*B*) Two-day cumulative food intake of weight-matched chow-fed mice ($n = 4$ per group). (*C*) Daily food intake of weight-matched mice averaged over 5 d. (*D*) Body weight curves of pair-fed mice on a HFD ($n = 5$ per group). (*E*) Percent body fat before and after 8 wk of HFD pair feeding ($n = 5$ per group). (*F*) Energy expenditure in HFD pair-fed animals (24-h averages over 5 d in metabolic cages; $n = 4$ per group; mice were 18 wk of age). (*G*) Oxygen consumption from mitochondrial complex 2 was measured on liver homogenates from HFD-fed mice ($n = 8$ per group). (Black) Wild-type (WT); (red) *Maf1*$^{-/-}$ (KO). All values are presented as the mean ± SEM.

plasma glucose levels in the chow-fed state and after an overnight fast showed no differences between wild-type and *Maf1*$^{-/-}$ mice at 4 mo of age, and pancreatic insulin content and islet insulin secretion ex vivo were normal (Fig. 3A–C). In a hyperinsulinemic–euglycemic clamp study, *Maf1*$^{-/-}$ mice on a chow diet required higher glucose infusion rates to achieve euglycemia (Fig. 3D–F) and showed increased whole body glucose disposal as well as increased suppression of hepatic glucose production (Fig. 3G–J). These results indicate that *Maf1*$^{-/-}$ mice are slightly more sensitive to insulin than control animals. However, these differences are associated with the lower body weight of *Maf1*$^{-/-}$ mice (Fig. 3K). We conclude that insulin sensitivity is slightly increased in *Maf1*$^{-/-}$ mice due to their lean phenotype rather than as a direct consequence of the absence of MAF1.

Given the marked reduction in body fat in *Maf1*$^{-/-}$ mice (Fig. 1B), we assayed for lipid metabolites in plasma. The concentrations of free fatty acids and cholesterol were normal in chow-fed knockout mice compared with controls (Fig. 4A,B). However, targeted metabolomics identified distinct differences between the two groups, including reductions in the levels of multiple glycerophospholipids in *Maf1*$^{-/-}$ plasma (Fig. 4C; Supplemental Fig. S4; Supplemental Table S1). Basal lipolysis in eWAT explants was elevated in the knockout, comparable with wild-type tissue in which lipolysis was activated by the β3-adrenergic agonist CL-316243 (Fig. 4D). Notably, incubation of *Maf1*$^{-/-}$ eWAT with the agonist did not substantially increase glycerol output over the untreated tissue, suggesting that lipolysis was close to maximally stimulated (Fig. 4D). Consistent with this possibility, the level of activated hormone-sensitive lipase (HSL) was greater than fourfold higher in eWAT of ad libitum chow-fed *Maf1*$^{-/-}$ mice relative to controls (Fig. 4E,F). The observation that dopamine levels were elevated in the plasma of *Maf1*$^{-/-}$ mice (Supplementary Table S1; Supplemental Fig. 4B) raises the possibility that activation of HSL may be achieved via Gαs-coupled dopamine D1 receptors on the adipocytes (Borcherding et al. 2011). Lipid metabolism was also

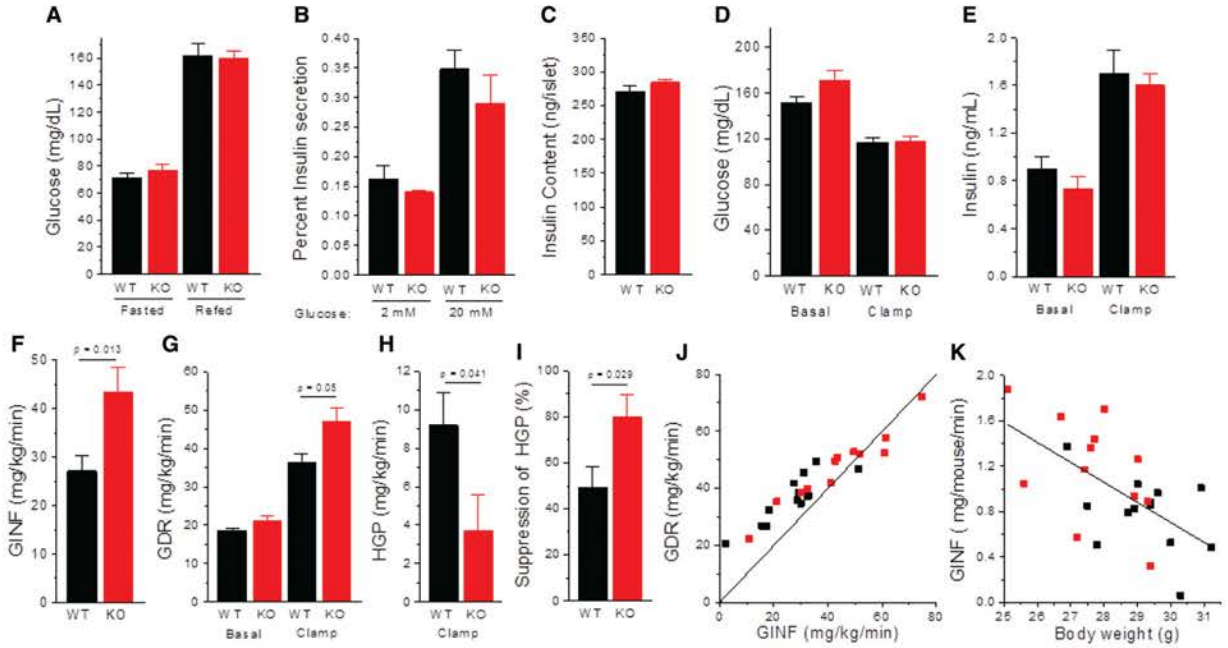

Figure 3. Blood glucose, insulin secretion, and analysis of insulin sensitivity. (*A*) Blood glucose concentrations were determined from tail vein bleeds after an overnight fast and following a 4-h refeed. Mice were 4 mo of age and were maintained on a breeder chow diet. ($n = 7$ mice per group). (*B*) Insulin secretion ex vivo was assayed in the presence of 2 mM and 20 mM glucose (five islets per well; $n = 8$ per condition per genotype; chow diet). Results are expressed as a percentage of the total insulin content of the islets used in the assay. (*C*) Insulin content of islets was calculated from five islets per sample ($n = 16$ per group). (*D–K*) Hyperinsulinemic–euglycemic clamp analysis of insulin sensitivity in 5-h-fasted mice. (*D*) Plasma glucose levels before and during the clamp. (*E*) Plasma insulin levels before and during the clamp. (*F*) Glucose infusion (GINF) rate needed to maintain euglycemia. (*G*) Glucose disposal rate (GDR) before and during the clamp was measured by the tracer dilution technique using [3-^{3}H]glucose as tracer. (*H*) Hepatic glucose production (HGP) during the clamp. (*I*) Suppression of hepatic glucose production was calculated as the difference in HGP in the basal state (=basal GDR) and during the clamp divided by the basal HGP. (*J*) Rates of glucose disposal versus glucose infusion are shown for all of the mice in the study relative to a line with a slope of 1. HGP is the vertical difference between each data point and the line. (*K*) Glucose infusion rate (insulin sensitivity) is inversely correlated with the body weight of the mice. A linear fit is shown to all of the data. All values are presented as the mean ± SEM. Clamp data in *D–K* were obtained from 13 wild-type and 12 *Maf1*$^{-/-}$ mice. (Black) Wild type (WT); (red) *Maf1*$^{-/-}$ (KO).

altered in the livers of *Maf1*$^{-/-}$ mice, which displayed increased de novo lipogenesis (Fig. 4G). Thus, *Maf1*$^{-/-}$ mice exhibit altered lipid metabolism in the liver and WAT and a different profile of glycerophospholipids in plasma.

Energy expenditure associated with futile synthesis of tRNA

To investigate global changes in gene expression in a tissue exhibiting *Maf1*$^{-/-}$ phenotypes, deep sequencing was performed on eWAT RNA. Although MAF1 has been reported to regulate transcription of several protein-coding genes (Johnson et al. 2007; Palian et al. 2014), we did not identify any significant, reproducible changes in the Pol II transcriptome in this tissue (Supplemental Fig. S5A; Supplemental Table S2). Importantly, although the observed increase in energy expenditure could in principle reflect higher levels of adaptive thermogenesis, we observed no induction of known activators or markers of BAT or beige adipose tissue, including UCP1, which regulates proton leak in thermogenic tissues (Walden et al. 2012; Wu et al. 2012; Harms and Seale 2013). Indeed, Western blotting showed that UCP1 was unchanged in BAT and undetectable in eWAT (Supplemental Fig. S5B–D), and the body temperature and cold stress resistance of *Maf1*$^{-/-}$ mice was normal (Supplemental Fig. S5E,F). These observations suggest that enhanced energy dissipation in *Maf1*$^{-/-}$ mice does not result from recruitment of brown-like adipocytes in WAT or UCP1-mediated uncoupling of oxidative phosphorylation.

Previous studies of *Maf1* knockdown and overexpression in glioblastoma cells found inverse changes in the expression of the TATA-box-binding protein (TBP) at the RNA and the protein level that correlated with changes in RNA Pol I transcription (Johnson et al. 2007). MAF1 effects on TBP expression were due to its recruitment to the TBP promoter, whereas changes at the rDNA were thought to be mediated by the promoter selectivity factor SL1, which contains TBP as a central component (Grummt 2013). Although TBP expression was not affected in *Maf1*$^{-/-}$ eWAT RNA (Supplemental Table S2), we examined this issue further in *Maf1*$^{-/-}$ livers and also

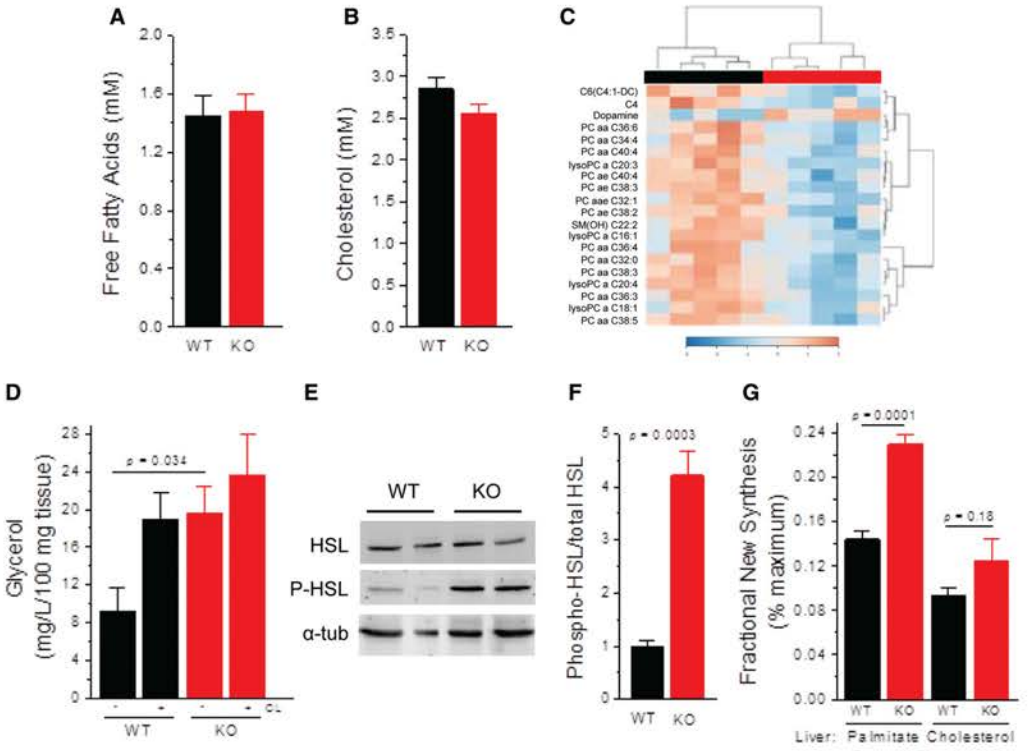

Figure 4. Altered lipid metabolism in *Maf1*$^{-/-}$ mice. (*A*,*B*) Serum-free fatty acids and serum cholesterol were measured in overnight-fasted mice maintained on a standard chow diet ($n = 6$ per group). (*C*) Hierarchical clustering of plasma metabolite profiles from Biocrates AbsoluteIDQ p180 analysis performed with mice on a breeder chow diet. The top 20 metabolites by *t*-test ($P < 0.025$) were clustered using Pearson's correlation to measure similarity and Ward's linkage to minimize the sum of the squares of the clusters (MetaboAnalyst) (see also Supplemental Figure S4 and Supplemental Table S1). (*D*) Lipolysis in eWAT explants from mice on a breeder chow diet. Glycerol release in explants was measured in the presence and absence of the β3-adrenergic receptor agonist CL-316,243 (CL, $n = 8$ for wild-type under both treatments; $n = 7$ for untreated *Maf1*$^{-/-}$; $n = 4$ for CL-316,243-treated *Maf1*$^{-/-}$ explants). (*E*) Western blot of phospho-HSL (P-HSL) and total HSL from eWAT. (*F*) Quantitation of activated phospho-HSL over total HSL in eWAT (wild type, $n = 8$; *Maf1*$^{-/-}$, $n = 7$; breeder chow diet). (*G*) De novo lipogenesis and cholesterol synthesis in livers from mice on a breeder chow diet were measured by tracer enrichment after 5 d of receiving 6% D_2O in drinking water ($n = 5$ per group). All values are presented as the mean ± SEM.

looked for changes in rDNA transcription (Supplemental Fig. S5G–I; Oie et al. 2014). No significant differences were detected in these assays. We infer that the effects of MAF1 on TBP expression and potentially other protein coding genes may be context-dependent.

eWAT RNA sequencing (RNA-seq) data were analyzed to determine the effect of the knockout on the synthesis of precursor tRNAs. These molecules are short-lived and are widely used to assess the level of transcription by RNA Pol III (Upadhya et al. 2002; Michels et al. 2010). Consistent with the increase in polymerase occupancy of Pol III genes in *Maf1*$^{-/-}$ tissue (Bonhoure et al. 2014), pre-tRNA-specific reads representing >100 different tRNA genes were markedly increased in the knockout (Fig. 5A; Supplemental Table S3). In contrast, mature tRNA-specific reads increased significantly for only a few tRNA genes, and the magnitude of these changes was much lower (Fig. 5B; Supplemental Table S3). Similar findings were obtained by Northern blotting of tRNA species from WAT and numerous other tissues (Fig. 5C,D; Table 1). For example, pre-tRNA^{Ile} (TAT) levels increased from approximately threefold in the liver and quadriceps to approximately ninefold in WAT and the spleen, while the levels of five different mature tRNAs, including initiator methionine tRNA (tRNA$_i^{Met}$), in various tissues showed only minor variations (Fig. 5C,D; Table 1). Additionally, quantitation of the tRNA fraction in the liver indicated only a modest 15% ± 3% increase in the knockout ($P = 0.008$, $n = 7$ per group), and total tRNA levels in a range of other tissues showed minimal changes (Supplemental Fig. 5J). Mature tRNA is reported to have a long (2- to 3-d) half-life in chicken livers and mouse uteruses (Miller 1973; Nwagwu and Nana 1980), so a large (greater than threefold) increase in Pol III transcription in the absence of MAF1 (Fig. 5A,C,D) should have been readily apparent in the steady-state abundance of the mature tRNA population. Since most mature tRNAs as well as bulk tRNA levels were not substantially affected (Table 1; Fig. 5B–D; Supplemental Fig. 5J), we conclude that increased tRNA synthesis in the knockout must be largely matched by increased turnover of nascent tRNA transcripts, pre-tRNAs, and/or mature tRNAs. Support for

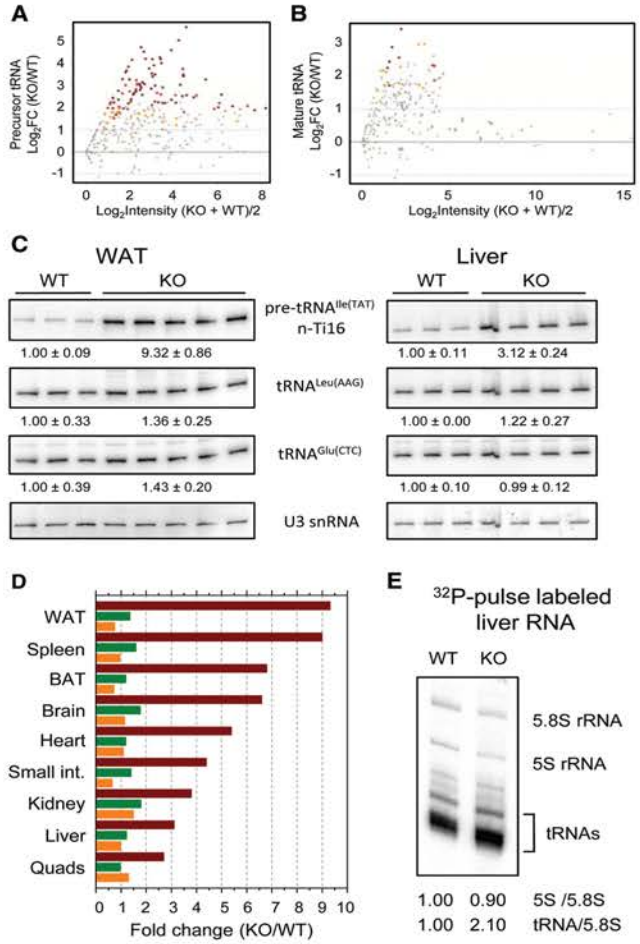

Figure 5. Futile cycling of tRNAs as a mechanism for energy expenditure. (*A*) Log ratio versus abundance (MA plot) of uniquely mapped precursor tRNA-specific RNA-seq reads in eWAT of breeder chow-fed mice ($n = 3$ per group). Yellow and red dots correspond to loci exhibiting significant changes called by limma or GLM, respectively. Brown dots correspond to loci with significant changes called by both methods. Gray dots correspond to loci with scores that are not statistically different. (*B*) MA plot of uniquely mapped mature tRNA reads in eWAT. The color scheme is the same as in *A*. (*C*) Northern blots of precursor and mature tRNA species from the eWAT and livers of breeder chow-fed mice. The fold change normalized to U3 snRNA is shown *below* each panel. (*D*) Precursor $tRNA^{Ile}$ (TAT) n-Ti16 (maroon), mature $tRNA^{Leu}$ (AAG) (green), and mature $tRNA_i^{Met}$ (CAT) (orange) levels were surveyed by Northern analysis in the indicated tissues of breeder chow-fed mice. The fold change was normalized to U3 snRNA. (*E*) Newly synthesized 5.8 S rRNA, 5S rRNA, and tRNAs from breeder chow-fed mice were quantified in total liver RNA following i.p. injection of ^{32}P-orthophosphate and labeling for 4 h.

this view is provided by in vivo ^{32}P pulse-labeling of liver RNA. Compared with the Pol I-derived 5.8S rRNA, labeling of Pol III-derived 5S rRNA was unaffected, and labeling of the newly synthesized mature tRNA population increased twofold (Fig. 5E); i.e., less than the threefold level measured for specific precursor tRNAs in this tissue (Table 1), suggesting that some turnover has occurred. In addition, since tRNA synthesis during the pulse was increased twofold but steady-state tRNA levels were not substantially changed (Supplemental Fig. 5J), tRNA turnover is again indicated. We conclude that increased synthesis and turnover of Pol III transcripts—most notably tRNAs, which account for ~10% of total RNA—constitutes a futile cycle that is likely to be an important driver of energy expenditure in mice.

Spermidine, autophagy, and life span extension

We hypothesized that a pervasive whole-body effect of the *Maf1* knockout on Pol III transcription and energy expenditure was likely to generate a common metabolic signature in different tissues. To assess this possibility, we conducted targeted metabolite profiling in liver and skeletal muscle. Multivariate partial least squares discriminant analysis (PLS-DA) of the aggregated data showed that wild-type and knockout tissues are readily distinguished by their metabolite profiles (Fig. 6A). Multiple statistical measures (variable importance in projection [VIP] scores and *t*-tests) indicate that $Maf1^{-/-}$ tissues have significantly elevated levels of many amino acids and polyamine pathway metabolites, including ornithine, putrescine, and spermidine (Fig. 6B; Supplemental Fig. S6B; Supplemental Table S1). Perturbations of polyamine synthesis have been linked to changes in adiposity (Jell et al. 2007; Pirinen et al. 2007), and mice expressing reduced levels of nicotinamide *N*-methyltransferase (NNMT), which influences polyamine synthesis, are obesity-resistant (Kraus et al. 2014). Consistent with these observations and the increased level of spermidine in $Maf1^{-/-}$ tissues, the expression of *Nnmt* mRNA was significantly reduced in the liver, as was the level of NNMT protein in the liver and muscle (Fig. 6C,D; Supplemental Fig. S6C,D). NNMT methylates nicotinamide using S-adenosyl methionine (SAM) as a methyl donor. Thus, in addition to its potential to affect SAM-dependent methylation reactions and the supply of propylamine groups for polyamine synthesis, NNMT can regulate the availability of NAD^+ for cellular redox metabolism (Supplemental Fig. S6A; Kraus et al. 2014). To examine this issue, we measured the total cellular concentration of NAD^+ in wild-type and $Maf1^{-/-}$ livers and skeletal muscle by liquid chromatography-mass spectrometry (LC-MS). Consistent with the view that NAD^+ synthesis in the liver is not limited by the activity of the nicotinamide salvage pathway (Houtkooper et al. 2010; Kraus et al. 2014), the level of NAD^+ in $Maf1^{-/-}$ livers was the same as for wild-type tissue (Fig. 6E). In contrast, the level of NAD^+ was increased ~40% in $Maf1^{-/-}$ muscle (Fig. 6E). Similar increases have been reported in the muscles of mice with a whole-body deletion of poly(ADP-ribose) polymerase, a major consumer of NAD^+, and in mice whose diet has been supplemented with the NAD^+ precursor nicotinamide ribonucleoside (Cantó et al. 2012; Houtkooper et al. 2012). Importantly, these animal models have increased energy expenditure and are protected from HFD-induced obesity. In light of these studies, it appears likely that

Table 1. Quantitation of Northern blotting data on liver RNA

tRNA species	*Maf1*$^{+/+}$	*Maf1*$^{-/-}$	*P*-value
Pre-tRNA^{Ile} n-Ti16	1.00 ± 0.08 (6)	2.98 ± 0.09 (6)	0.00032
Pre-tRNA^{Tyr} n-Ty2	1.00 ± 0.31 (3)	3.28 ± 0.28 (5)	0.002
Pre-tRNA^{Leu} n-Tl12	1.00 ± 0.12 (3)	3.09 ± 0.31 (5)	0.0027
Mature tRNA^{Leu} (CAA)	1.00 ± 0.09 (6)	1.05 ± 0.07 (6)	0.71
Mature tRNA^{Meti} (CAT)	1.00 ± 0.10 (6)	1.04 ± 0.09 (6)	0.77
Mature tRNA^{Glu} (CTC)	1.00 ± 0.01 (3)	1.06 ± 0.05 (5)	0.4
Mature tRNA^{Leu} (AAG)	1.00 ± 0.07 (3)	1.02 ± 0.02 (5)	0.74
Mature tRNA^{Ser} (GCT)	1.00 ± 0.15 (3)	0.83 ± 0.08 (5)	0.28
U6 snRNA	1.00 ± 0.05 (6)	1.09 ± 0.03 (6)	0.18
U1 snRNA	1.00 ± 0.16 (6)	1.06 ± 0.09 (6)	0.75

Oligonucleotide probes to various precursor and mature tRNAs as well as U6 and U1 snRNAs were used to quantify RNA levels in total liver RNA preparations from overnight-fasted mice. Hybridization signals were normalized to U3 snRNA as in Figure 5. The number of biological replicates is given in parentheses.

altered NAD$^+$ metabolism contributes to the obesity resistance of *Maf1*$^{-/-}$ mice.

Spermidine is a known inducer of autophagy in yeast, flies, worms, and mammalian cells, and enhanced autophagy is critical for the life span-extending effects of spermidine in these organisms (Eisenberg et al. 2009). Accordingly, livers from overnight-fasted *Maf1*$^{-/-}$ mice displayed increased autophagic activity compared with controls, as shown by the elevated delivery of LC3-II-positive autophagosomes to lysosomes (net LC3-II flux) and their subsequent lysosomal fusion (Fig. 6F–H; Klionsky et al. 2007). Lysosomal degradation of proteins is consistent with the observed increase in amino acid levels (Fig. 6B; Supplemental Fig. S6B; Supplemental Table S1). In addition, enhanced autophagic activity in the knockout was also associated with increased colocalization of LC3 with BODIPY-stained LDs and increased sequestration of hepatic LDs by LC3-II-positive autophagosomes (Fig. 6I,J). Moreover, we observed a significant reduction in hepatic triglycerides but not free hepatic glycerol in *Maf1*$^{-/-}$ mice (Fig. 6K,L). Together, these findings indicate activated mobilization of hepatocellular lipids via lipophagy (Singh et al. 2009). Increased lipid consumption through autophagy together with the increase in de novo lipogenesis in the *Maf1*$^{-/-}$ liver (Fig. 4G) reveals contributions to metabolic inefficiency and energy expenditure in the mice via increased futile cycling of hepatic lipids. Finally, Kaplan-Meier survival curves revealed a statistically significant extension of mean and maximal life span for female *Maf1*$^{-/-}$ mice, in accordance with the effects of spermidine and autophagy in other model organisms (Fig. 6M; Eisenberg et al. 2009). A similar trend was observed for male mice (Supplemental Fig. S6E).

Discussion

Our work shows that the loss of *Maf1*, a ubiquitous global regulator of transcription by RNA Pol III, significantly impacts whole-body metabolism and energy expenditure while providing health benefits. These benefits include resistance to diet-induced obesity and nonalcoholic fatty liver disease as well as an extension of life span that can be attributed to previously documented effects of spermidine on the induction of autophagy and longevity in yeast, flies, and worms (Eisenberg et al. 2009). Obesity resistance in *Maf1*$^{-/-}$ mice is achieved through reduced food intake and increased metabolic inefficiency. In this study, we focused on the metabolic component. At the whole-body level, *Maf1*$^{-/-}$ mice demonstrate metabolic inefficiency by their reduced growth rate under paired-feeding conditions (i.e., lower body weight despite equal caloric intake). At the molecular level, metabolic inefficiency is apparent from the increased synthesis and turnover (futile cycling) of tRNAs and hepatic lipids. We infer that the increased energetic cost of these processes alters the balance between fuel utilization and storage and contributes to the lean phenotype. Additional factors contributing to the energy expenditure and obesity resistance of the mice include the reduced expression of NNMT in the liver, muscle, and potentially other tissues and downstream effects on NAD$^+$ metabolism and/or the polyamine pathway (Kraus et al. 2014; Liu et al. 2014). How the different molecular effects of the *Maf1* knockout are partitioned in terms of energy expenditure and obesity resistance has yet to be determined, but our current results already establish MAF1 as a novel and unconventional therapeutic target for the treatment of obesity and related diseases.

Reduced expression of *Nnmt*, which we observed in the liver and muscle but not in eWAT, can increase the level of SAM and/or SAM/SAH ratios and the supply of nicotinamide (Supplemental Fig. S6A; Kraus et al. 2014). Increased SAM levels in turn can lead to increased polyamine synthesis, and, indeed, the liver and muscle showed increased levels of polyamine pathway metabolites, including spermidine. Perturbations of polyamine pathway flux are associated with obesity resistance or sensitivity in several mouse models (Jell et al. 2007; Pirinen et al. 2007; Kraus et al. 2014; Liu et al. 2014). In addition to oligonucleotide-directed knockdown of *Nnmt*, which confers obesity resistance primarily by affecting *Nnmt* expression in the liver and adipose tissue (Kraus et al. 2014), whole-body changes in polyamine catabolism have been engineered by overexpression and underexpression of spermidine/spermine-N^1-acetyltransferase (SSAT) (Supplemental Fig. S6A). By increasing or decreasing polyamine acetylation in these models, acetyl-CoA and malonyl CoA pools were altered with corresponding changes in fatty acid synthesis, fatty acid oxidation, and body fat accumulation. These studies implicate enhanced polyamine pathway cycling in the obesity resistance of *Maf1*$^{-/-}$ mice.

Elevated nicotinamide supply resulting from decreased *Nnmt* can lead to increased NAD$^+$ levels (Kraus et al. 2014), which we observed in muscle tissue. Multiple genetic and pharmacological interventions that raise the level of NAD$^+$ are known to enhance oxidative metabolism and provide protection against diet-induced obesity (Bai et al. 2011; Cantó et al. 2012; Pirinen et al. 2014). Along with its role as a cofactor in oxidoreductase

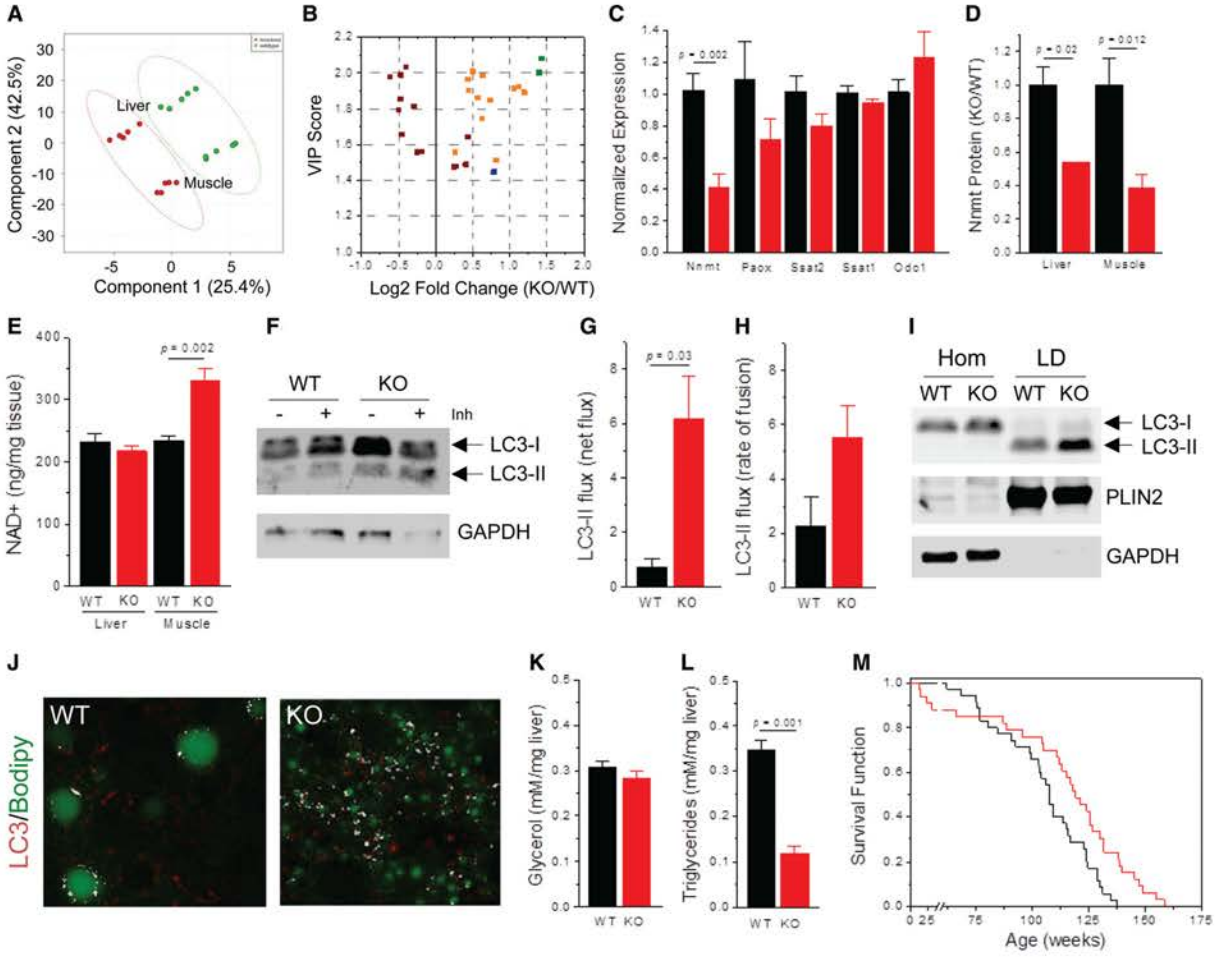

Figure 6. Elevated amino acid and polyamine levels in *Maf1*$^{-/-}$ tissues correlate with induction of autophagy and life span extension. (*A*) Two-dimensional score plot of principal components from PLS-DA of liver and skeletal muscle metabolite profiles from mice on a breeder chow diet. The variance explained by each component is in brackets. Ellipses define regions of 95% confidence. (Green) Wild type (WT); (red) knockout (KO). (*B*) VIP scores (>1.0 is considered significant) obtained by PLS-DA are plotted against the fold change in metabolite concentration (normalized per milligram of tissue) in quadriceps. All metabolites had *P*-values <0.05 ($n = 5$ per group). (Green) Putrescine and spermidine; (orange) amino acids; (maroon) glycerolphospholipids; (blue) C5 acylcarnitine. (*C*) RT-qPCR analysis of polyamine pathway gene expression in the livers ($n = 5$ per group) of chow-fed mice. (*D*) Normalized NNMT protein levels from Supplemental Figure 6, C and D ($n = 3$ per group, chow-fed mice). (*E*) NAD$^+$ levels in the liver and quadriceps as determined by LC-MS ($n = 5$ per group, breeder chow-fed mice). (*F*) Examination of autophagic flux in liver explants from mice on a breeder chow diet. The level of LC3-II, the lipidated autophagosome-associated form of LC3, was monitored in the presence or absence of lysosomal inhibitors (Inh). A representative blot is shown from three biological replicates per genotype. (*G*) Net flux shows the normalized difference in LC3-II ± Inh for each genotype ($n = 3$ per group). (*H*) Rate of autophagolysosome fusion compares the normalized ratio of LC3-II ± Inh. (*I*) Immunoblots of liver homogenates (Hom) and hepatic LD fractions. PLIN2 shows the equivalence of LD content, and GAPDH shows the lack of cytosolic contamination. (*J*) Colocalization (white) of BODIPY 493/503-stained LDs (green) and LC3 (red) in overnight-fasted livers. Images are at the same magnification and are representative of data from four wild-type and three *Maf1*$^{-/-}$ mice. (*K*) Quantitation of liver glycerol ($n = 4$ per group). (*L*) Quantitation of liver triglycerides ($n = 4$ per group). The data in *F*–*L* were from the same cohort of breeder chow-fed mice. (*M*) Kaplan-Meier survival curves of female mice on a breeder chow diet (mean life span of wild type 113 wk, $n = 35$ [black]; mean life span of *Maf1*$^{-/-}$ 121 wk, $n = 33$ [red]; $P = 0.0054$, log rank test; maximal life span assessed on the oldest quartile: 130 wk for wild type and 146 wk for *Maf1*$^{-/-}$; $P = 0.00013$, *t*-test).

reactions, NAD$^+$ is a rate-limiting cosubstrate for the sirtuin family of NAD$^+$-dependent deacetylases, which regulate the activity of several key transcription factors controlling nuclear and mitochondrial metabolism (Houtkooper et al. 2012). Our RNA-seq analysis of *Maf1*$^{-/-}$ eWAT did not find any significant changes in gene expression for SIRT1 target genes (or other protein-coding genes), but since *Nnmt* expression was not affected in this tissue, NAD$^+$ levels may not have been elevated. Gene expression and metabolic profiling of additional *Maf1*$^{-/-}$ tissues will further clarify the relationship between NNMT, NAD$^+$, and metabolism in these mice.

The finding that the synthesis of precursor tRNAs can be increased 10-fold or more, depending on the gene and the tissue, without significant changes at the level of mature tRNA suggests the existence of a robust homeostatic mechanism to prevent the global accumulation of these molecules. Although we did not explore the mechanism of tRNA turnover, it seems likely that the large amount of precursor tRNAs generated in the *Maf1* knockout leads to defects in tRNA processing and/or modification, and such molecules—in particular hypomodified tRNAs—are known to be rapidly degraded (Kadaba et al. 2004; Alexandrov et al. 2006; Chernyakov et al. 2008; Wilusz et al. 2011). Even with rapid tRNA turnover largely offsetting elevated precursor tRNA synthesis, subtle changes in the composition of the tRNA pool in the knockout are likely (Dittmar et al. 2006; Ciesla et al. 2007; Pang et al. 2014), and this in turn has the potential to alter the expression of genes whose codon usage is sensitive to these changes (Gingold et al. 2014). The recent identification of unique translational programs for proliferation and differentiation genes that reflect differences in codon usage and corresponding changes in the tRNA pool (Gingold et al. 2014) may well apply in other situations such as metabolic disease and the response to stress. In this regard, it is likely significant that the effect of deleting *Maf1* on Pol III gene transcription is not equal among different tissues and thus may lead to tissue-specific effects on gene expression.

The lower growth rate of *Maf1*$^{-/-}$ mice is consistent with their reduced feeding and metabolic inefficiency but is strikingly different from the increased cell growth and accelerated larval development seen upon *Maf1* knockdown in *Drosophila* (Rideout et al. 2012). Importantly, these *Drosophila* phenotypes were recapitulated in flies overexpressing tRNA$_i^{Met}$, which promoted growth by stimulating protein synthesis. Our examination of tRNA$_i^{Met}$ levels in multiple mouse tissues found no evidence of its overexpression and thus provides a logical explanation for the growth-related phenotypic difference.

The normal levels of tRNA$_i^{Met}$ in *Maf1*$^{-/-}$ mice are also consistent with these mice not being prone to tumorigenesis, as demonstrated by their extended life span. Until now, the tumorigenic potential of a *Maf1* knockout in mammals has been an open, intriguing question given (1) substantial correlative data linking deregulated Pol III transcription and increased tRNA$_i^{Met}$ levels to cell transformation and tumorigenesis (White 2008; Pavon-Eternod et al. 2013), (2) the requirement for elevated levels of Pol III transcripts for Myc-driven tumorigenesis (Johnson et al. 2008), and (3) the ability of *Maf1* overexpression to suppress anchorage-independent growth of transformed cells and tumor formation in a xenograft mouse model (Johnson et al. 2007; Palian et al. 2014). While the mouse *Maf1* knockout does not promote tumorigenesis or add to the role of Pol III transcription in the development of cancer, the likely explanation and important insight is that not all interventions that increase Pol III synthesis are capable of increasing the level of tRNA$_i^{Met}$ or other mature tRNAs.

Studies in mammalian cells and worms have recently reported that perturbing the expression of MAF1 affects lipogenesis (Khanna et al. 2014; Palian et al. 2014). Notably, RNAi-mediated knockdown of MAF1 increased de novo lipogenesis in these studies, consistent with our observations in the livers of *Maf1*$^{-/-}$ mice (Fig. 4G). However, the apparent mechanism and the net effect on lipid accumulation in these studies differ from our findings. Whereas Maf1 overexpression or knockdown had reciprocal effects on the mRNA levels of key lipogenic enzymes (e.g., fatty acid synthase [FASN]) in worms and mammalian cells (Khanna et al. 2014; Palian et al. 2014), we did not detect significant changes in FASN expression in the liver by either RT-qPCR or Western blotting (RD Moir and A Byrnes, unpubl.). Also, liver triglycerides were lower (Fig. 6L), not higher, in the knockout mice, in keeping with the induction of lipophagy, the increase in whole-body energy expenditure, and the lean phenotype. At the present time, we can only speculate about the basis of the differences between our results and these other studies. Possibilities include partial versus complete ablation of *Maf1*, differences in diet and/or nutrients supplied in growth media, and effects due to short-term versus long-term changes in gene expression and/or metabolism.

The obesity and fatty liver disease resistance of the whole-body *Maf1* knockout may have, in part, a basis in metabolic inefficiency similar to that of the liver-specific knockout of NML. Hepatic NML deficiency leads to obesity resistance due to a failure to repress rDNA transcription by RNA Pol I, the main consumer of nucleotides among the RNA polymerases (Oie et al. 2014). This effect is extreme on a HFD. Thus, it appears that the normal function of NML and MAF1 in transcriptional repression by RNA Pol I and Pol III, respectively, is critical for the conservation of metabolic energy and the storage of excess calories as fat. The liver-specific phenotype of the NML knockout coupled with differences in nucleotide consumption between Pol I and Pol III (~60% vs. 15% in growing cell populations) argues that a knockout of *Maf1* in any single tissue is unlikely to generate the full complement of phenotypes or provide the same level of protection against diet-induced obesity as the whole-body knockout. For MAF1, the overall health benefit is likely to be derived from reducing food intake and spreading the increase in energy expenditure over virtually every cell in the body.

In summary, our findings indicate that obesity resistance in *Maf1*$^{-/-}$ mice is achieved through multiple mechanisms. In addition to the loss of repression of RNA Pol III transcription and the futile cycling of tRNAs in the whole animal, other contributions to energy expenditure are provided by the futile cycling of hepatic lipids and potentially polyamines, with enhanced oxidative metabolism enabled by the elevated level of NAD^+. Both direct and indirect effects of the *Maf1* knockout on gene expression are involved, and we suggest that changes in some processes may be driven by an increase in the demand for nucleotides. Finally, we note that the lower caloric intake of the mice may be due to the loss of MAF1 function in the brain and/or may reflect a differential response of the CNS to factors secreted from peripheral *Maf1*$^{-/-}$ tissues.

Materials and methods

Animals

All experiments involving mice were performed using protocols approved by the Institutional Animal Care and Use Committee (IACUC) of the Albert Einstein College of Medicine or the Veterinary Office of the Canton of Vaud (SCA-EXPANIM, Service de la Consommation et des Affaires Vétérinaires, Epalinges, Switzerland) in accordance with the Federal Swiss Veterinary Office guidelines. *Maf1*$^{+/-}$ mice were generated in the C57Bl/6J background (Ozgene). Details of the targeting vector, breeding, housing, and diets are given in the Supplemental Material. All experiments were performed with male mice except for body weight (growth rate) and life span studies, which were performed with animals of both sexes.

Histology and cell size and cell number determination

Adipose and liver samples were fixed in 10% buffered formalin prior to paraffin-embedding, sectioning, and staining by hematoxylin and eosin (H&E). Livers were frozen in OCT cryo-embedding medium for Oil-Red-O staining. Adipose cell volume was determined from measurements of the cell radius (>250 cells per condition, two mice per genotype, $v = 4/3\pi r^3$). Error estimates of the cell radius were propagated to volume as $4\pi r^2$. Cell numbers were determined by dissecting and weighing eWAT fat pads from chow-fed mice (12 mo of age). A tissue sample (100 mg) was digested with collagenase, the mixture was centrifuged at 200*g* for 10 min, and the cells in the supernatant were counted in a hemocytometer.

Body composition, fecal lipids, and indirect calorimetry

Body composition was determined by EchoMRI. The lipid content of mouse feces was determined by gravimetry with [^{14}C] triolein as a radioactive tracer to normalize for the recovery of neutral lipids (Argmann et al. 2006). Measurements of food intake, oxygen consumption, CO_2 production, respiratory exchange ratio (RER), and locomotor activity were performed using an indirect calorimetry eight-cage system (Oxymax) as described in the Supplemental Material.

Mitochondrial respiration

Oxygen consumption in liver homogenates of HFD-fed mice was measured using the Oxygraph-2k (Oroboros Instruments). Mitochondrial complexes 1 and 2 were stimulated by injection of 5 mM pyruvate, 2 mM malate, 10 mM glutamate, 2.5 mM ADP, and 10 mM succinate followed by inhibition of the mitochondrial complex 1 by injection of 0.5 µM rotenone.

Insulin secretion and content

Pancreatic islets were isolated from 17-wk-old mice by digestion with collagenase and separation of exocrine tissue (Gotoh et al. 1987). After 24 h in suspension culture, the islets were distributed into wells (five islets per well) of a 12-well plate, incubated for 1 h at 37°C at a low-glucose concentration (2.8 mM), transferred into wells containing 2 or 20 mM glucose in triplicate, and incubated for another hour. The islets were then separated from the supernatant and lysed in acidic ethanol to extract the insulin. Insulin content of the islets and the supernatant was determined, and insulin secretion was expressed as percent of insulin content.

Hyperinsulinemic–euglycemic clamp

A dual tracer clamp ([3-^{3}H]glucose infusion and 2-deoxy-d-[1-^{14}C] glucose bolus) was performed in 3-mo-old male mice. Mice received an indwelling silicone catheter in the femoral vein and were allowed to recover for 4–7 d before a hyperinsulinemic–euglycemic clamp study was conducted (see the Supplemental Material). Rates of basal and insulin-stimulated glucose disposal and hepatic glucose production were determined by the [3-^{3}H]glucose dilution method.

Metabolite profiling

Biocrates AbsoluteIDQ p180 analysis of metabolites in plasma was performed according to the manufacturer's instructions. Plasma was prepared from retroorbital bleeds of overnight-fasted mice (19 wk of age). Tissue samples from overnight-fasted mice (22–24 wk of age) were freeze-clamped in liquid nitrogen and ground to powder with a mortar and pestle on dry ice. The powdered tissue (50–100 mg) was extracted for analysis. NAD^+ levels were determined by LC-MS. Metabolites with CVs >30% were excluded from the analysis. Supervised PLS-DA was performed using MetaboAnalyst or SIMCA-P software.

Assays of lipogenesis and lipolysis

Lipogenesis and cholesterol synthesis were measured with deuterated water as a tracer (Vaitheesvaran et al. 2012). Mice were provided with 6% D_2O in their drinking water for 5 d. Palmitate in liver triglyceride and cholesterol was analyzed by gas chromatography-MS (GC-MS) to determine D_2O enrichment relative to body water. Lipolysis assays were performed on epididymal fat pads harvested from preprandial ad libitum-fed mice (Marcelin et al. 2012). Glycerol concentration was measured using a colorimetric assay kit (Cayman Chemical).

Tissue extracts and Western blotting

BAT and WAT were homogenized in lysis buffer (50 mM Tris-HCl at pH 7.4, 1 mM EDTA, 1 mM EGTA, 50 mM NaF, 10 mM sodium glycerophosphate, 20 mM sodium pyrophosphate) containing Complete Mini and PhosSTOP (Roche). Samples were spun at 14,000*g* for 15 min at 4°C, and the interphase was transferred to a new tube. Triton was added to 1% (v/v), and samples were incubated for 30 min at 4°C with agitation and then centrifuged as above to obtain the supernatant. Extracts from other tissues were prepared in RIPA buffer with inhibitors. Protein concentrations were determined by BCA assay (Pierce). Details of the antibodies used are provided in the Supplemental Material.

RNA-seq analysis

Epididymal adipose tissue was harvested and freeze-clamped in liquid nitrogen from overnight-fasted 22- to 24-wk-old mice maintained on a breeder chow diet. Total RNA was prepared (Qiagen miRNeasy) and digested with DNase I, and RNA quality was assessed by capillary electrophoresis (Agilent 2100 Bioanalyzer). Library preparation and directional RNA-seq were performed at the Einstein Epigenomics Core Facility. Data analysis is described in the Supplemental Material. RNA-seq data have been deposited in NCBI's Gene Expression Omnibus under accession number GSE65976.

Northern blotting and in vivo labeling of RNA

Tissue samples (50–100 mg, flash-frozen in liquid N_2) were homogenized into Qiazol lysis reagent (Qiagen), and RNA was

purified according to the manufacturer's directions. RNA was precipitated twice, quantified, and resolved by denaturing polyacrylamide electrophoresis before electrophoretic transfer to Nytran Plus membranes (GE Healthcare) and hybridization with [^{32}P]-end labeled oligonucleotide probes at 42°C (Li et al. 2000). tRNA signals detected by phosphorimaging were quantified and normalized to U3 snRNA to compare expression in wild-type and knockout samples. For in vivo labeling, mice (23 wk of age) maintained on a breeder chow diet were fasted overnight and injected i.p. with 0.5 mCi ^{32}P-orthophosphate (carrier-free) in Tris-buffered saline. After 4 h, the animals were sacrificed, tissues were dissected and freeze-clamped, and total RNA was prepared for electrophoresis on denaturing polyacrylamide gels.

Autophagy assays

In vivo LC3 autophagic flux analyses determined the amount of LC3-II that accumulates in lysosomes when exposed to lysosomal inhibitors, 20 mM ammonium chloride, and 100 µM leupeptin. Briefly, freshly harvested liver explants were rapidly placed in dishes containing high-glucose DMEM in the presence or absence of inhibitors and transferred to a CO_2 incubator for 2 h at 37°C and 5% CO_2. Following incubation, explant lysates were generated and subjected to immunoblotting for LC3. Autophagic flux, expressed as rate of autophagolysosome fusion, was determined by the ratio of normalized intensities for LC3-II in inhibitor-treated versus untreated explants. Net flux was determined by subtracting the normalized intensity of untreated LC3-II from the corresponding inhibitor-treated value. Mouse liver LD fractions were isolated as previously described (Singh et al. 2009). Methods for immunohistochemistry are described in the Supplemental Material.

Liver glycerol and triglyceride analyses

Liver glycerol was measured in tissue aqueous homogenates. Triglyceride content was analyzed in liver samples subjected to lipid extraction in a 2:1 chloroform:methanol mixture containing 0.05% sulfuric acid for 24 h at −20°C. Tissue glycerol and triglyceride analyses were carried out using a commercial kit from Sigma-Aldrich as per the manufacturer's instructions.

Statistics

Results are expressed as mean ± SEM. Differences between animals and/or treatments were tested for statistical significance using Student's unpaired *t*-test unless otherwise indicated.

Acknowledgments

We thank Gary Schwartz for helpful discussions on indirect calorimetry, Rani Sellers for histopathology, Manuel Sanchez-Casalongue for experimental insights on mouse biology, Anabela Pimentel for technical assistance in the clamp study, José Iglesias and Walter Wahli for assistance in the ex vivo insulin secretion and content study, Bernard Thorens for helpful discussions, Pascal Cousin for assistance with various mouse experiments, Edith Hummler and the Transgenic Animal Facility of the University of Lausanne for the generation of the *Maf1*-null mutant mice with a targeted zinc finger nuclease, and Xu Wang for help with the analysis of gene expression data. The work was supported by National Institutes of Health grants GM085177 (I.M.W.), AG043930 (J.A.), and T32 GM07491 (A.B.); the University of Lausanne, Swiss National Science Foundation grants 31003A_132958 (N.H.) and 31003A-140780 (J.A.); the Ecole Polytechnique Fédérale de Lausanne; SystemsX.ch SySX.ch 2013/153 (J.A.); and funds from the Albert Einstein College of Medicine supporting stable isotope and metabolomic studies and deep sequencing.

References

Alekseev AE, Reyes S, Yamada S, Hodgson-Zingman DM, Sattiraju S, Zhu Z, Sierra A, Gerbin M, Coetzee WA, Goldhamer DJ, et al. 2010. Sarcolemmal ATP-sensitive K^+ channels control energy expenditure determining body weight. *Cell Metab* **11:** 58–69.

Alexandrov A, Chernyakov I, Gu W, Hiley SL, Hughes TR, Grayhack EJ, Phizicky EM. 2006. Rapid tRNA decay can result from lack of nonessential modifications. *Mol Cell* **21:** 87–96.

Anunciado-Koza RP, Zhang J, Ukropec J, Bajpeyi S, Koza RA, Rogers RC, Cefalu WT, Mynatt RL, Kozak LP. 2011. Inactivation of the mitochondrial carrier SLC25A25 (ATP-Mg^{2+}/Pi transporter) reduces physical endurance and metabolic efficiency in mice. *J Biol Chem* **286:** 11659–11671.

Argmann CA, Champy MF, Auwerx J. 2006. Evaluation of energy homeostasis. *Curr Protoc Mol Biol* **73:** 29B.1.1–29B.1.17.

Bai P, Cantó C, Oudart H, Brunyánszki A, Cen Y, Thomas C, Yamamoto H, Huber A, Kiss B, Houtkooper RH, et al. 2011. PARP-1 inhibition increases mitochondrial metabolism through SIRT1 activation. *Cell Metab* **13:** 461–468.

Bonhoure N, Bounova G, Bernasconi D, Praz V, Lammers F, Canella D, Willis IM, Herr W, Hernandez N, Delorenzi M. 2014. Quantifying ChIP-seq data: a spiking method providing an internal reference for sample-to-sample normalization. *Genome Res* **24:** 1157–1168.

Borcherding DC, Hugo ER, Idelman G, De Silva A, Richtand NW, Loftus J, Ben Jonathan N. 2011. Dopamine receptors in human adipocytes: expression and functions. *PLoS One* **6:** e25537.

Cantó C, Houtkooper RH, Pirinen E, Youn DY, Oosterveer MH, Cen Y, Fernandez-Marcos PJ, Yamamoto H, Andreux PA, Cettour-Rose P, et al. 2012. The NAD^+ precursor nicotinamide riboside enhances oxidative metabolism and protects against high-fat diet-induced obesity. *Cell Metab* **15:** 838–847.

Chernyakov I, Whipple JM, Kotelawala L, Grayhack EJ, Phizicky EM. 2008. Degradation of several hypomodified mature tRNA species in *Saccharomyces cerevisiae* is mediated by Met22 and the 5′–3′ exonucleases Rat1 and Xrn1. *Genes Dev* **22:** 1369–1380.

Cherry JM, Hong EL, Amundsen C, Balakrishnan R, Binkley G, Chan ET, Christie KR, Costanzo MC, Dwight SS, Engel SR, et al. 2012. *Saccharomyces* genome database: the genomics resource of budding yeast. *Nucleic Acids Res* **40:** D700–D705.

Ciesla M, Towpik J, Graczyk D, Oficjalska-Pham D, Harismendy O, Suleau A, Balicki K, Conesa C, Lefebvre O, Boguta M. 2007. Maf1 is involved in coupling carbon metabolism to RNA polymerase III transcription. *Mol Cell Biol* **27:** 7693–7702.

Clapham JC, Arch JR. 2011. Targeting thermogenesis and related pathways in anti-obesity drug discovery. *Pharmacol Ther* **131:** 295–308.

Dittmar KA, Goodenbour JM, Pan T. 2006. Tissue-specific differences in human transfer RNA expression. *PLoS Genet* **2:** e221.

Eisenberg T, Knauer H, Schauer A, Buttner S, Ruckenstuhl C, Carmona-Gutierrez D, Ring J, Schroeder S, Magnes C, Antonacci L, et al. 2009. Induction of autophagy by spermidine promotes longevity. *Nat Cell Biol* **11:** 1305–1314.

Flegal KM, Carroll MD, Ogden CL, Curtin LR. 2010. Prevalence and trends in obesity among US adults, 1999–2008. *JAMA* **303:** 235–241.

Gingold H, Tehler D, Christoffersen NR, Nielsen MM, Asmar F, Kooistra SM, Christophersen NS, Christensen LL, Borre M, Sorensen KD, et al. 2014. A dual program for translation regulation in cellular proliferation and differentiation. *Cell* **158:** 1281–1292.

Gotoh M, Maki T, Satomi S, Porter J, Bonner-Weir S, O'Hara CJ, Monaco AP. 1987. Reproducible high yield of rat islets by stationary in vitro digestion following pancreatic ductal or portal venous collagenase injection. *Transplantation* **43:** 725–730.

Grummt I. 2013. The nucleolus-guardian of cellular homeostasis and genome integrity. *Chromosoma* **122:** 487–497.

Guh DP, Zhang W, Bansback N, Amarsi Z, Birmingham CL, Anis AH. 2009. The incidence of co-morbidities related to obesity and overweight: a systematic review and meta-analysis. *BMC Public Health* **9:** 88.

Harms M, Seale P. 2013. Brown and beige fat: development, function and therapeutic potential. *Nat Med* **19:** 1252–1263.

Houtkooper RH, Canto C, Wanders RJ, Auwerx J. 2010. The secret life of NAD^+: an old metabolite controlling new metabolic signaling pathways. *Endocr Rev* **31:** 194–223.

Houtkooper RH, Pirinen E, Auwerx J. 2012. Sirtuins as regulators of metabolism and healthspan. *Nat Rev Mol Cell Biol* **13:** 225–238.

Jell J, Merali S, Hensen ML, Mazurchuk R, Spernyak JA, Diegelman P, Kisiel ND, Barrero C, Deeb KK, Alhonen L, et al. 2007. Genetically altered expression of spermidine/spermine N1-acetyltransferase affects fat metabolism in mice via acetyl-CoA. *J Biol Chem* **282:** 8404–8413.

Johnson SS, Zhang C, Fromm J, Willis IM, Johnson DL. 2007. Mammalian Maf1 is a negative regulator of transcription by all three nuclear RNA polymerases. *Mol Cell* **26:** 367–379.

Johnson SA, Dubeau L, Johnson DL. 2008. Enhanced RNA polymerase III-dependent transcription is required for oncogenic transformation. *J Biol Chem* **283:** 19184–19191.

Kadaba S, Krueger A, Trice T, Krecic AM, Hinnebusch AG, Anderson J. 2004. Nuclear surveillance and degradation of hypomodified initiator tRNAMet in *S. cerevisiae*. *Genes Dev* **18:** 1227–1240.

Khanna A, Johnson DL, Curran SP. 2014. Physiological roles for mafr-1 in reproduction and lipid homeostasis. *Cell Rep* **9:** 2180–2191.

Klionsky DJ, Cuervo AM, Seglen PO. 2007. Methods for monitoring autophagy from yeast to human. *Autophagy* **3:** 181–206.

Kraschnewski JL, Boan J, Esposito J, Sherwood NE, Lehman EB, Kephart DK, Sciamanna CN. 2010. Long-term weight loss maintenance in the United States. *Int J Obes (Lond)* **34:** 1644–1654.

Kraus D, Yang Q, Kong D, Banks AS, Zhang L, Rodgers JT, Pirinen E, Pulinilkunnil TC, Gong F, Wang YC, et al. 2014. Nicotinamide N-methyltransferase knockdown protects against diet-induced obesity. *Nature* **508:** 258–262.

Li Y, Moir RD, Sethy-Coraci IK, Warner JR, Willis IM. 2000. Repression of ribosome and tRNA synthesis in secretion-defective cells is signaled by a novel branch of the cell integrity pathway. *Mol Cell Biol* **20:** 3843–3851.

Liu C, Perez-Leal O, Barrero C, Zahedi K, Soleimani M, Porter C, Merali S. 2014. Modulation of polyamine metabolic flux in adipose tissue alters the accumulation of body fat by affecting glucose homeostasis. *Amino Acids* **46:** 701–715.

Maclean PS, Bergouignan A, Cornier MA, Jackman MR. 2011. Biology's response to dieting: the impetus for weight regain. *Am J Physiol Regul Integr Comp Physiol* **301:** R581–R600.

Marcelin G, Liu SM, Li X, Schwartz GJ, Chua S. 2012. Genetic control of ATGL-mediated lipolysis modulates adipose triglyceride stores in leptin-deficient mice. *J Lipid Res* **53:** 964–972.

Michels AA, Robitaille AM, Buczynski-Ruchonnet D, Hodroj W, Reina JH, Hall MN, Hernandez N. 2010. mTORC1 directly phosphorylates and regulates human MAF1. *Mol Cell Biol* **30:** 3749–3757.

Miller BG. 1973. The biological half-lives of ribosomal and transfer RNA in the mouse uterus. *J Endocrinol* **59:** 81–85.

Moir RD, Willis IM. 2013. Regulation of pol III transcription by nutrient and stress signaling pathways. *Biochim Biophys Acta* **1829:** 361–375.

Murayama A, Ohmori K, Fujimura A, Minami H, Yasuzawa-Tanaka K, Kuroda T, Oie S, Daitoku H, Okuwaki M, Nagata K, et al. 2008. Epigenetic control of rDNA loci in response to intracellular energy status. *Cell* **133:** 627–639.

Nwagwu M, Nana M. 1980. Ribonucleic acid synthesis in embryonic chick muscle, rates of synthesis and half-lives of transfer and ribosomal RNA species. *J Embryol Exp Morphol* **56:** 253–267.

Oie S, Matsuzaki K, Yokoyama W, Tokunaga S, Waku T, Han SI, Iwasaki N, Mikogai A, Yasuzawa-Tanaka K, Kishimoto H, et al. 2014. Hepatic rRNA transcription regulates high-fat-diet-induced obesity. *Cell Rep* **7:** 807–820.

Palian BM, Rohira AD, Johnson SA, He L, Zheng N, Dubeau L, Stiles BL, Johnson DL. 2014. Maf1 is a novel target of PTEN and PI3K signaling that negatively regulates oncogenesis and lipid metabolism. *PLoS Genet* **10:** e1004789.

Pang YL, Abo R, Levine SS, Dedon PC. 2014. Diverse cell stresses induce unique patterns of tRNA up- and down-regulation: tRNA-seq for quantifying changes in tRNA copy number. *Nucleic Acids Res* **42:** e170.

Parsons PA. 2007. Energetic efficiency under stress underlies positive genetic correlations between longevity and other fitness traits in natural populations. *Biogerontology* **8:** 55–61.

Pavon-Eternod M, Gomes S, Rosner MR, Pan T. 2013. Overexpression of initiator methionine tRNA leads to global reprogramming of tRNA expression and increased proliferation in human epithelial cells. *RNA* **19:** 461–466.

Pirinen E, Kuulasmaa T, Pietila M, Heikkinen S, Tusa M, Itkonen P, Boman S, Skommer J, Virkamaki A, Hohtola E, et al. 2007. Enhanced polyamine catabolism alters homeostatic control of white adipose tissue mass, energy expenditure, and glucose metabolism. *Mol Cell Biol* **27:** 4953–4967.

Pirinen E, Canto C, Jo YS, Morato L, Zhang H, Menzies KJ, Williams EG, Mouchiroud L, Moullan N, Hagberg C, et al. 2014. Pharmacological inhibition of poly(ADP-ribose) polymerases improves fitness and mitochondrial function in skeletal muscle. *Cell Metab* **19:** 1034–1041.

Reina JH, Azzouz TN, Hernandez N. 2006. Maf1, a new player in the regulation of human RNA polymerase III transcription. *PLoS One* **1:** e134.

Rideout EJ, Marshall L, Grewal SS. 2012. Drosophila RNA polymerase III repressor Maf1 controls body size and developmental timing by modulating tRNAiMet synthesis and systemic insulin signaling. *Proc Natl Acad Sci* **109:** 1139–1144.

Rosen ED, Spiegelman BM. 2014. What we talk about when we talk about fat. *Cell* **156:** 20–44.

Singh R, Kaushik S, Wang Y, Xiang Y, Novak I, Komatsu M, Tanaka K, Cuervo AM, Czaja MJ. 2009. Autophagy regulates lipid metabolism. *Nature* **458:** 1131–1135.

Tseng YH, Cypess AM, Kahn CR. 2010. Cellular bioenergetics as a target for obesity therapy. *Nat Rev Drug Discov* **9:** 465–482.

Unger RH, Scherer PE. 2010. Gluttony, sloth and the metabolic syndrome: a roadmap to lipotoxicity. *Trends Endocrinol Metab* **21:** 345–352.

Upadhya R, Lee J, Willis IM. 2002. Maf1 is an essential mediator of diverse signals that repress RNA polymerase III transcription. *Mol Cell* **10:** 1489–1494.

Vaitheesvaran B, Yang L, Hartil K, Glaser S, Yazulla S, Bruce JE, Kurland IJ. 2012. Peripheral effects of FAAH deficiency on fuel and energy homeostasis: role of dysregulated lysine acetylation. *PLoS One* **7:** e33717.

Walden TB, Hansen IR, Timmons JA, Cannon B, Nedergaard J. 2012. Recruited vs. nonrecruited molecular signatures of brown, 'brite,' and white adipose tissues. *Am J Physiol Endocrinol Metab* **302:** E19–E31.

Warner JR. 1999. The economics of ribosome biosynthesis in yeast. *Trends Biochem Sci* **24:** 437–440.

White RJ. 2008. RNA polymerases I and III, non-coding RNAs and cancer. *Trends Genet* **24:** 622–629.

Wilusz JE, Whipple JM, Phizicky EM, Sharp PA. 2011. tRNAs marked with CCACCA are targeted for degradation. *Science* **334:** 817–821.

Wu C, Orozco C, Boyer J, Leglise M, Goodale J, Batalov S, Hodge CL, Haase J, Janes J, Huss JW III, et al. 2009. BioGPS: an extensible and customizable portal for querying and organizing gene annotation resources. *Genome Biol* **10:** R130.

Wu J, Bostrom P, Sparks LM, Ye L, Choi JH, Giang AH, Khandekar M, Virtanen KA, Nuutila P, Schaart G, et al. 2012. Beige adipocytes are a distinct type of thermogenic fat cell in mouse and human. *Cell* **150:** 366–376.

Zoncu R, Efeyan A, Sabatini DM. 2011. mTOR: from growth signal integration to cancer, diabetes and ageing. *Nat Rev Mol Cell Biol* **12:** 21–35.

SUPPLEMENTAL MATERIAL LIST

SUPPLEMENTAL MATERIALS AND METHODS

SUPPLEMENTAL REFERENCES

SUPPLEMENTAL FIGURE LEGENDS

Figure S1. Targeting, genotyping, breeding and phenotyping. (A) Schematic of the construct used to direct homologous recombination at the *Maf1* locus in ES cells. (B) PCR genotyping of tail DNA. Diagnostic products for $Maf1^{+/+}$ (421 bp) and $Maf1^{-/-}$ (376 bp). (C) RT-qPCR of *Maf1* and β-actin mRNAs from wild type and $Maf1^{-/-}$ mouse embryo fibroblasts (Reina et al., 2006). n.d. : not detected. (D) Frequency of genotypes from heterozygous crosses. (E) Fertility and fecundity in homozygous crosses. (F) Body weights of $Maf1^{+/+}$ and $Maf1^{-/-}$ female mice fed *ad libitum* on breeder chow (mean ± s.e.m.). (G) H&E-stained sections of eWAT and oil red O-staining of liver are compared as indicated. Images are at the same magnification and include a 100 μm scale bar. Average cell diameters and estimated cell volumes were determined from multiple fields (see Materials and Methods and Fig. 1I).

Figure S2. Body weights of *Maf1* null mutant mice created using a targeted zinc finger nuclease. (A) Schematic of the *Maf1* locus before and after zinc finger nuclease genome editing. The targeted *Fok*1 cutting site in the wild type *Maf1* sequence is indicated in red. Edited alleles are indicated in blue and the new amino acid sequences are in green followed by a asterisk representing the stop codon. Green and red polygons correspond to the start and the end of the wild type *Maf1* coding sequence. (B) Body weights of male wild type and *Maf1* null mice from homozygous crosses fed *ad libitum* on a high fat diet (mean ± s.e.m.).

Figure S3. Locomotor activity, respiratory exchange ratios, mitochondrial copy number and complex abundance. (A) Total locomotor activity (IR beam breaks in the X and Z dimensions) of high fat pair-fed mice during the light and dark cycle (daily averages from 5 days

in metabolic cages, $n = 4$ per group). (B) Respiratory exchange ratios of high fat pair-fed mice during the light and dark cycle (daily averages from 3 days in metabolic cages, $n = 4$ per group) (C) Mitochondrial copy number in mouse liver was calculated using two different mitochondrial genes (CytB and ND1) relative to the nuclear H19 gene ($n = 9$ per group). (D) Representative proteins in different complexes of the electron transport chain were examined in total mouse liver homogenates using MitoProfile® Total OXPHOS Rodent WB Antibody Cocktail.

Figure S4. Targeted metabolite profiling of plasma. The Biocrates Absolute*IDQ* p180 system was used to quantify the levels of 186 metabolites representing glycerophospholipids, sphingolipids , acyl carnitines, amino acids and other biologic amines. Mice (4 months of age) were fasted overnight and retro-orbital bleeds were taken to prepare plasma. Multivariate partial least squares discriminant analysis (PLS-DA) was performed (MetabolAnalyst) on 159 metabolites that returned values for each of the five wild-type and five knockout plasma samples. (A) 2D score plot of principal components 1 and 2 shows that wild-type and *Maf1*$^{-/-}$ mice are readily distinguished by their plasma metabolite profiles (ellipses define the region of 95% confidence). Leave one out cross validation indicates that the data is best described by a single-component (accuracy 0.8, R2 0.88, Q2 0.54). (B) Fold change in plasma metabolites (KO/WT). The top 31 scoring plasma metabolites are rank ordered, top to bottom, by p value (p values < 0.05). Metabolite concentrations and p values are provided in Supplemental Table S1.

Figure S5. *Maf1*$^{-/-}$ mice do not expend energy by inducing UCP1-mediated adaptive thermogenesis. (A) RNA-seq analysis of eWAT. The MvA plot shows the log2 fold change (KO/WT) versus the log2 average abundance (counts per million reads) for uniquely mapped

reads obtained from biological triplicate RNA samples. Statistical analysis of differential gene expression was performed using EdgeR (Supplemental Table S2). The output was filtered by requiring a >two-fold difference in gene expression, an adjusted *p* value < 0.05 (EdgeR) and >50 reads (normalized) per KO sample for up-regulated genes or >50 reads per WT sample for down-regulated genes. The 13 genes satisfying these criteria are highlighted in red. Due to the sensitivity of EdgeR to outliers, differential gene expression was also evaluated using DESeq. None of the 13 genes scored as statistically significant using this approach. (B) Western blotting of UCP1 and β tubulin in brown adipose tissue. Animals were housed at 22°C and fed *ad libitum* on a breeder chow diet. (C) UCP1 signal intensities from panel B were quantified and normalized to β tubulin. (D) Western blotting of UCP1 in white adipose tissue. Animals were raised as in panel B. BAT lysate was loaded as a positive control. (E) Body temperature of animals housed at 22 ºC (*n* = 7 mice per group). (F) A cold stress test was performed by placing the mice at 4 ºC in individual cages without bedding or food and measuring their body temperature using a rectal thermocouple microprobe (Physiotemp IT-23) at hourly intervals. Four mice at 5 months of age were used per group. WT, blue; KO, orange) (G) Quantitation of TBP expression in total liver RNA was performed as in Fig. 6C (*n* = 5 per group). (H) Western blotting of TBP in nuclear extracts from WT and Maf1 KO liver. (I) Pre-rRNA levels in liver were calculated in the chow-fed and the fasted (16 hr) state by RT-qPCR using primers specific for the 5' external transcribed spacer with normalization to GAPDH (*n* = 3 WT fed, *n* = 2 WT fasted and KO fed, *n* = 4 KO fasted). Comparable results were obtained using cyclophilin for normalization. (J) Quantitation of total tRNA ratios (KO/WT) relative to 5.8S rRNA in different tissues from ethidium bromide-stained denaturing polyacrylamide gels (*n* = 7 per group for liver,

n = 2 per group for eWAT and brain, other tissues represent single determinations). Values are presented as the mean ± SEM.

Figure S6. Polyamine pathway, liver metabolites and lifespan of male wild-type and *Maf1*$^{-/-}$ mice. (A) Polyamine biosynthetic pathway showing inputs from amino acids, methionine, arginine and ornithine along with enzymes and cofactors (Ac-CoA, acetyl coenzyme A; SAM, S-adenosyl methionine, dcSAM, decarboxylated SAM; SAH, S-adenosyl homocysteine; Nam, nicotinamide; Me-Nam, N-methyl Nam). The ability of NNMT (green) to influence polyamine (blue) synthesis by affecting the availability of SAM is indicated. (B) Variable importance in projection (VIP) scores (>1.0 is considered significant) obtained by PLS-DA of liver metabolite profiles (Biocrates p180) are plotted against the fold change in metabolite concentration (normalized per mg tissue) ($p < 0.05$, n = 5 per group). Spermidine, green; amino acids, orange; glycerophospholipids, maroon; acylcarnitines, blue. Ornithine, an amino acid precursor for the polyamine pathway is indicated by a dotted circle. Metabolite concentrations and p values are provided in Supplemental Table S1. (C) Immunoblot of liver NNMT and γ tubulin. (D) Immunoblot of NNMT and γ tubulin in quadriceps. Data in panels C and D are quantified in Fig. 6D. (E) Kaplan-Meier survival curves of male mice (mean lifespan WT 109 weeks, n = 21, black; *Maf1*$^{-/-}$ 120 weeks, n = 32, red, p = 0.24 logrank test).

SUPPLEMENTAL TABLES

Table S1. Metabolite concentrations in plasma, skeletal muscle and liver. Concentrations ± SEM, fold change and p values are tabulated for the top scoring 31 metabolites in plasma, 28 metabolites in skeletal muscle and 22 metabolites in liver determined using the Biocrates

Absolute*IDQ* p180 system. Data are represented graphically in Fig. 4 and in Supplemental Figs. S4 and S6.

Table S2. RNA-seq analysis of wild-type and Maf1 KO eWAT.

This table contains raw and normalized RNA-seq read count data and EdgeR analysis of differential gene expression for reads that were uniquely mapped using HTseq-count. Data are represented graphically in Supplemental Fig. S5A.

Table S3. Pol III transcriptome RNA-seq scores.

This table contains RNA-seq scores for Pol III transcribed genes (see Materials and Methods). Data for precursor and mature tRNAs are represented graphically in Figs. 5A and 5B.

SUPPLEMENTAL MATERIALS AND METHODS

Animals, diets and analysis of lifespan

The *Maf1* targeting vector (Figure S1A) using for homologous recombination contained *loxP* sites in intron 1, 481 bp 5' of the start codon and in exon 8, 221 bp 3' of the stop codon. Chimeric mice were crossed to C57Bl/6 mice expressing Cre recombinase to obtain germ line transmission of the knockout allele. Wild-type and homogygous knockout mice were obtained by further breeding. The majority of the experiments were performed on animals obtained from homozygous crosses. Genotyping primers were Maf1 fwd: 5' AGG CTT GCA GGG CAG CAA TG 3', Maf1 WT rev: 5' CAC TGG CTG ACA GGG AGA TG 3' and Maf1 KO rev: 5' TGG CCC TTA GAG CTG GAG TG 3'. Mice were housed in barrier facilities at 22°C with a 12 h light/dark cycle and were fed *ad libitum* unless otherwise stated on a standard chow diet (KLIBA NAFAG #3436, 13% calories from fat), a breeder chow diet (PicoLab Rodent Diet 20, #5058, 21% calories from fat) or a high fat diet (Bio-Serv, 60% calories from fat). For pair-feeding, a

limiting amount of HFD (2.2 g per day) was determined for *Maf1*$^{-/-}$ mice from *ad libitum* feeding studies. Mice at 10 weeks of age that had been maintained on breeder chow were housed separately in standard cages and provided with pre-weighed high fat pellets every evening for eight weeks. Body weight was measured every three days. For lifespan studies, mice were maintained on breeder chow, *ad libitum,* until their natural end of life. A small number of animals were euthanized based on a veterinarian's independent assessment in accordance with AAALAC guidelines. These animals are represented in the lifespan analysis only if the condition of the animal was considered incompatible with continued survival.

A construct coding for a zinc finger nuclease targeting the *Maf1* gene, as well as corresponding mRNA, were obtained from Sigma-Aldrich (CompoZr®). Mice were produced by the Transgenic Mouse Facility of the University of Lausanne by injection of the zinc finger nuclease mRNA at a concentration of 40 ng/µl (Meyer et al. 2010). A total of 782 injected oocytes were transferred to 29 pseudopregnant females, of which 12 became pregnant and gave birth to 61 live pups. To detect founders, DNA was extracted from toe clips and mutations were identified by DNA sequencing with the primers Fwd 5'- ATG ACT CTG CCT GCG TTC TT-3' and Rev 5'-ACT CAT TGA GGG TGG CAA TC-3'.

Indirect calorimetry

Mice were housed individually at 22°C with a 12 h light/dark cycle and allowed to acclimate for 48 h before data collection. Gas exchange measurements were made under the following Oxymax system settings: air flow, 0.6 l/min; sample flow, 0.5 l/min; settling time, 55 sec; measuring time, 5 sec. Energy expenditure was calculated as recommended by the manufacturer using the following formulas. Heat = CV × VO2 and CV = 3.815 +1.232 × RER

where CV is the calorific value and RER is the respiratory exchange ratio. Calculations of energy expenditure were normalized for lean body mass.

Hyperinsulinemic-Euglycemic Clamp

The hyperinsulinemic-euglycemic clamp study was conducted over 180 min. in awake, freely moving mice following a 5 h fast. HPLC-purified [3-^{3}H]-glucose (NEN Life Sciences, Boston, MA) was prime-infused throughout the clamp [5 μCi bolus, followed by 0.05 μCi/min (basal) and 0.1 μCi/min (clamp)] to estimate the glucose disposal rate and hepatic glucose production. After an 80 min. basal period, a blood sample was collected from the tail tip for determination of basal glucose disposal rate (which equals basal hepatic glucose production in basal conditions). The clamp was initiated by prime-infusion of human insulin (Actrapid, Novo Nordisk, Denmark, 25mU/kg bolus, then 2.5 mU/kg/min), and 50% glucose was infused at variable rates and adjusted every 10 min. to clamp plasma glucose levels around 120 mg/dL as measured by glucometers on 2 μl blood samples (Ascensia Breeze2, Bayer Healthcare, Switzerland). After a 2 h stabilization period, blood was sampled from the tail tip 5 times at 10 minutes intervals for determination of glucose turnover under hyperinsulinemic, steady-state conditions. Hepatic glucose production (HGP) was measured as the difference between the Glucose Disposal Rate (GDR) anf the Glucose Infusion rate (GINF).

Western blotting and antibodies

Cell extracts (50 ug protein) were resolved by 7-11% SDS-PAGE and transferred to nitrocellulose membranes for antibody probing and detection with an Odyssey imager (LI-COR). Primary antibodies were obtained against HSL, phospho-HSL and LC3 (Cell Signaling Technology), UCP1 (Abcam ab47687), Nnmt (H-68, Santa Cruz Biotechnology), PLIN2, (OriGene Technologies, Inc.), α and γ tubulins (clone B-5-1-2 and GTU-88, Sigma-Aldrich),

GAPDH (GeneTex, GT239), and HADC (Abcam ab7030). Antibodies against full-length recombinant TBP were raised in rabbits. MitoProfile® Total OXPHOS Rodent WB Antibody Cocktail was from Abcam. Secondary antibodies were from LI-COR.

Mitochondrial-nuclear DNA ratio measurement.

Total DNA was isolated from the livers of 9 WT and 9 *Maf1*$^{-/-}$ (3 months old) mice under HFD with the Nucleospin kit from Macherey-Nagel. qPCRs were performed with equal amounts of DNA from each sample using SYBERGreen Master mix (Roche) and 5 μM of the following primers: mouse mitochondrial DNA measurements: Cyt B [forward, 5'-GTG AAC GAT TGC TAG GGC C-3'; reverse, 5'- CGA TTC TTC GCT TTC CAC TTC AT-3'], and ND1 [forward, 5'- CTC TTA TCC ACG CTT CCG TTA CG-3'; reverse, 5'-GAT GGT GGT ACT CCC GCT GTA-3']; mouse nuclear DNA measurements: H19 [forward, 5'-GTA CCC ACC TGT CGT CC-3'; reverse, 5'-GTC CAC GAG ACC AAT GAC TG-3']. Ratios of CytB:H19 and Nd1:H19 were calculated.

RNA-seq analysis of pol II and pol III transcriptomes and RT-qPCR

Three biologically independent samples (RNA integrity numbers >7.5, Agilent Bioanalyzer) from wild-type and *Maf1*$^{-/-}$ mice were sequenced. For analysis of the pol II transcriptome, uniquely mapped reads were aligned to the mouse genome (mm9) and counted using GSNAP and HTseq-counts, respectively (Wu and Nacu 2010;Anders et al. 2014). Normalization and statistical evaluation of differential gene expression was performed using EdgeR and DESeq (Robinson et al. 2010;Anders et al. 2013). In the analysis of the pol III transcriptome, sequence tags were mapped in three sequential steps. The first mapping was performed with Bowtie on the Mm9 Mouse genome assembly release. The tags left unmapped were then aligned with BLAT on the pol III loci listed in Table S3. As twenty four tRNA genes

contain introns, the remaining tags were aligned in a third round with BLAT to sequences corresponding to spliced tRNAs. The results of the three alignment steps were pooled and the tags aligning in the pol III loci listed in Table S3 were counted. The tags were scaled to the total number of tags aligning in pol II genes, and tags with multiple matches in the genome were given a weight corresponding to the number of matches divided by the number of times they were sequenced. Scores corresponding to the log2 of tags per gene were then calculated. Tags were considered derived from precursor tRNAs when they extended either upstream or downstream of the mature tRNA coding region or overlapped with tags extending upstream or downstream of the tRNA coding region or for tRNA genes containing an intron, when they contained intron sequences. Sequence tags were considered derived from mature tRNAs when they had 5' and 3' ends that mapped entirely within the mature RNA, and for tRNA genes containing an intron, when they spanned the exon-exon junction. For the differential analyses, two different approaches were used. In the first, we fitted the generalized linear model (GLM) from EdgeR(Robinson et al. 2010) on the scaled tag counts per gene for the three *Maf1*$^{-/-}$ versus the three WT samples; in the second, we applied the limma linear model fitting(Smyth 2004;Smyth et al. 2005) on the log2 of the scaled tag counts per gene, again for the three *Maf1*$^{-/-}$ versus the three WT samples. RT-qPCR was performed using SybrGreen detection as described previously (Reina et al. 2006). For the measurement of pre-rRNA, primers specific for the 5' external transcribed spacer were employed as reported previously (Oie et al. 2014). Differential gene expression was calculated using the ΔΔCt method using GAPDH as the internal reference.

Quantitation of total tRNA

Total RNA (5 μg) was resolved on denaturing polyacrylamide gels, stained with ethidium bromide, imaged and quantified using ImageQuant software. Amounts of total tRNA were

normalized to 5.8S rRNA. The intensity of tRNA and 5.8S rRNA staining was empirically determined to be in the linear range under these conditions.

Immunohistochemistry and fluorescence microscopy

Liver sections were stained for LC3B (Cell Signaling Technology, Inc., MA, USA) overnight at 4°C and incubated with Alexa Fluor® 647 Goat Anti-Rabbit secondary antibody for 1hr at room temperature (RT). For lipid droplet detection, sections were incubated with BODIPY 493/503 for 20 min. at RT. Images were acquired using a Leica DMI6000B microscope/DFC360FX 1.4-megapixel monochrome digital camera (Leica Microsystems, Germany) with a X100 objective/1.4 numerical aperture. All images were acquired at same exposure times. Image slices of 0.2μm thickness were captured and deconvolved using the Leica MetaMorph acquisition/analysis software. All images were prepared using Adobe Photoshop and subjected to identical post-acquisition brightness/contrast effects. Native images were processed with the "colocalization finder" plugin of the NIH ImageJ software, and areas of colocalization are shown as white pixels.

SUPPLEMENTAL REFERENCES

Anders S, McCarthy DJ, Chen Y, Okoniewski M, Smyth GK, Huber W, Robinson MD. 2013. Count-based differential expression analysis of RNA sequencing data using R and Bioconductor. *Nat Protoc.* **8**: 1765-1786.

Anders S, Pyl PT, Huber W. 2014. HTSeq - A Python framework to work with high-throughput sequencing data. *Bioinformatics.*

Meyer M, de Angelis MH, Wurst W, Kuhn R. 2010. Gene targeting by homologous recombination in mouse zygotes mediated by zinc-finger nucleases. *Proc.Natl.Acad.Sci.U.S.A* **107**: 15022-15026.

Oie S, Matsuzaki K, Yokoyama W, Tokunaga S, Waku T, Han SI, Iwasaki N, Mikogai A, Yasuzawa-Tanaka K, Kishimoto H et al. 2014. Hepatic rRNA transcription regulates high-fat-diet-induced obesity. *Cell Rep.* **7**: 807-820.

Reina JH, Azzouz TN, Hernandez N. 2006. Maf1, a new player in the regulation of human RNA polymerase III transcription. *PLoS One.* **1**: e134.

Robinson MD, McCarthy DJ, Smyth GK. 2010. edgeR: a Bioconductor package for differential expression analysis of digital gene expression data. *Bioinformatics.* **26**: 139-140.

Smyth GK. 2004. Linear models and empirical bayes methods for assessing differential expression in microarray experiments. *Stat.Appl.Genet Mol Biol* **3**: Article3.

Smyth GK, Michaud J, Scott HS. 2005. Use of within-array replicate spots for assessing differential expression in microarray experiments. *Bioinformatics* **21**: 2067-2075.

Wu TD, Nacu S. 2010. Fast and SNP-tolerant detection of complex variants and splicing in short reads. *Bioinformatics.* **26**: 873-881.

Bonhoure_Fig S1

A

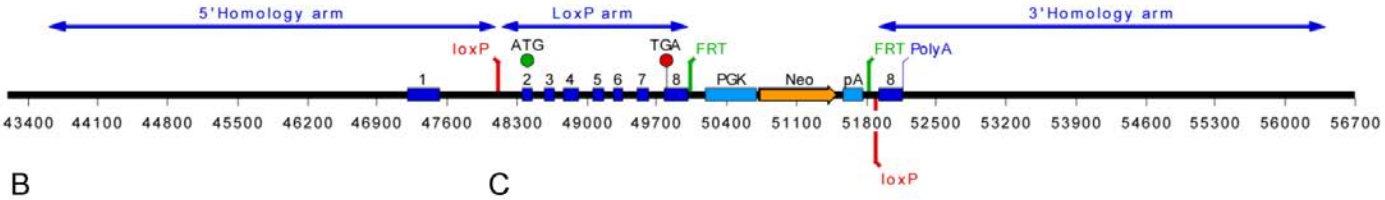

B

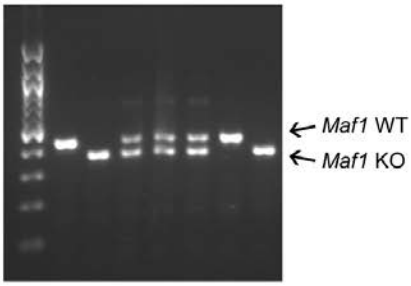

C

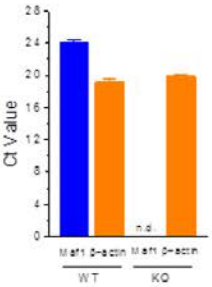

D

Genotypes of progeny from *Maf1*$^{+/-}$ crosses		
Maf1$^{+/-}$	*Maf1*$^{+/+}$	*Maf1*$^{-/-}$
148	79	56

Chi-squared test for independence $p = 0.11$

E

Genotype	Time between litters in homozygous crosses			Litter size in homozygous crosses		
	Breeding pairs	Litters	Time between litters (days)	Breeding pairs	Litters	Pups/litter
WT	18	76	25 ± 1	25	102	6.0 ± 0.2
Maf1$^{-/-}$	30	119	35 ± 1 *	39	165	4.8 ± 0.2 †

Values were calculated for breeding pairs having seven or fewer litters and report the mean ± s.e.m.
* $p = 1.9$ E-9, † $p = 2.3$ E-4.

F

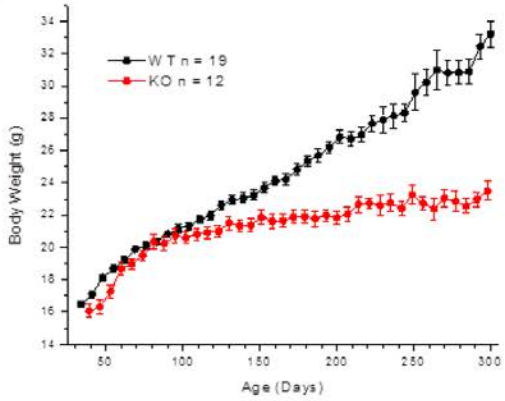

G

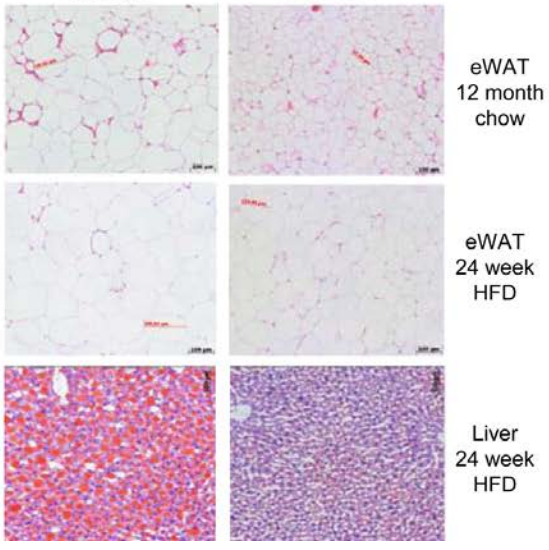

Bonhoure_Fig S2

A

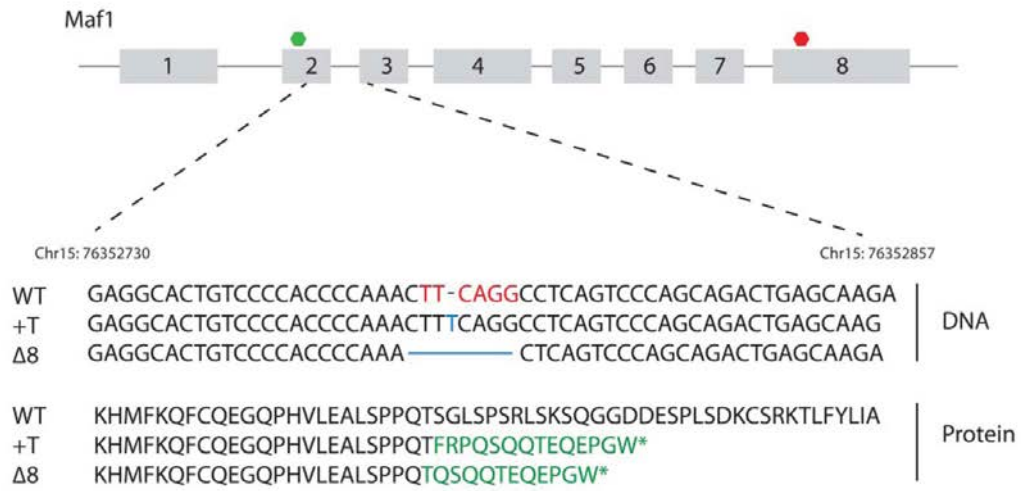

B

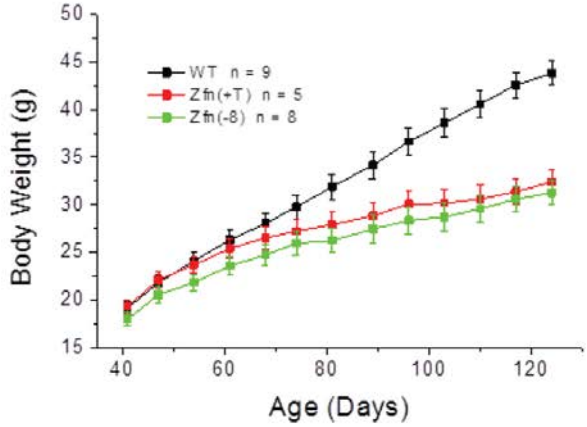

Bonhoure_Fig S3

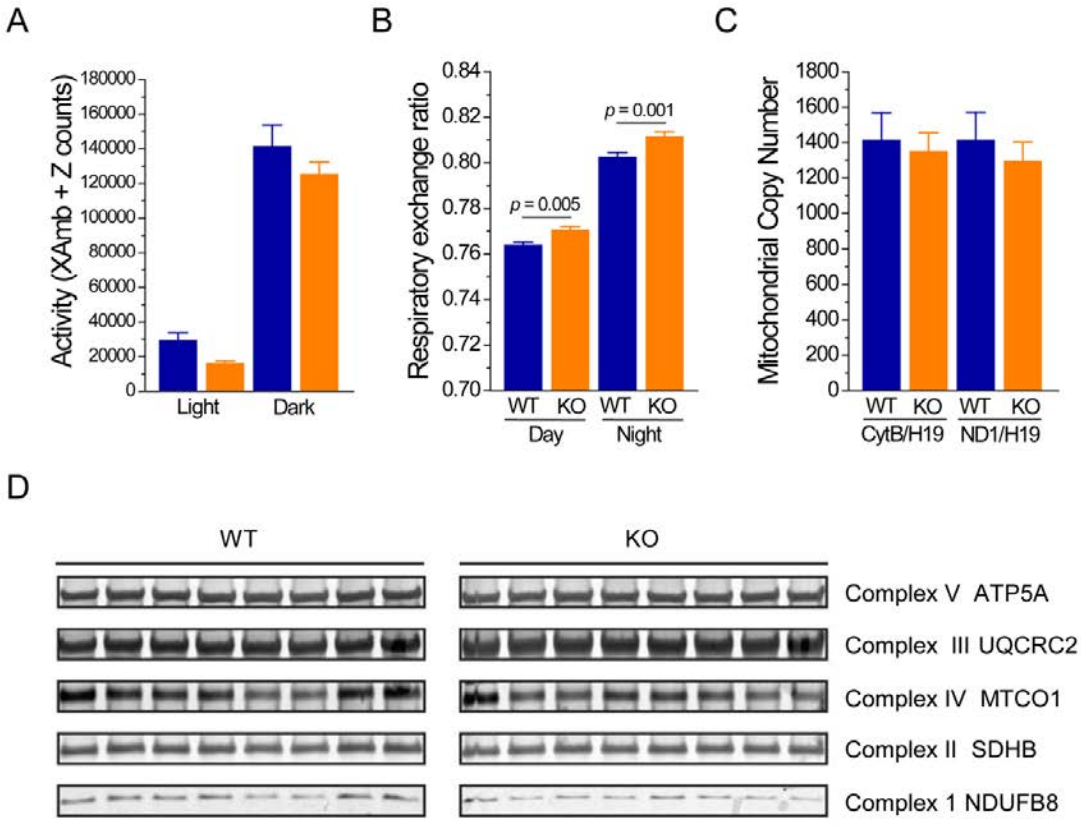

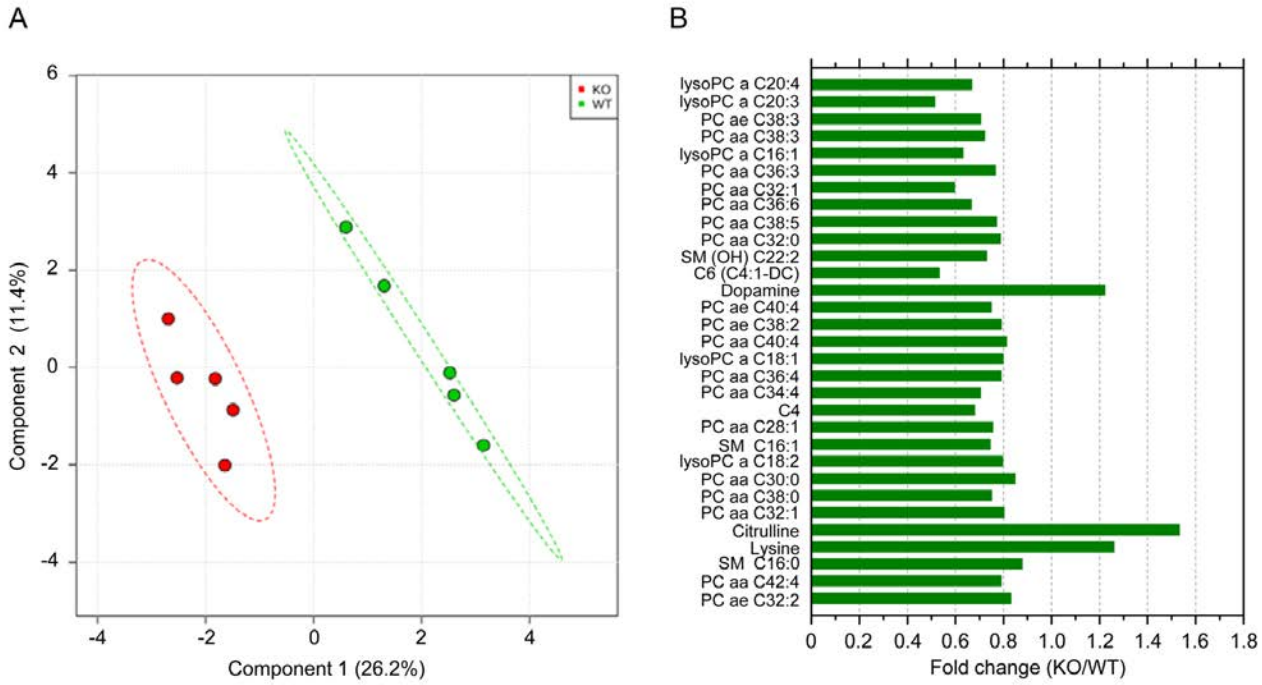
A
B
KO
WT
Component 2 (11.4%)
Component 1 (26.2%)
lysoPC a C20:4
lysoPC a C20:3
PC ae C38:3
PC aa C38:3
lysoPC a C16:1
PC aa C36:3
PC aa C32:1
PC aa C36:6
PC aa C38:5
PC aa C32:0
SM (OH) C22:2
C6 (C4:1-DC)
Dopamine
PC ae C40:4
PC ae C38:2
PC aa C40:4
lysoPC a C18:1
PC aa C36:4
PC aa C34:4
C4
PC aa C28:1
SM C16:1
lysoPC a C18:2
PC aa C30:0
PC aa C38:0
PC aa C32:1
Citrulline
Lysine
SM C16:0
PC aa C42:4
PC ae C32:2
Fold change (KO/WT)

Bonhoure_Fig S5

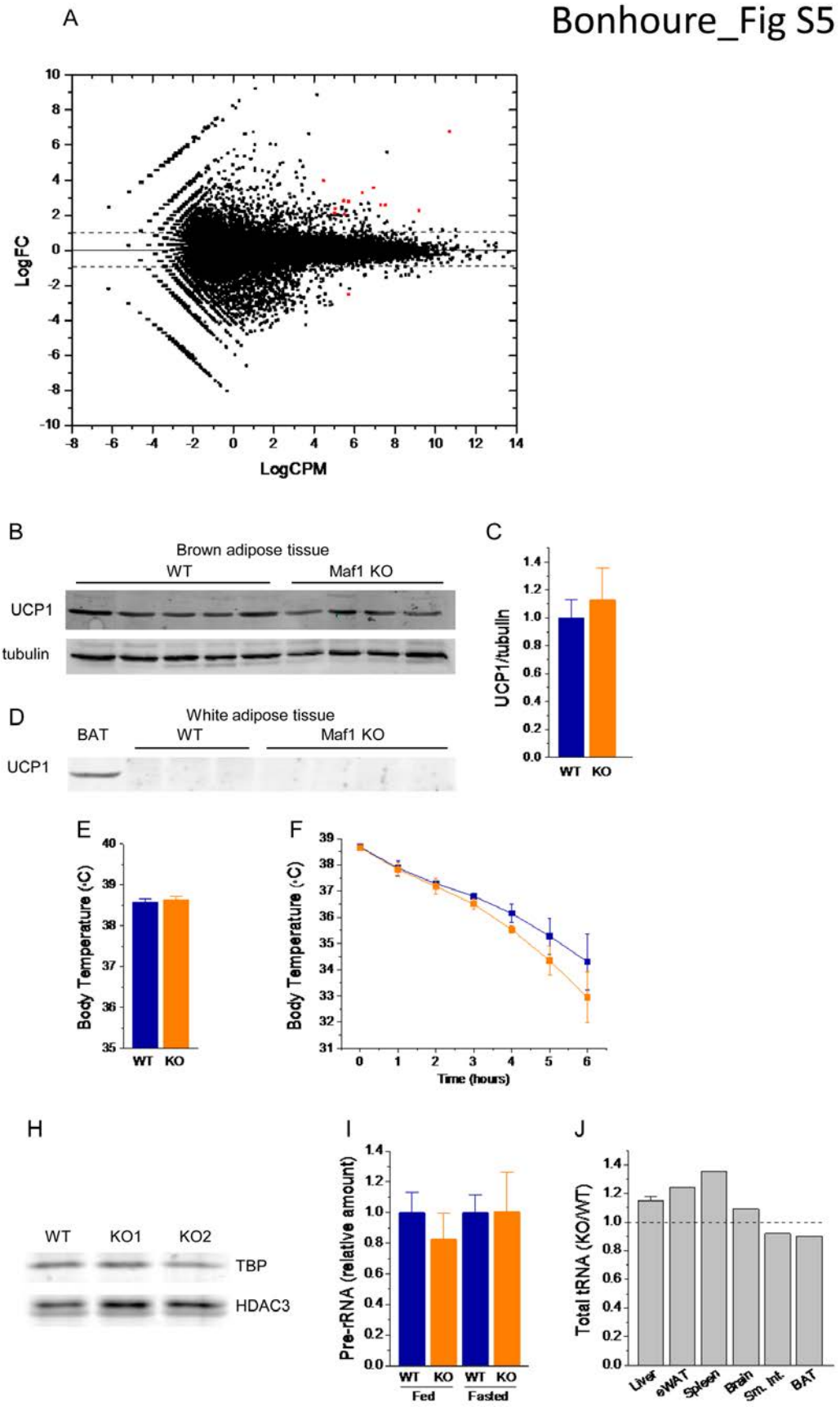

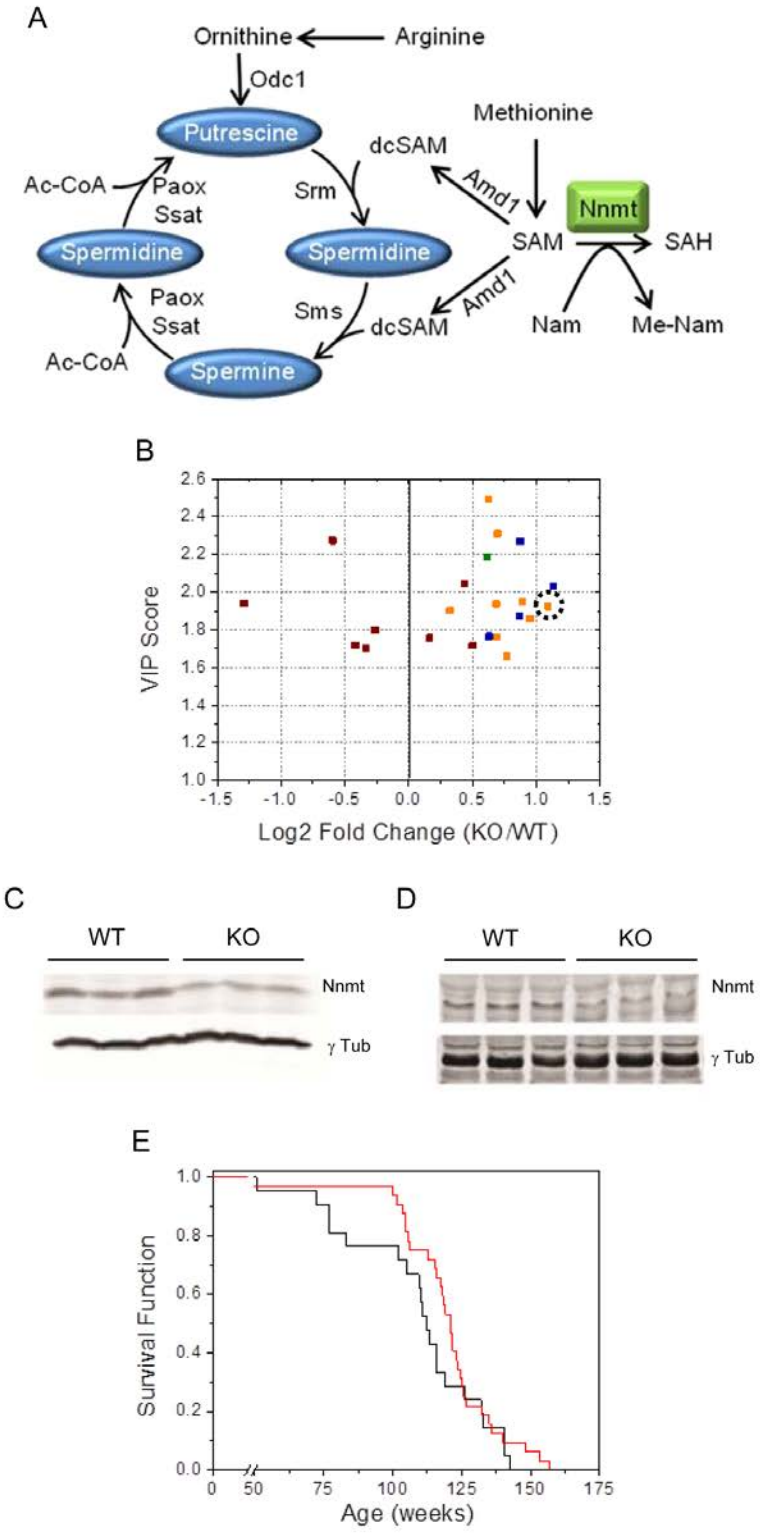
A
Ornithine
Arginine
Odc1
Putrescine
Methionine
dcSAM
Amd1
Nnmt
Ac-CoA
Paox
Ssat
Srm
Spermidine
Spermidine
SAM
SAH
Amd1
Paox
Ssat
Sms
dcSAM
Nam
Me-Nam
Ac-CoA
Spermine
B
VIP Score
Log2 Fold Change (KO/WT)
C
WT
KO
Nnmt
γ Tub
D
WT
KO
Nnmt
γ Tub
E
Survival Function
Age (weeks)

Supplemental tables S1, S2, and S3 can be found online at the address:
http://genesdev.cshlp.org/content/29/9/934/suppl/DC1

Chapter III – Development of a method to normalize ChIP-seq data

Abstract

In the mouse, Pol 3 transcribes more than 600 genes involved in different molecular functions. Pol 3 activity can be measured by chromatin immunoprecipitation performed with antibodies directed against Pol 3 subunits followed by deep sequencing (ChIP-seq). ChIP-seq allows the identification, genome wide, of the Pol 3 binding sites but should in principle also allow the quantification of the level of Pol 3 binding onto the different loci. Theoretically, after normalization of the data, the user should be able to compare the levels of occupancy among different conditions or different cell types. Highly used normalization methods always include, as a first step, a scaling to the total number of sequenced tag to correct for sequencing depth, often followed by quantile normalization to identify specific enriched regions for a given condition. When I started this project, a previous post-doctoral fellow in our group had monitored Pol 3 occupancy in mouse liver every four hours around the clock using ChIP-seq to check for the effects of the circadian clock on Pol 3 activity. However, applying the normalization methods described above, no significant changes in Pol 3 activity were found around the clock. We realized that although the standard normalization methods are efficient to define a set of enriched genes, they fail to identify global changes in which all the genes are enriched for a factor in one condition compared to another, a situation likely to occur for Pol 3 genes. To be able to monitor global changes, we sought to use an internal control that would allow us to normalize samples between different conditions. We added a small amount of chromatin (spike) from a foreign organism (in our case, spiking human chromatin into mouse chromatin) at the earliest possible step in the experiment and used the signal of the spike chromatin to normalize the data. This method relies on the antibody used for the immunoprecipitation working efficiently with both species.

For a “perfect” experiment, the spiked material should be added before sonication, ensuring that both chromatins are sheared similarly. However, working with an animal tissue (i.e. mouse liver) complicated the cell number quantification, making it difficult to be accurate for the addition of the spiked material. We therefore decided to add the spike chromatin just after sonication of the mouse liver chromatin, using DNA concentration for quantification. I developed the experimental part of the method, and the analysis was performed in collaboration with the group of Mauro Delorenzi (Swiss Institute of Bioinformatics). We defined which percentage of spiked material was optimal for the normalization and also tested how different extents of chromatin sonication impacted on the normalization. We observed that the spike-adjustment method improved reproducibility between replicate samples and, more importantly, revealed changes in global occupancy between different conditions that were not seen with the previous methods of normalization. We validated the method using antibodies directed against Pol 2 and Pol 3 subunits to show that the usefulness of the spike-adjusting method to normalize ChIP-seq data was not limited to a single antibody. The method development, the step-by-step analysis, and the results are described in the attached paper.

Quantifying ChIP-seq data: a spiking method providing an internal reference for sample-to-sample normalization

Nicolas Bonhoure,[1,6] Gergana Bounova,[1,2,6] David Bernasconi,[1,2,8] Viviane Praz,[1,3] Fabienne Lammers,[1] Donatella Canella,[1] Ian M. Willis,[4] Winship Herr,[1] Nouria Hernandez,[1,9] Mauro Delorenzi,[2,5,9] and The CycliX Consortium[7]

[1]*Center for Integrative Genomics, Faculty of Biology and Medicine, University of Lausanne, 1015 Lausanne, Switzerland;* [2]*Bioinformatics Core Facility, SIB Swiss Institute of Bioinformatics, 1015 Lausanne, Switzerland;* [3]*Swiss Institute of Bioinformatics, 1015 Lausanne, Switzerland;* [4]*Department of Biochemistry, Albert Einstein College of Medicine, Bronx, New York 10461, USA;* [5]*Department of Oncology and the Ludwig Center for Cancer Research, Faculty of Biology and Medicine, University of Lausanne, 1011 Lausanne, Switzerland*

Chromatin immunoprecipitation followed by deep sequencing (ChIP-seq) experiments are widely used to determine, within entire genomes, the occupancy sites of any protein of interest, including, for example, transcription factors, RNA polymerases, or histones with or without various modifications. In addition to allowing the determination of occupancy sites within one cell type and under one condition, this method allows, in principle, the establishment and comparison of occupancy maps in various cell types, tissues, and conditions. Such comparisons require, however, that samples be normalized. Widely used normalization methods that include a quantile normalization step perform well when factor occupancy varies at a subset of sites, but may miss uniform genome-wide increases or decreases in site occupancy. We describe a spike adjustment procedure (SAP) that, unlike commonly used normalization methods intervening at the analysis stage, entails an experimental step prior to immunoprecipitation. A constant, low amount from a single batch of chromatin of a foreign genome is added to the experimental chromatin. This "spike" chromatin then serves as an internal control to which the experimental signals can be adjusted. We show that the method improves similarity between replicates and reveals biological differences including global and largely uniform changes.

[Supplemental material is available for this article.]

In chromatin immunoprecipitation (ChIP) followed by deep sequencing (ChIP-seq) (Barski et al. 2007; Johnson et al. 2007a; Mikkelsen et al. 2007), chromatin is first treated, within intact cells, with a cross-linking reagent such as formaldehyde. The cross-linked chromatin is then isolated and fragmented, often by sonication, and used as starting material for immunoprecipitations with antibodies directed against the factors of interest. The immunoprecipitated material, containing the protein targeted by the antibody as well as any DNA cross-linked to it, is heated to reverse the crosslinks, the DNA is purified, and an amplified representation of this DNA is submitted to deep sequencing. Deep sequencing generates sequence "tags" of commonly 35 to ~100 nucleotides (nt), which are then aligned onto the genome. Genomic regions enriched in aligned tags over noise (variously defined in different works) are interpreted as regions of factor occupancy. This method has proven immensely powerful in characterizing chromatin organization, i.e., in identifying sites bound, for example, by transcription factors, by histones carrying (or not) specific modifications, or by RNA polymerases.

Apart from identifying regions of factor occupancy within a single chromatin sample, ChIP-seq is invaluable for comparing the level of occupancy at a set of loci (e.g., previously identified targets of a specific transcription factor) between different chromatin samples from various cell types or tissues, from cells submitted to different conditions, or from cells at different developmental stages, etc. Unlike measurements of mature mRNAs, such experiments inform on changes occurring at the very first steps of gene expression, i.e., changes in chromatin structure and gene transcription. In such experiments, however, reliable sample normalization has proven difficult.

There are a number of different methods to normalize ChIP-seq samples including scaling to total amounts of tags (i.e., normalizing for sequencing depth), quantile normalization, and other methods. Scaling to the total amount of sequence tags that can be aligned onto the genome is usually the first step (for examples, see Li et al. 2011; Landt et al. 2012; Le Martelot et al. 2012). Quantile normalization is also broadly applied because it can reveal differ-

[6]These authors contributed equally to this work.
[7]A complete list of consortium authors appears at the end of this article.
[8]Present address: Biocartis SA, EPFL Innovation Square, Lausanne, Switzerland
[9]Corresponding authors
E-mail nouria.hernandez@unil.ch
E-mail mauro.delorenzi@unil.ch

Article published online before print. Article, supplemental material, and publication date are at http://www.genome.org/cgi/doi/10.1101/gr.168260.113. Freely available online through the *Genome Research* Open Access option.

ences at specific loci even in samples displaying relatively uniform global differences at all enriched loci (for examples, see Rahl et al. 2010; Le Martelot et al. 2012). Scaling to total tag amounts and quantile normalization can have very different effects, particularly in cases of global differences; for example, if all regions enriched in one sample are uniformly enriched to a higher or lower degree in another sample. With just scaling to total amount of aligned tags, these differences might persist, but their interpretation will be difficult because scaling will not distinguish whether the differences result from technical experimental variations or from genuine biological differences. With quantile normalization, on the other hand, the distributions of the various samples are made identical so that they can be easily compared, thus masking any uniform changes, whether genuine or not, from one sample to another.

Here we describe a spike adjustment procedure (SAP) designed to allow comparison of occupancy levels for a set of loci of interest. Unlike the above, this method addresses the problem via an experimental procedure conducted prior to immunoprecipitation. It consists of adding a constant, low amount of a single batch of foreign chromatin (e.g., human) as an internal control to each sample of the chromatin of interest (e.g., mouse) before immunoprecipitation. This allows adjustment of the signals in each sample to the internal control. We show that unlike only scaling to the total amount of aligned sequence tags or quantile normalization, the SAP allows the scoring of global and largely uniform changes when they result from biological differences.

Results

To illustrate the approach, Figure 1A shows a hypothetical experiment in which all ChIP-seq peaks are higher in a first sample (light blue) compared with a second sample (purple). The global change in peak size could in principle be the result of a biological difference, e.g., occupancy in the second example might be reduced because of some change in cell metabolism; or it might reflect a technical problem such as reduced immunoprecipitation efficiency. In this hypothetical example, scaling to total amount of tags maintains the differences because the total number of sequenced and aligned tags is roughly similar in both samples (Fig. 1B). In contrast, scaling followed by quantile normalization reveals almost no differences between the samples (Fig. 1C), because the peaks in the second experiment are more or less uniformly lower than in the first. Thus, in this example the two methods give different results and do not allow one to distinguish between the two scenarios, genuine biological difference or technical variability. The two scenarios should be distinguishable, however, by adjustment to an internal reference. In panels D and E, the same experiment is shown as in panel A but this time with a spike signal, symbolized by the yellow bars. Replicates (or similar biological samples) displaying apparent different occupancy due to technical problems would display a lower spike signal in the second sample and, after normalization to this internal reference by the SAP, little or no change (Fig. 1F). In contrast, biologically different samples would reveal a global negative fold change (Fig. 1G).

Addition of different percentages of human chromatin to mouse chromatin

An internal reference is most useful when included as early as possible in an experimental procedure. We therefore sought to include the internal reference before the immunoprecipitation step, which is one of the steps likely to generate variation from one sample to another in the ChIP-seq protocol. We tested the usefulness of adding spikes of human chromatin to mouse chromatin samples for ChIP-seq experiments performed with two antibodies: one directed against POLR3D (RPC4), a subunit of RNA polymerase (Pol) III; and the other against POLR2B (RPB2), the second largest subunit of Pol II (for a list of the samples used in this work and their nomenclature, see Table 1). Both antibodies are directed against peptides that are 100% conserved in mouse and human Pol III and Pol II, respectively. We first focused on experiments using the anti-POLR3D antibody and tested mixing different amounts of human chromatin with the mouse chromatin, with the aim of using the smallest possible amount of human chromatin so as to avoid unnecessary contamination of the mouse sample, and yet obtaining a robust signal on a sufficient number of human genes.

The various mixtures were used for ChIP-seq and the resulting 100-nt-long sequence tags were aligned with both the mouse (NCBI37/mm9) and human (GRCh37/hg19) genomes. Supplemental Table S1, A and B, lists the tag counts that aligned to the mouse genome, the human genome, or to both genomes (ambiguous tags). Adding 2.5%, 5%, or 10% human chromatin derived from HeLa cells resulted in an increase in the number of reads aligning to the human genome, as expected, but had little influence on the amount of ambiguous reads, indicating that most of the ambiguous reads originate from the mouse chromatin, which is not surprising since this chromatin represents in all cases most of the material. Moreover, the ambiguous tags represented only a small proportion of the tags mapping to human Pol III regions (see Supplemental Table S1B [sheet 2], last column) such that there was little loss of sensitivity in the human signal due to the exclusion of tags that cannot be unequivocally mapped to the mouse or human genomes. For subsequent analyses, we thus used 2.5% human chromatin, as this amount produced a usable signal on human genes (see below).

Spiking samples allows quality control

Figure 2 summarizes the steps in the SAP. After tag alignment to the human and the mouse genomes and removal of ambiguous tags, we first tested whether the human spike signal can be used for quality control evaluation. Indeed, since the human chromatin added to the experimental mouse samples is constant from one sample to another, the quality of the human signal should in principle attest to the technical quality of the experiment, unlike experimental mouse samples where the mouse signal may vary according to biological differences. We thus compared a sample generated with our standard protocol (90_R1) (see Table 1) to a "poor" sample (97.5_P1) (see Table 1) in which we deliberately contaminated the immunoprecipitated material by adding back 1.5% of the supernatant obtained after immunoprecipitation. Figure 3 shows, for each of these two spiked-in samples, a mean-difference scatter plot comparing spike human tag counts in 400-bp genomic bins obtained in the ChIP versus the input. The red dots indicate bins that overlap with what we refer to hereafter as "Pol III loci," i.e., annotated Pol III genes (whether occupied by Pol III or not) as well as previously identified Pol III–occupied loci (see Table S2 in Renaud et al. 2014). With the standard protocol (upper panel), many of the bins overlapping with spike human Pol III loci showed strong enrichment in the ChIP sample with respect to the

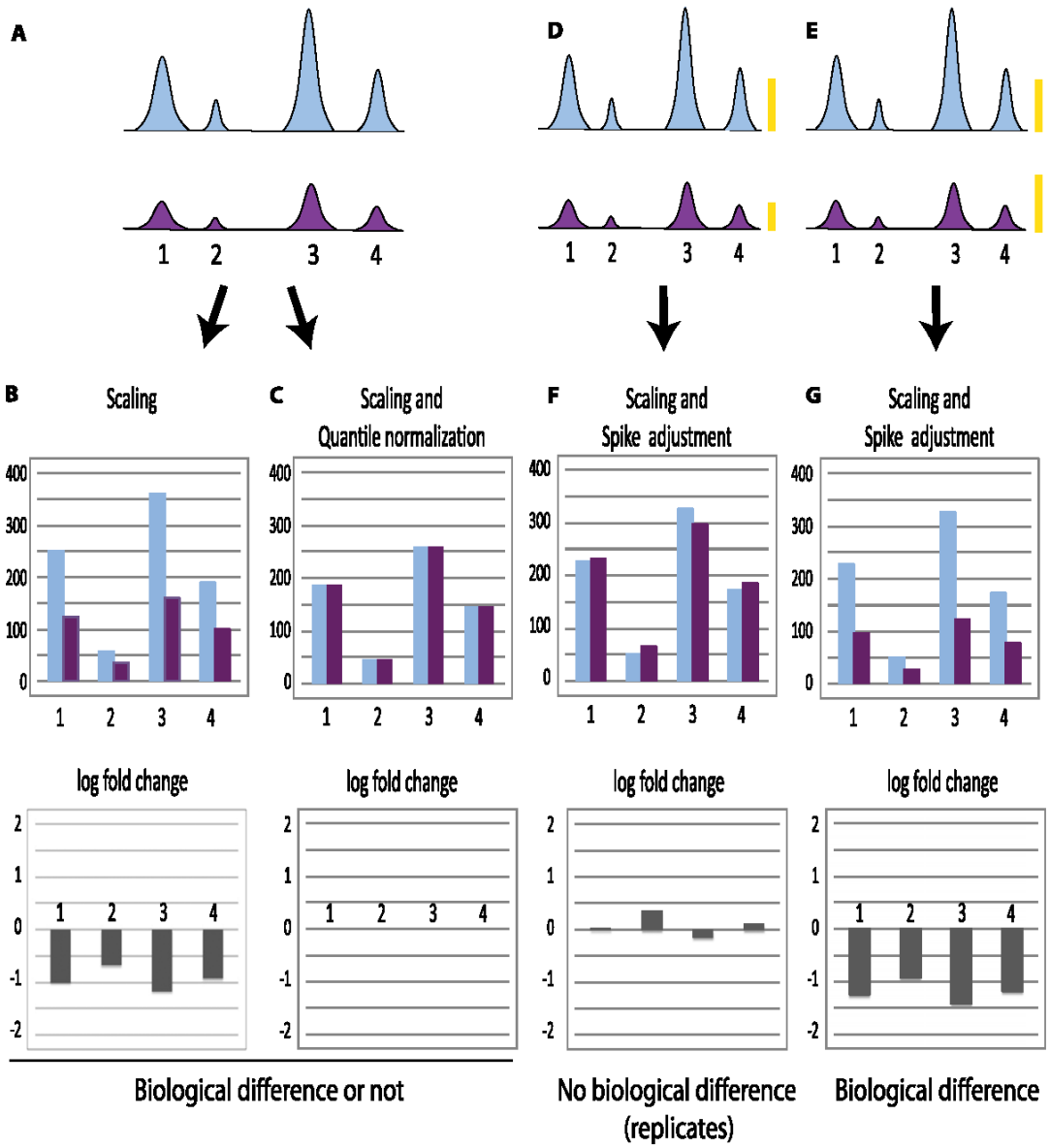

Figure 1. Normalization can obscure global effects. (*A*) Schematic representation of peaks obtained after ChIP-seq in a hypothetical example where all peaks are uniformly diminished in the second (purple) sample compared with the first (light blue). These samples can represent a replicate experiment, in which case the overall decrease observed in the second sample is the result of experimental variation, or they can represent experiments performed with samples collected under different conditions, in which case the global decrease might reflect a biological difference. No spike chromatin is included. (*B*) Normalization by scaling to total number of tags aligned onto the genome (i.e., normalization for sequencing depth) showing tag counts (*top*) and $\log_2$ fold change (*bottom*). In this hypothetical example, the number of tags aligned onto the genome is quite similar in both samples, and this type of normalization indicates a general decrease for each peak in the second sample, whether the two samples are biologically different (and thus should indeed indicate a protein occupancy decrease in sample 2) or similar (and thus should in fact display similar signals). (*C*) Normalization by scaling followed by quantile normalization showing tag counts (*top*) and $\log_2$ fold change (*bottom*). In this example, the second step—quantile normalization—will equalize the sample distributions whether the samples are biologically different or not, because the decrease in sample 2 is uniform. In *D* and *E*, spike chromatin is included in the sample and gives rise to signals symbolized by the yellow bars. (*F*,*G*) Normalization by scaling followed by spike adjustment showing tag counts (*top*) and $\log_2$ fold change (*bottom*). In *F*, the spike adjustment factor increased the signals in sample 2 by a factor of about two, in *G*, the spike adjustment factor decreased the signal in sample 2 by a factor of about 0.8 (see yellow bars). Spike adjustment reveals whether the samples are in fact similar (example in *F*) or are in fact biologically different (example in *G*).

input. In contrast, the poor sample (lower panel) showed almost no enrichment. Thus, the amount of signal in human Pol III loci reflects sample quality, as expected, and can be used for quality control. A quantitative metric to characterize signal content can be the percentage of tags aligning in gene regions. Indeed, as shown in Supplemental Table S1B (sheet 2), the percentage of human tags

Table 1. Samples used in this work

Sample name	Mouse chromatin (%)	Human chromatin (%)	Antigen	Amount of antibody used (μL)	Number of sonication cycles
97.5_R1	97.5	2.5	POLR3D	10	10
95_R1	95.0	5	POLR3D	10	10
90_R1	90.0	10	POLR3D	10	10
97.5_P1	97.5	2.5	POLR3D	10 (1.5% supernatant added back)	10
97.5_S5	97.5	2.5	POLR3D	10	5
97.5_S10	97.5	2.5	POLR3D	10	10
97.5_S15	97.5	2.5	POLR3D	10	15
mR1_WT	97.5	2.5	POLR3D	10	10
mR1_KO	97.5	2.5	POLR3D	10	10
mR2_WT	97.5	2.5	POLR3D	10	10
mR2_KO	97.5	2.5	POLR3D	10	10
RPB2_95	95	5	POLR2B	10	10
RPB2_90	90	10	POLR2B	10	10

The numbers in the names (97.5, 95, or 90) refer to the percentage of mouse chromatin in the sample (the rest correspond to human chromatin). R1 or R2 refer to technical replicates (separate immunoprecipitations performed with the same chromatin sample); P1 refers to a "poor" sample in which the immunoprecipitation conditions were changed with the aim of reducing efficiency; and S5, S10, and S15 refer to different sonication conditions. mR1_WT and mR2_WT, as well as mR1_KO and mR2_KO, are in each case replicate ChIP-seq performed at a 10-mo interval with the same batch of wild-type (WT) and *Maf1* knockout (KO) mouse liver chromatin. The replicates were spiked with the same batch of human chromatin. All samples were immunoprecipitated with antibodies directed against the POLR3D subunit of Pol III, except for the samples labeled "RPB2," which were immunoprecipitated with antibodies directed against the POLR2B subunit of Pol II.

in human Pol III loci was 8.7- to 16.7-fold lower for the poor 97.5_P1 sample compared with the standard 97.5_R1 or any of the other standard replicate (R) samples (column G). Together with visual inspection of scatter plots as shown above, this information can be used to identify samples that should be discarded (and experiments that should be redone).

The next step after assessing sample quality consisted in scaling the samples relative to the total number of aligned tags (scaling for sequencing depth) in each experiment, which was performed separately for the mouse and human tags (Fig. 2, step 2). We then selected signal loci (step 3; see Methods) and calculated scores for the human sample and preliminary scores for the mouse sample (step 4). We then used the sample-to-sample differences in human signals to compute a spike adjustment factor for each sample. This spike adjustment factor was applied to the preliminary scores of the mouse Pol III loci (for a list of these loci, see Table S3 in Renaud et al. 2014) to obtain final scores (step 5; see Methods).

Effect of sonication on the spike signal

As sonication is performed before addition of the spiking material, a possible problem with the SAP might arise as a result of sonication of the human and mouse samples to different average fragment sizes. This is illustrated in Figure 4A. In this example, the human chromatin, which is from a single batch, is sonicated to an average size of 500 bp. In contrast, the first mouse chromatin is sonicated to a larger average size (upper panel), whereas the second sample is sonicated to a smaller average size (lower panel). Size selection of DNA fragments from 200 to 400 bp during library preparation (indicated by the rectangle) would result in a smaller percentage of mouse chromatin in the first case compared with the second case. This problem should be in large part circumvented by the first normalization step, in which we scale independently the human and mouse signals to the total number of aligned sequence tags.

To directly test the effects of different average sizes of the mouse sample, we sonicated mouse chromatin for five, 10, and 15 cycles. As expected, increasing the number of sonication cycles resulted in shorter average mouse chromatin fragment lengths, as visualized after analysis on a Bioanalyzer 2100 from Agilent (Fig. 4B, upper panel, lanes S5, S10, S15) or after agarose gel electrophoresis (lower panel). Figure 4B also shows the human spike chromatin, which was fragmented less completely than the mouse samples but nevertheless contained an abundance of fragments <1000 bp.

Despite the variable length distributions of the mouse chromatin samples, the SAP did not disrupt the data and sample alignments remained very high in all cases, as illustrated by the scatter plots in Figure 4C (for Pearson and Spearman correlations, see Figure 4 legend). Thus, spike adjustment is quite impervious to differences in sample sonication.

Spike adjustment both improves similarity between biological replicates and reveals biological differences

To test the usefulness of the SAP to both improve similarity between replicates and reveal biological differences, we made use of two experiments that are part of an independent study (N Bonhoure, V Praz, RD Moir, IM Willis, and N Hernandez, unpubl.). In these experiments, which were performed at different times, before and after upgrade of the sequencer, but with the same batches of mouse and human chromatin, we compared Pol III occupancy in the liver of wild-type (WT) mice (samples mR1_WT and mR2_WT) (see Table 1) and mice lacking the *Maf1* gene (mR1_KO and mR2_KO). MAF1 is a repressor of Pol III transcription, both in yeast (Pluta et al. 2001; Upadhya et al. 2002) and in mammalian cells (Reina et al. 2006; Johnson et al. 2007b; Rollins et al. 2007), which prevents transcription complex assembly by binding to Pol III as well as to BRF1, a member of the Pol III preinitiation complex (Desai et al. 2005; Oficjalska-Pham et al. 2006; Reina et al. 2006; Goodfellow and White 2007; Vannini et al. 2010). In the absence of MAF1, one might expect a difference in Pol III occupancy at Pol III loci.

We first compared the replicates before and after spike adjustment (step 5 in Fig. 2). As shown in the scatter plots in Figure 5, A and B, the scores for Pol III–occupied loci were closer to the $x = y$

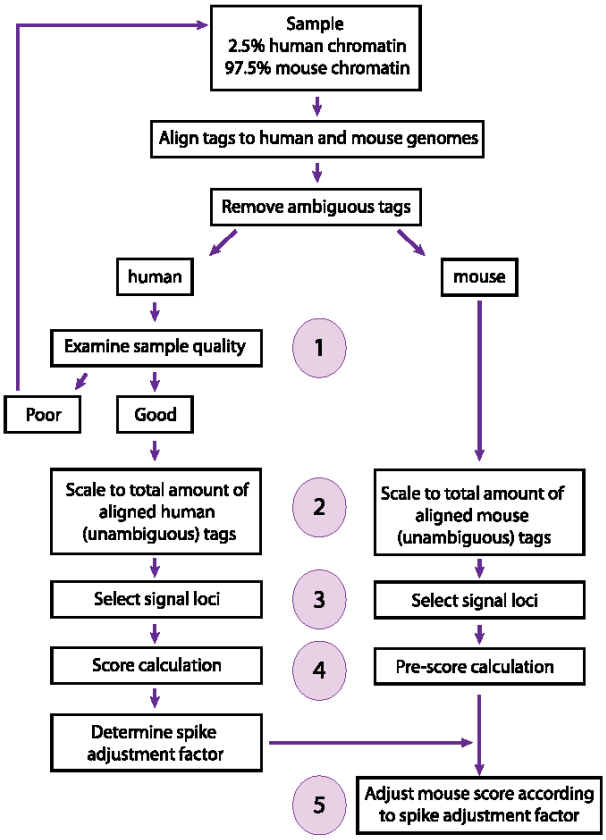

Figure 2. Schematic diagram summarizing the SAP. The main steps, i.e., examination of sample quality, scaling to total amount of genome-aligned tags, selection of signal genes, score calculation, and spike adjustment, are numbered.

line after (black) than before (orange) spike adjustment, both for the replicate samples from WT mice (panel A) and for those of the *Maf1* KO mice (panel B).

We then compared the four samples using scaling to total number of tags (Fig. 1, cf. A and B), scaling and quantile normalization (Fig. 1, cf. A and C), or scaling and spike adjustment (Fig. 1, cf. D–G). Figure 5, C through E, shows the resulting boxplots of the occupancy scores on Pol III loci in WT (green) and *Maf1* KO mice (blue), in the first (light colors) or second (dark colors) experiments. After just scaling (panel C), the average and median occupancy were in each case higher in the *Maf1* KO samples compared with the corresponding WT sample. However, the average and mean of the first *Maf*1 KO sample (mR1_KO) were very similar to the average and mean of the second WT sample (mR2_WT; cf. the second and third box plots), making the results difficult to interpret. Upon scaling and quantile normalization, the distributions of all samples became similar, as expected (panel D). In contrast, the SAP not only remarkably improved the agreement between replicates, in particular for the KO samples, but also revealed a clear difference between the WT and KO samples, with higher average Pol III occupancy in the KO samples (panel E). This was also evident in the empirical cumulative distribution function (ECDF) graphs (panels F–H), showing identical distributions for all samples after scaling and quantile normalization (panel G), but more similar distributions for the two WTand the two KO samples, as well as better separation of the WT and KO sample pairs, for the samples normalized with SAP (cf. panels F and H).

To examine the effect of scaling and quantile normalization versus the SAP on a locus per locus basis, we performed a differential analysis with the two sets of normalized scores. The results are displayed as mean-difference plots in Figure 5, I and J, with the scores showing a significant difference in the WT versus *Maf1* KO samples in yellow ($P \leq 0.01$) and red ($0.01 < P \leq 0.05$). With the scaling and quantile normalization method (panel I), 34 loci had significantly different occupancy, but the minimum false-discovery rate (FDR = 0.045) was close to the cutoff 0.05, and there was a roughly equal number of loci with higher and lower scores in the *Maf1* KO compared with the WT samples. With the SAP, 490 loci scored as having significantly different Pol III occupancy, and all but one (with a very low score) showed higher Pol III occupancy in the KO compared with the WT samples (panel J). Thus, the SAP both improves similarity of replicates and reveals biological differences, even when these are quite uniform for all loci.

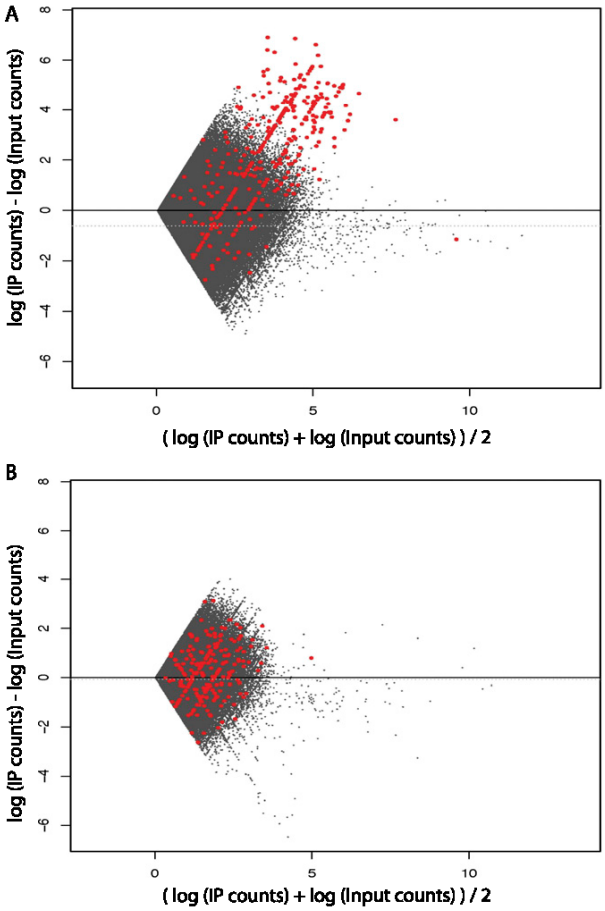

Figure 3. The spike chromatin can be used for quality control. Mean-difference scatter plot of human Pol III genome bin counts (in log scale). Red dots indicate genomic bins that overlap with Pol III loci. The genome was binned into 400-bp bins (corresponding to a typical Pol III gene length [~100 bp] extended by 150 bp in both the upstream and downstream directions). Zero-count bins were filtered out prior to plotting. (*A*) An example of a good-quality sample (90_R1). (*B*) An example of a poor-quality sample (97.5_P1).

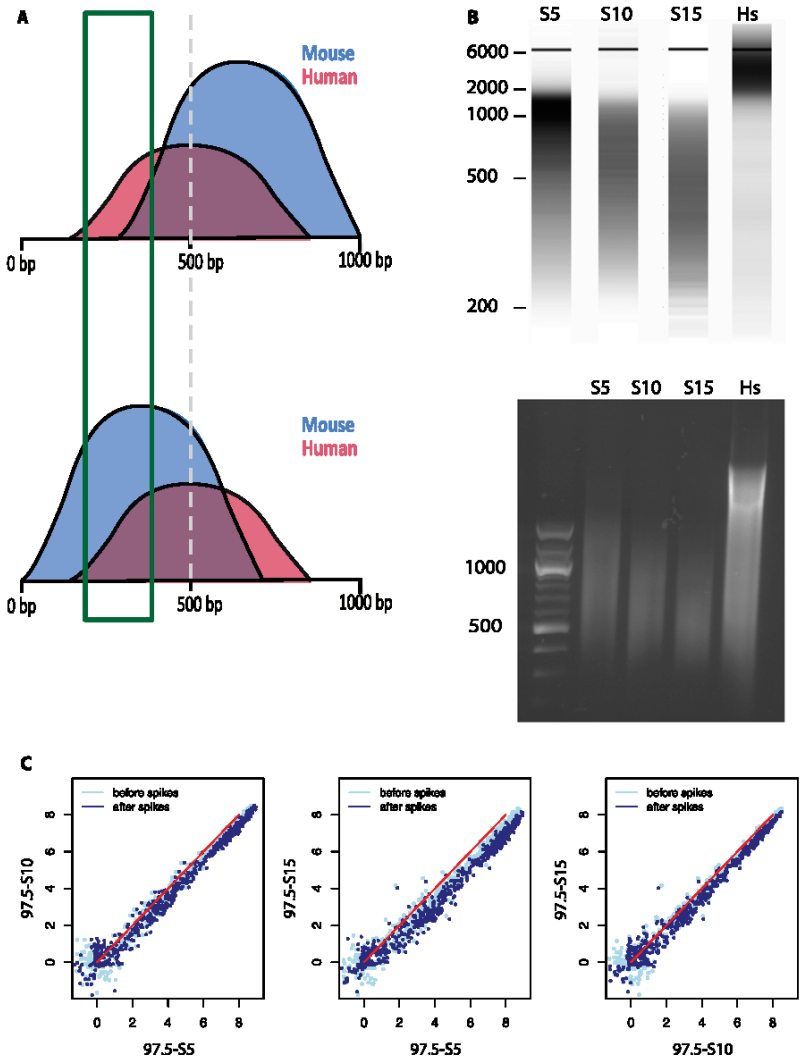

Figure 4. The SAP tolerates sample-to-sample differences of average chromatin fragment length. (*A*) Illustration of two hypothetical cases. (*Top*) The mouse chromatin sample (blue) is sonicated to an average size >500 bp; (*bottom*) the average size is <500 bp. The human chromatin (red) used to spike the samples is from the same batch and has an average size of 500 bp. Size selection from 200 to 400 bp is expected to result in a smaller proportion of mouse chromatin in the first case than in the second case. (*B*) Size representation obtained by fragment analyzer (*top*) and 1% agarose gel electrophoresis (*bottom*) of three mouse chromatin samples sonicated for 5 (S5), 10 (S10), and 15 (S15) cycles of 10 sec, as indicated *above* the lanes. The position of DNA size markers (in bp) is indicated on the *left*. The last lane shows the human chromatin spike sample. (*C*) Scatter plots showing the relation of mouse Pol III loci scores before and after spike adjustment for the three pairs of samples sonicated for different amounts of time. The Pearson and Spearman correlations before and after spike adjustment were as follows: 97.5_S5 versus 97.5_S10, 0.9927→0.9935 and 0.9678→0.9653; 97.5_S5 versus 97.5_S15, 0.9900→0.9885 and 0.9728→0.9663; and 97.5_S10 versus 97.5_S15, 0.9917→0.9926 and 0.9626→0.9636.

Improvement of Pol II ChIP-seq biological replicate similarity by spike adjustment

In the examples above, we used a method to calculate preliminary scores (Fig. 2, step 4) that is tailored to ChIP-seq experiments where the total genomic target of the factor of interest is relatively small and where, therefore, the tags mapping to this target represent a small percentage of the total amount of tags aligning onto the genome, as is the case for many factors (Landt et al. 2012). Indeed, for Pol III occupancy, tags mapping to known targets for both human and mouse Pol III (Canella et al. 2010, 2012; Renaud et al. 2014) represented 0.01%–1% of the total number of aligned tags (see Supplemental Table S1A,B). To determine whether the spike adjustment method might be more generally applicable, we applied it to chromatin samples immunoprecipitated with anti-POLR2B antibodies, and we calculated preliminary scores around TSSs using the SPP software (https://sites.google.com/a/brown.edu/bioinformatics-in-biomed/spp-r-from-chip-seq) (Kharchenko et al. 2008). The samples, referred to as RPB2_95 and RPB2_90 (see Table 1), contained different percentages of human chromatin (which was managed in the analysis by the species-specific scaling) (step 2 in Fig. 2) but otherwise were derived from the same batch of mouse chromatin and processed similarly (for numbers of tags aligned to mouse and human genomes, see Supplemental Table S2A,B) and can thus be considered technical replicates. We calculated Pol II scores in mouse regions extending from −250 to +250 bp around 11,217 annotated TSSs selected to be separated by at least 1000 bp from any other annotated TSS or polyadenylation site (see Le Martelot et al. 2012).

Figure 6A, left and right panels, show ECDF graphs of the samples after SPP score calculation, or after SPP score calculation and spike adjustment. The replicates were of high quality such that they were very close even before spike adjustment. Nevertheless, spike adjustment decreased the Kolmogorov-Smirnov distance between the two samples by more than half. The improvement is also visible in the scatter plot in Figure 6B, showing a tightening of the scores along the x = y line after spike adjustment. Thus, spike adjustment performs well not only for samples immunoprecipitated with an antibody targeting Pol III, but also for samples immunoprecipitated with an antibody targeting Pol II. Moreover, it can be applied to scores calculated by a method other than the one we specifically developed for Pol III occupancy. As further discussed below, this method is thus likely to be widely applicable.

Discussion

We describe a normalization method for ChIP-seq experiments that is not confined to computational treatment of the data but includes an experimental step, namely the addition of an internal reference to each sample. This internal reference consists of a small

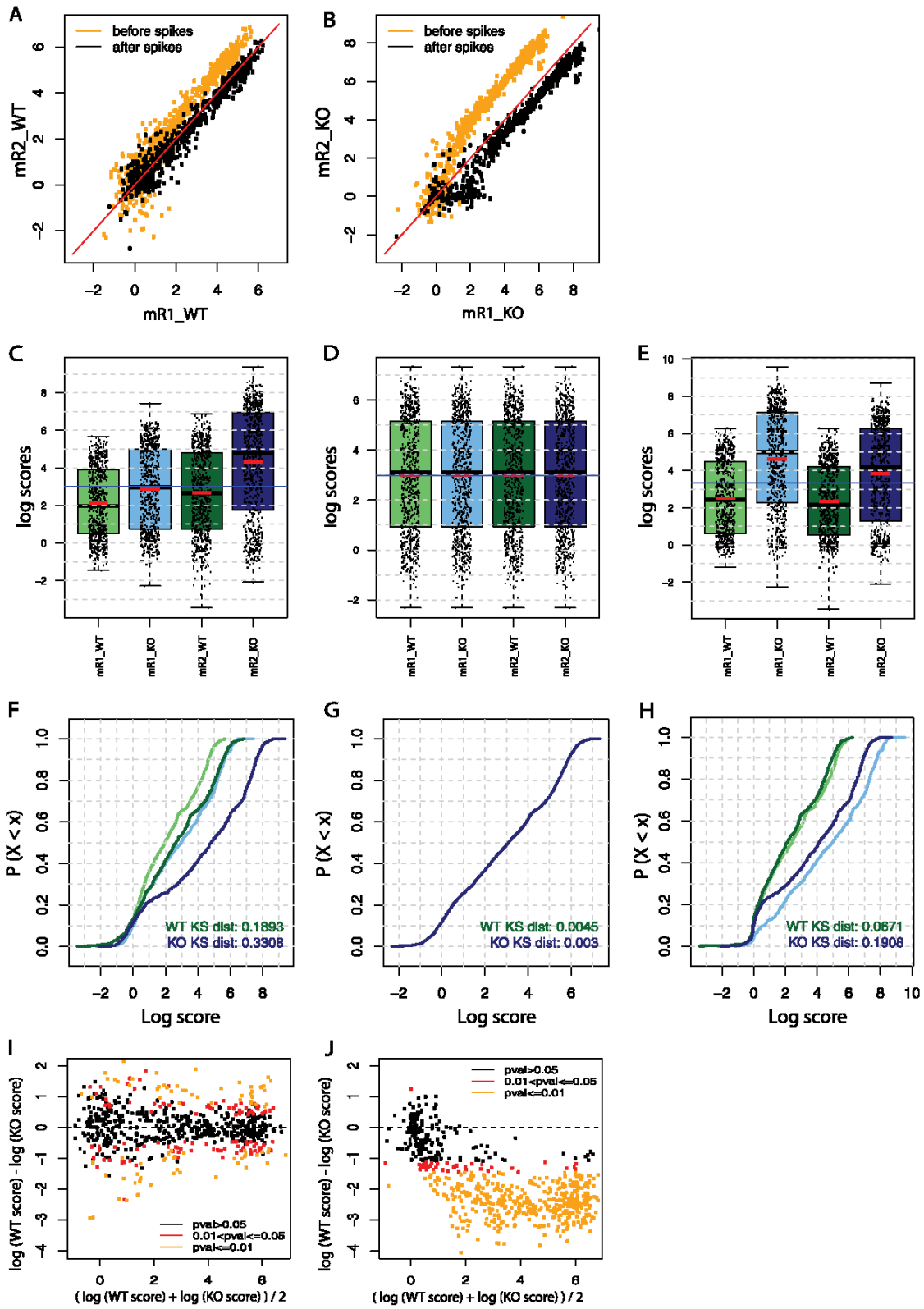

Figure 5. (Legend on next page)

amount of chromatin (spike) from a different species than the chromatin being tested, but a species close enough that the factors of interest share conserved epitopes, in our case human chromatin added to mouse chromatin. The internal reference is mixed with the experimental sample and undergoes all experimental steps following fragmentation of the chromatin, i.e., immunoprecipitation, library preparation, and sequencing. The method is related, in its principle of introducing an internal reference into each sample, to the method recently described by Loven et al. (2012) to normalize RNA-seq data. In that case, a synthetic RNA standard is added to each RNA sample to be analyzed in proportion to the starting number of cells, thus allowing quantification of RNA relative to starting cell number (Loven et al. 2012).

We show that the spike signal allows quality control. Indeed, it is in principle affected only by experimental (rather than biological) variations, and thus allows one to pinpoint dubious experimental samples that should be considered with circumspection and possibly discarded. For samples passing this quality control test, the SAP both improves similarity between replicates, without disrupting the distribution of the data, and reliably reveals true biological differences. Thus, on one hand, spike adjustment prevents the erroneous perception of differences when there are no genuine differences in protein occupancy; i.e., it reduces false-positive calls. On the other hand, it allows reliable recognition of real differences in occupancy; i.e., it also reduces false-negative calls.

The amount of spike material to be added to the sample should be as low as possible to give a robust spike signal and yet to contribute as few ambiguous tags as possible. This amount will vary with sequencing depth and size of the ChIP genomic target (for an exploration of this relationship, see Methods). We tested adding different amounts of human "spike" chromatin to the mouse chromatin and found that for our experiments, 2.5% was sufficient to provide a robust spike signal (Fig. 3). It might be advantageous to use as much as 5% spike chromatin because this may allow the "rescue" of poorer quality experimental samples. On the other hand, an increase in spike material might result in an increase in the number of ambiguous tags, i.e., tags that map to both the mouse and the human genomes, and this in turn might affect the mouse scores, especially for lowly occupied genes near the detection limit and in genes highly conserved in mouse and humans, as these tags are removed from the analysis. Thus, for analyses focusing on individual gene scores rather than on score distributions, it may be beneficial to add the ambiguous tags to the mouse tags, their most likely origin given that most of the starting material is mouse chromatin, with some attention to cases where a highly expressed spiked-in gene shares tags with a lowly expressed mouse gene.

The spike chromatin was added to the sample chromatin after the sonication step. Indeed, although it would in principle be preferable to mix the two materials before sonication, the difficulty of precisely quantifying tissue, cells, or the viscous presonication chromatin makes it impractical. Thus, when samples with different fragment size distributions are mixed with the same batch of sonicated spike chromatin, the proportion of spike chromatin fragments will differ in different samples. This is in principle corrected by the scaling to total number of tags, as this scaling is performed separately for the human and the mouse tags. Indeed, we found that the SAP gave very similar results for chromatin samples varying up to threefold in sonication time.

We tested the SAP in the study of Pol III occupancy, because this is one case where genome occupancy is likely to vary in a global manner and where current normalization methods are prone to failure. Indeed, Pol III transcription is, for example, elevated in cancer cells, and is globally diminished under certain conditions such as nutrient deprivation or other kinds of stress (for reviews, see White 2004; Goodfellow and White 2007; Gjidoda and Henry 2013). In yeast, a global Pol III transcription decrease upon nutrient deprivation is accompanied by a general decrease in Pol III occupancy at Pol III loci (Roberts et al. 2003, 2006; Oficjalska-Pham et al. 2006). Consistent with such global regulation, most known regulators of Pol III transcription act on general transcription factors used by all Pol III promoters such as TFIIIB or, in the case of the general Pol III repressor MAF1, on the polymerase itself (for reviews, see Geiduschek and Kassavetis 2006; Willis and Moir 2007; Ciesla and Boguta 2008). Indeed, we show here that deletion of the mouse *Maf1* gene leads to generally increased Pol III occupancy at Pol III loci in a tissue, the mouse liver. Such global changes in chromatin occupancy are likely to be more common than generally appreciated. For example, it has recently been shown that an increase in MYC protein leads to a general "transcriptional amplification," which is accompanied by increased MYC and Pol II occupancy at most promoters (Lin et al. 2012; Nie et al. 2012). The SAP can make detection of such global changes by ChIP-seq experiments more reliable.

Although we developed the SAP for the specific purpose of comparing Pol III occupancy under various biological conditions, the method is not limited to this particular application. We have also shown that the SAP improved similarity of replicate samples for Pol II ChIP-seq scores calculated with the SPP software; spike adjustment can thus be applied for ChIP-seq results other than Pol III and for scores calculated by different methods. Moreover, although the SAP is in principle limited by the availability of an antibody capable of recognizing the target of interest in different species, such antibodies are in fact common for many factors widely studied by ChIP-seq experiments, such as RNA polymerases and other members of the general transcription machinery, or histones and their modifications, as these are in general highly conserved in different species. Indeed, in this work we used antibodies that recognize human and mouse Pol III as well as human and mouse Pol II, and showed that for both of these factors, the method performs well. We have used human chromatin to spike mouse chromatin, but the reverse can be done, and chromatin from other species could be used for spiking according to needs, as long as the epitopes in the targets

Figure 5. Spike adjustment improves similarity between replicates and reveals genuine differences in Pol III occupation. (*A*,*B*) Scatter plots showing the relation of Pol III loci scores between the two WT (*A*) and the two *Maf1* KO (*B*) replicate samples before (orange) and after (black) spike adjustment. The red line corresponds to x = y. (*C*–*E*) Boxplot representations of the Pol III loci score distributions for the two WT samples (light and dark green, mR1_WT and mR2_WT) and the two *Maf1* KO samples (light and dark blue, mR1_KO and mR2_KO). The scores were normalized to total number of tags aligned onto the genome (*C*) followed by either quantile normalization (*D*) or spike adjustment (*E*). (*F*–*H*) Empirical cumulative frequency distributions functions (ECDFs) of the log scores of the indicated distribution. Samples were normalized to the total number of tags aligned onto the genome (*F*) followed by either quantile normalization (*G*) or spike adjustment (*H*). The Kolmogorov-Smirnov (KS) distance for the two WT (green lines) and the two *Maf1* KO (blue lines) samples is shown at the *bottom right* of each panel. (*I*,*J*) Mean difference scatter plots illustrating Pol III occupancy in WT and *Maf1* KO livers. Samples were normalized to the total number of tags aligned onto the genome followed by quantile normalization (*I*), respectively by spike adjustment (*J*). Scores for WT and KO conditions are the average of the two replicates. Loci with scores showing a significant difference in the WT versus *Maf1* KO samples are represented with yellow ($P \leq 0.01$) and red ($0.01 < P \leq 0.05$) dots.

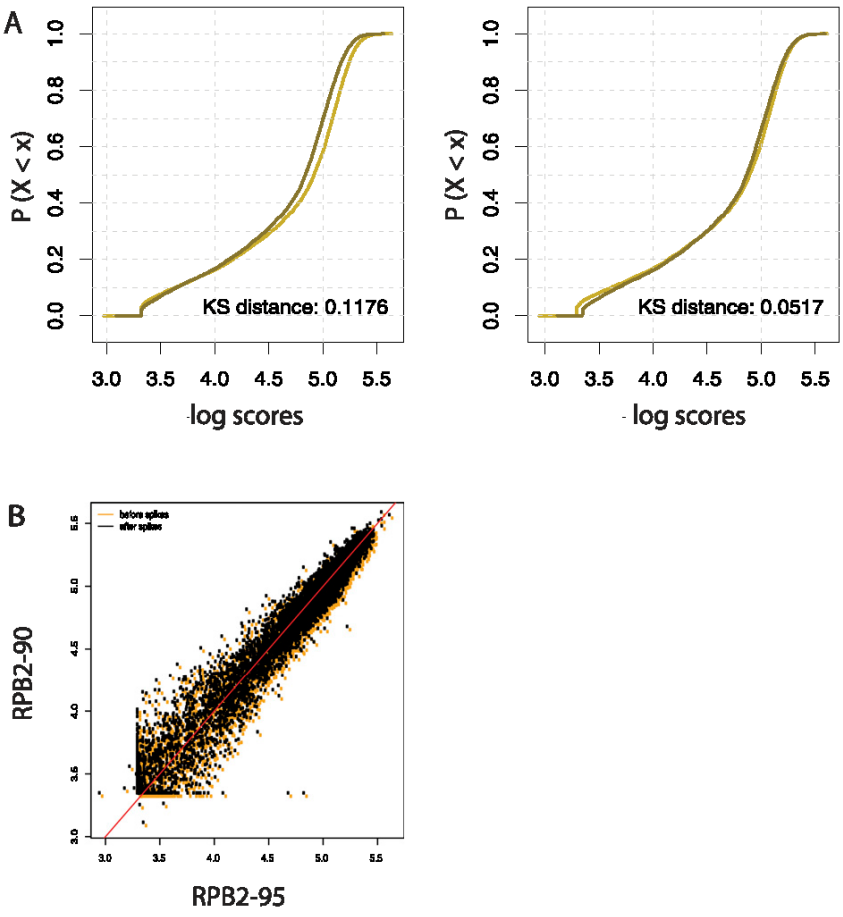

Figure 6. Spike adjustment improves the similarity of two Pol II ChIP-seq replicate experiments. (*A*) ECDFs of the scores of the indicated distributions. Preliminary scores were computed around the TSS (±250 bp) with the SPP software. The KS distance is shown at the *bottom right* of each panel. (Dark line) RPB2_90 sample; (light line) RPB2_95 sample. (*B*) Scatter plots showing the relation between the RPB2_90 and RPB2_95 scores before (orange dots) and after (black dots) spike adjustment. The red line corresponds to x = y.

studied are conserved. Further, when using cells or organisms expressing tagged proteins combined with antibodies directed against the tags, an internal control chromatin, i.e., chromatin from cells expressing a chosen factor carrying the same tag, can be designed. The spike adjustment method should thus be widely applicable.

Methods

Spiked mouse ChIP

Perfused C57BL/6 mice liver were homogenized in 4 mL of PBS containing 1% of formaldehyde and left in the same buffer for cross-linking for a total of 10 min. Nuclei were isolated as described in Ripperger and Schibler (2006). Nuclear lysis was performed in 1.2 mL of 50 mM Tris/HCl (pH 8.1), 10 mM EDTA, 1% SDS, 50 μg/mL PMSF, 1 μg/mL leupeptin. The nuclear lysate was then supplemented with 0.92 mL of 20 mM Tris/HCl (pH 8.1), 150 mM NaCl, 2 mM EDTA, 1% Triton X-100, 0.01% SDS, 50 μg/mL PMSF, 1 μg/mL leupeptin and sonicated with a Branson SLPe sonicator during 10 cycles of 10 sec at 50% amplitude, resulting in an average fragment size between 300 and 1000 bp. Between each sonication cycle, the chromatin was kept in an ice-cold bath during 20 sec. The samples 97.5_S5 and 97.5_S15 were sonicated with five and 15 cycles, respectively, of 10 sec each. Chromatin samples from three mice were pooled and de-cross-linked, and an aliquot was extracted for DNA quantification. Human HeLa cell chromatin was prepared as described in Canella et al. (2010), and DNA concentration was assessed.

ChIPs were performed with 30.8 μg of total DNA in the appropriate mouse/human chromatin ratio and 10 μL of rabbit serum immunized against a peptide 100% conserved in human and mouse POLR3D (CS681 antibody, C-terminal peptide CSPDFESLLDHKHR) (Chong et al. 2001). This antibody has been used extensively for ChIP-seq experiments, in both human and mouse cells (Canella et al. 2010, 2012; Renaud et al. 2014). For the anti-Pol II ChIPs, the commercial antibody anti-POLR2B (H-201; catalog no. sc-67318, Santa Cruz Biotechnology) recognizing human, mouse, and rat POLR2B was used. The ChIPs were performed as described previously in Forsberg et al. (2000) and Dhami et al. (2010) with a few modifications. Briefly, the chromatin samples were incubated with the antibodies overnight at 4°C. The next day, 20 μL of protein A–sepharose beads (CL4B GE Healthcare) was added and the samples were further incubated for 3 h. The beads were next washed once with 20 mM Tris/HCL (pH 8.1), 50 mM NaCl, 2 mM EDTA, 1% Triton X-100, 0.1% SDS; twice with 10 mM Tris/HCL (pH 8.1), 250 mM LiCl, 1 mMEDTA, 1% NP-40, 1% deoxycholic acid; and twice with TE buffer 1× (10 mM Tris-Cl at pH 7.5. 1 mM EDTA). Bound material was then eluted from the beads in 300 μL of elution buffer (100 mM $NaHCO_3$, 1% SDS), treated first with RNase A (final concentration 8 μg/mL) during 6 h at 65°C and then with proteinase K (final concentration 345 μg/mL) overnight at 45°C. The next day, the samples were purified with a PCR clean-up kit from Macherey Nagel and eluted in 50 μL of elution buffer. Sample 97.5_P1 was prepared as described above except that 1.5% of the immunoprecipitation supernatant was added back to the bead-eluted immunoprecipitated material.

Ultra-high-throughput sequencing

Ten nanograms of DNA from each ChIP was next used to prepare sequencing libraries according to the Illumina ChIP-seq DNA sample prep protocol (Illumina, catalog no. IP-102-1001), except that size selection of the samples was performed after, rather than before, library amplification. Sequencing libraries were loaded onto one lane of a HiSeq 2000 flow cell and sequenced at 100 cycles. For each condition, we sequenced input chromatin sample and the corresponding ChIP sample(s).

Analysis method principle

Samples contain a fixed amount of added-in reference (human) chromatin (spike). We assume that any variation in the background-adjusted counts from this constant reference chromatin

reflects technical experimental variations and that, therefore, a scaling factor estimated from the reference chromatin can be used to adjust tag counts in the experimental chromatin. Tags are assigned to the reference (human) or the experimental (mouse) chromatin and analyzed separately, each according to the model below. For both, the input samples are used for computing background-adjusted counts. To simplify notation, we consider that there is only one ChIP sample per condition, indicated by the index k. We assume, as in Enroth et al. (2012), that tags in the ChIP sample come from the following sources: specific binding to the antibody (true enrichment), nonspecific binding (to the antibody and the beads), and random noise.

The genome is partitioned into segments roughly the size of the regions of interest. Tag counts are computed for all such genomic segments. The probability distribution for the nonspecific tag counts is denoted as x_i, where i indicates a genomic segment (or $x_{i,k}$ for segment i in sample k). The distribution of the specific tags for condition k is denoted as $y_{i,k}$. The observed counts for the segments in the input sample are denoted as $b_{i,k}$ and are a multiple of $x_{i,k}$ with experimental errors $\varepsilon_{i,k}$:

$$b_{i,k} = \gamma_k x_{i,k} + \varepsilon_{i,k}. \quad (1)$$

For the ChIP samples, the observed counts $z_{i,k}$ are given by

$$z_{i,k} = \alpha_k y_{i,k} + \beta_k x_{i,k} + \varepsilon_{i,k}, \quad (2)$$

where $\alpha_k y_{i,k}$ are the specific tag counts corresponding to protein occupancy scores (signal), $x_{i,k}$ is the nonspecific tag distribution, as in Equation 1, and $\varepsilon_{i,k}$ is random noise. Equation 1 is used to estimate $\beta_k x_{i,k}$ in Equation 2.

Analysis method principle: preliminary score calculation for Pol III data

Our goal is to estimate the signal counts in regions of interest, namely $\alpha_k y_{i,k}$ in Equation 2. A key assumption is that the nonspecific segment counts in ChIP are proportional to their observed input segment counts. When most segments are not enriched by ChIP, this implies a linearity of segment counts in the ChIP sample versus the input sample. As shown in Supplemental Figure S1, this is indeed the case for our data, in which tags mapping to the regions of interest (400-bp bins overlapping with "Pol III loci," i.e., annotated Pol III genes [whether occupied by Pol III or not] as well as other previously identified Pol III–occupied loci; for the list, see Tables S2 [human loci] and S3 [mouse loci] in Renaud et al. 2014) represent a small percentage of the total amount of tags aligning onto the genome (0.01%–1%) (see Supplemental Table S1A,B). To adjust for variation in the amount of specific counts in segments of interest, i.e., here Pol III loci, we consider the signal $\alpha_k y_{i,k}$. Formally, from Equation 2,

$$\widehat{\alpha_k y_{i,k}} = z_{i,k} - \widehat{\beta_k x_{i,k}}, \quad (3)$$

where β_k is estimated from 400-bp genomic bin counts outside of the regions being scored. In practice, using the observed background (Equation 1) we estimate them as the positive residuals of the regression of ChIP counts $z_{i,k}$ on input counts:

$$\widehat{w_{i,k}} := \max\left(0, \widehat{\alpha_k y_{i,k}}\right). \quad (4)$$

The above scoring scheme is applied to calculate preliminary signal counts in both human and mouse samples independently.

Note that the principle of the SAP can also be performed successfully with simple log ratio scores (of ChIP with input, data not shown), as well as SPP scores (Fig. 6; Kharchenko et al. 2008).

Analysis method principle: determination of the spike adjustment factor

For the spike chromatin, we expect that background-adjusted counts should in principle be identical from sample to sample and that any difference reflects technical experimental variations. Thus, we use the human spike chromatin to compute a scaling factor to adjust for different yields in specific background-subtracted counts. Let $\widehat{w_{j,k}}$ and $\widehat{w_{j,r}}$ be the set of positive residuals computed from Equation 4 for a single sample k and a reference r. In practice, as reference we take the mean of positive residuals across all samples. Then the spike-adjustment scaling factor for sample k can be written using the means of signals in spike chromatin as

$$\eta_k := mean_k\left(\widehat{w_{j,k}}\right) / mean_r\left(\widehat{w_{j,r}}\right) = \sum_j \widehat{w_{j,k}} \Big/ \sum_j \widehat{w_{j,r}}, \quad (5)$$

where the index j is used instead of i to indicate that only a selected set of regions with reliable signals in the spike material is used in Equation 5.

The adjustment is then applied to the spike material for quality control and to the experimental chromatin to obtain adjusted protein occupancy scores:

$$\widetilde{w_{i,k}} := \widehat{w_{i,k}} / \widehat{\eta_k}, \quad (6)$$

where the tilde symbol ($\sim$) is used to refer to scores obtained after spike adjustment. The $\widetilde{w_{i,k}}$ values are non-negative and can be used for analysis of relative occupancy in linear or log scale.

To obtain (log) ratios between the counts in the IP sample and in the input sample, we use the estimator:

$$\widetilde{Lz_{i,k}} = \log_2\left(\frac{\widehat{w_{i,k}} + \widehat{\beta_k x_{i,k}} + pc}{b_{i,k} + pc}\right), \quad (7)$$

where the pseudo counts (pc) are typically set to one but can be set higher to regularize ratios. In regions of high occupancy, $\widetilde{Lz_{i,k}}$ is positive, whereas in regions where $\widetilde{w_{i,k}}$ is very small or zero, the log ratio can be negative. These are the (log) scores we used in our analysis (Figs. 4–6).

Analysis method principle: sequencing depth and spike percentage

The calculation of the spike adjustment factor in Equation 6 is based on the mean of the sum of n signals in regions that, for us, correspond to annotated Pol III genes (whether or not occupied by Pol III) and other previously identified Pol III–occupied loci (Renaud et al. 2014). In principle, any set of known regions enriched in the factor of interest can be used. The efficiency of spike adjustment depends on sequencing depth and percentage of spike material. Here we make an estimate of the standard error of the adjustment factor considering the random variation of tag sampling. The adjustment factor is the ratio of the estimated means for the regions used (Equation 5). The sum of signals used for correction can be estimated as such: For the data in Figure 5, the sequencing depth is $R \approx 1.3 \times 10^8$. The spike percentage is s = 2.5%, and signal content in the entire sample, computed for our set of 700 loci, is p ≈ 0.2%. Therefore, the total signal count sum is $S = R \times s \times p \approx 6500$. Of the 700 human Pol III loci studied previously (Renaud et al. 2014), we singled out about 500 significantly occupied loci, which account for >90% of all Pol III loci counts ($S \approx 6000$). The mean count per locus used for adjustment is thus about $S/n \approx 13$, but it is the precision of S that determines the precision of the adjustment factor. Under the classic Poisson assumption for sampling error, the theoretical relative error r = sqrt(S)/S is about

0.013. For the adjustment factor, which is the ratio of two such quantities, the relative error is the double, thus ~2.5%. To halve the theoretical relative error, one needs about four times more sequence tags, for example by increasing the proportion of the spike material to s = 10%. If there are more counts in known sites in the spike chromatin, say p = 10%, then one could reduce the spike chromatin percentage or sequence less deeply. Exact conditions need, however, to be determined for the specific parameters of each experiment.

Data analysis: *tag alignment*

The 100-nt sequence tags obtained after ultra-high-throughput sequencing were mapped onto the UCSC genome versions mentioned in Supplemental Tables S1, A and B, and S2, A and B, via the eland_extended mode of ELAND v2e in the Illumina CASSAVA pipeline v1.8.2. Only the tags with perfect matches, which represented >85% of the data, were kept for the analysis. Tags sequenced more than 50 times were given a maximum score of 50.

For the Pol III samples, counts were assigned to previously defined lists of human and mouse annotated Pol III genes and Pol III–occupied loci (Tables S2 and S3 in Renaud et al. 2014). For each locus the annotated RNA-coding region (e.g., tRNA) was extended by 150 bp on each side. One tag sequence was worth one count, and fractional counts were attributed in the case of a partial overlap between tag and locus. For the Pol II samples, tag counts were attributed in the same manner to regions extended by 250 bp on each side of the 22,572 annotated RefSeq TSSs (human), and on 11,217 annotated TSSs selected to be separated by at least 1000 bp from any other annotated TSS or polyadenylation site (mouse) (Le Martelot et al. 2012). The total numbers of tags, with and without redundancy, aligned onto the mouse and human genomes, as well as the numbers of tags falling in either mouse or human Pol III loci, are listed in Supplemental Tables S1, A and B, and S2, A and B.

Data analysis: normalization for sequencing depth

We normalized the mouse and human tags separately. We took the median of the total numbers of aligned tags across all the samples. We used this median as a reference total count. We then scaled bin counts in all samples to obtain a new total sample count equal to the reference total count. The typical reference total count was 150 million tags for mouse and 3 million for human tags. The input samples were normalized to the same total reference count as the ChIP samples.

Data analysis: calculating preliminary scores

For the Pol III data, we calculated scores as the non-negative residuals of the regression of ChIP bin counts versus input bin counts (see Equations 2–4). For the Pol II data, we calculated spp scores (Fig. 6). The regression coefficients from Equation 3 were estimated based on genomic bin counts outside of the regions being scored. For the Pol III experiments, we thus used a set of 400-bp bins covering the genome (6,637,291 bins on the mouse genome and 7,739,205 on the human genome). For the Pol II experiments, we used 500-bp bins (5,309,835 bins on the mouse genome and 6,191,402 on the human genome). We calculated tag counts for all bins, for ChIP and input samples. After selecting bins that did not overlap with the regions to be scored, we performed a robust linear regression on ChIP versus input. We used the regression coefficients to compute $\widehat{\alpha_k y_{i,k}}$ in regions to be scored. The values $\widehat{w_{i,k}}$, which were background-adjusted, estimated the counts due to specific immunoprecipitation.

Data analysis: calculation of the spike adjustment factor and score adjustment

We used either a subset or all of the scored regions in the spike chromatin to calculate the score adjustment factor. Subselecting is inherent to our scoring method, since we select positive residuals only and set negative residuals to zero. Depending on the data analyzed, it might be appropriate to take upper quantiles or use a threshold score. The spike adjustment scaling (η) between two samples k and r was then computed as

$$\eta_k = \frac{\sum_j \widehat{w_{i,k}}}{\sum_j \widehat{w_{i,r}}},$$

where the $\hat{w}$'s were the preliminary scores in the human regions j for these two samples. The index r here indicates a "reference" sample. The spike adjustment factor η was then applied as scaling factor to adjust the corresponding mouse gene scores: $\widetilde{w_{i,k}} = \widehat{w_{i,k}}/\eta_k$. The example above considers the spike adjustment of one sample k with respect to a reference sample r. In practice, we adjusted multiple samples together. In our analysis and all figures, the reference was taken to be the mean of means of scores in all samples.

Data analysis: final scores for follow-up analysis

After spike adjustment, for final quantification we used the adjusted log ratios, as shown in Equation 7. The adjusted gene scores $\tilde{w}$ are still in linear scale. We re-added the estimated background and then took a log ratio with the observed background. These final scores were used in all figures in this manuscript.

Data access

The data from this study have been submitted to the NCBI Gene Expression Omnibus (GEO; http://www.ncbi.nlm.nih.gov/geo) under accession number GSE52049.

The CycliX Consortium

Nouria Hernandez,[1] Mauro Delorenzi,[2,3,4] Bart Deplancke,[5] Béatrice Desvergne,[1] Nicolas Guex,[6] Winship Herr,[1] Felix Naef,[5] Jacques Rougemont,[7] Ueli Schibler,[8] Teemu Andersin,[8] Pascal Cousin,[1] Federica Gilardi,[1] Pascal Gos,[8] Fabienne Lammers,[1] Sunil Raghav,[5] Dominic Villeneuve,[1] Roberto Fabbretti,[6] Volker Vlegel,[6] Ioannis Xenarios,[1,2,6] Eugenia Migliavacca,[1,6] Viviane Praz,[1,2] Fabrice David,[2,7] Yohan Jarosz,[2,7] Dmitry Kuznetsov,[6] Robin Liechti,[6] Olivier Martin,[6] Julien Delafontaine,[2,7] Julia Cajan,[5] Kyle Gustafson,[1] Irina Krier,[5] Marion Leleu,[2,7] Nacho Molina,[5] Aurélien Naldi,[7] Leonor Rib,[1] Laura Symul,[5] and Gergana Bounova[1,2]

[1]Center for Integrative Genomics, Faculty of Biology and Medicine, University of Lausanne, 1015 Lausanne, Switzerland
[2]Swiss Institute of Bioinformatics, 1015 Lausanne, Switzerland
[3]Bioinformatics Core Facility, Swiss Institute of Bioinformatics, 1015 Lausanne, Switzerland
[4]Department of Oncology and Ludwig Center for Cancer Research, Faculty of Biology and Medicine, University of Lausanne, 1011 Lausanne, Switzerland
[5]Interfaculty Institute of Bioengineering, School of Life Sciences, Ecole polytechnique Fédérale de Lausanne, 1015 Lausanne, Switzerland
[6]Vital IT, Swiss Institute of Bioinformatics, 1015 Lausanne, Switzerland
[7]Bioinformatics and Biostatistics Core Facility, School of Life Sciences, Ecole polytechnique Fédérale de Lausanne, 1015 Lausanne, Switzerland
[8]Department of Molecular Biology, Faculty of Sciences, University of Geneva, 1211 Geneva, Switzerland

Acknowledgments

We thank Michaël Wiederkehr for his assistance. We thank Keith Harshman, Director of the Lausanne Technologies Facility, where all the ultra-high-throughput sequencing was performed, and Ioannis Xenarios, Director of the Vital-IT (http://www.vital-it.ch) Center for High Performance Computing of the Swiss Institute of Bioinformatics. Maintenance of the CycliX servers was provided by Vital-IT. This work was financed by CycliX, a grant from the Swiss SystemsX.ch initiative evaluated by the Swiss National Science Foundation, Sybit, the SystemsX.ch IT unit, SNSF grant 31003A_132958 to N.H., and the University of Lausanne.

References

Barski A, Cuddapah S, Cui K, Roh TY, Schones DE, Wang Z, Wei G, Chepelev I, Zhao K. 2007. High-resolution profiling of histone methylations in the human genome. *Cell* **129:** 823–837.

Canella D, Praz V, Reina JH, Cousin P, Hernandez N. 2010. Defining the RNA polymerase III transcriptome: genome-wide localization of the RNA polymerase III transcription machinery in human cells. *Genome Res* **20:** 710–721.

Canella D, Bernasconi D, Gilardi F, LeMartelot G, Migliavacca E, Praz V, Cousin P, Delorenzi M, Hernandez N. 2012. A multiplicity of factors contributes to selective RNA polymerase III occupancy of a subset of RNA polymerase III genes in mouse liver. *Genome Res* **22:** 666–680.

Chong SS, Hu P, Hernandez N. 2001. Reconstitution of transcription from the human U6 small nuclear RNA promoter with eight recombinant polypeptides and a partially purified RNA polymerase III complex. *J Biol Chem* **276:** 20727–20734.

Ciesla M, Boguta M. 2008. Regulation of RNA polymerase III transcription by Maf1 protein. *Acta Biochim Pol* **55:** 215–225.

Desai N, Lee J, Upadhya R, Chu Y, Moir RD, Willis IM. 2005. Two steps in Maf1-dependent repression of transcription by RNA polymerase III. *J Biol Chem* **280:** 6455–6462.

Dhami P, Bruce AW, Jim JH, Dillon SC, Hall A, Cooper JL, Bonhoure N, Chiang K, Ellis PD, Langford C, et al. 2010. Genomic approaches uncover increasing complexities in the regulatory landscape at the human SCL (TAL1) locus. *PLoS ONE* **5:** e9059.

Enroth S, Andersson CR, Andersson R, Wadelius C, Gustafsson MG, Komorowski J. 2012. A strand specific high resolution normalization method for chip-sequencing data employing multiple experimental control measurements. *Algorithm Mol Biol* **7:** 2.

Forsberg EC, Downs KM, Christensen HM, Im H, Nuzzi PA, Bresnick EH. 2000. Developmentally dynamic histone acetylation pattern of a tissue-specific chromatin domain. *Proc Natl Acad Sci* **97:** 14494–14499.

Geiduschek EP, Kassavetis GA. 2006. Transcription: adjusting to adversity by regulating RNA polymerase. *Curr Biol* **16:** R849–R851.

Gjidoda A, Henry RW. 2013. RNA polymerase III repression by the retinoblastoma tumor suppressor protein. *Biochim Biophys Acta* **1829:** 385–392.

Goodfellow SJ, White RJ. 2007. Regulation of RNA polymerase III transcription during mammalian cell growth. *Cell Cycle* **6:** 2323–2326.

Johnson DS, Mortazavi A, Myers RM, Wold B. 2007a. Genome-wide mapping of in vivo protein–DNA interactions. *Science* **316:** 1497–1502.

Johnson SS, Zhang C, Fromm J, Willis IM, Johnson DL. 2007b. Mammalian Maf1 is a negative regulator of transcription by all three nuclear RNA polymerases. *Mol Cell* **26:** 367–379.

Kharchenko PV, Tolstorukov MY, Park PJ. 2008. Design and analysis of ChIP-seq experiments for DNA-binding proteins. *Nat Biotechnol* **26:** 1351–1359.

Landt SG, Marinov GK, Kundaje A, Kheradpour P, Pauli F, Batzoglou S, Bernstein BE, Bickel P, Brown JB, Cayting P, et al. 2012. ChIP-seq guidelines and practices of the ENCODE and modENCODE consortia. *Genome Res* **22:** 1813–1831.

Le Martelot G, Canella D, Symul L, Migliavacca E, Gilardi F, Liechti R, Martin O, Harshman K, Delorenzi M, Desvergne B, et al. 2012. Genome-wide RNA polymerase II profiles and RNA accumulation reveal kinetics of transcription and associated epigenetic changes during diurnal cycles. *PLoS Biol* **10:** e1001442.

Li QH, Brown JB, Huang HY, Bickel PJ. 2011. Measuring reproducibility of high-throughput experiments. *Ann Appl Stat* **5:** 1752–1779.

Lin CY, Loven J, Rahl PB, Paranal RM, Burge CB, Bradner JE, Lee TI, Young RA. 2012. Transcriptional amplification in tumor cells with elevated c-Myc. *Cell* **151:** 56–67.

Loven J, Orlando DA, Sigova AA, Lin CY, Rahl PB, Burge CB, Levens DL, Lee TI, Young RA. 2012. Revisiting global gene expression analysis. *Cell* **151:** 476–482.

Mikkelsen TS, Ku M, Jaffe DB, Issac B, Lieberman E, Giannoukos G, Alvarez P, Brockman W, Kim TK, Koche RP, et al. 2007. Genome-wide maps of chromatin state in pluripotent and lineage-committed cells. *Nature* **448:** 553–560.

Nie Z, Hu G, Wei G, Cui K, Yamane A, Resch W, Wang R, Green DR, Tessarollo L, Casellas R, et al. 2012. c-Myc is a universal amplifier of expressed genes in lymphocytes and embryonic stem cells. *Cell* **151:** 68–79.

Oficjalska-Pham D, Harismendy O, Smagowicz WJ, Gonzalez de Peredo A, Boguta M, Sentenac A, Lefebvre O. 2006. General repression of RNA polymerase III transcription is triggered by protein phosphatase type 2A-mediated dephosphorylation of Maf1. *Mol Cell* **22:** 623–632.

Pluta K, Lefebvre O, Martin NC, Smagowicz WJ, Stanford DR, Ellis SR, Hopper AK, Sentenac A, Boguta M. 2001. Maf1p, a negative effector of RNA polymerase III in *Saccharomyces cerevisiae*. *Mol Cell Biol* **21:** 5031–5040.

Rahl PB, Lin CY, Seila AC, Flynn RA, McCuine S, Burge CB, Sharp PA, Young RA. 2010. c-Myc regulates transcriptional pause release. *Cell* **141:** 432–445.

Reina JH, Azzouz TN, Hernandez N. 2006. Maf1, a new player in the regulation of human RNA polymerase III transcription. *PLoS ONE* **1:** e134.

Renaud M, Praz V, Vieu E, Florens L, Washburn MP, L'Hote P, Hernandez N. 2014. Gene duplication and neofunctionalization: POLR3G and POLR3GL. *Genome Res* **24:** 37–51.

Ripperger J, Schibler U. 2006. Rhythmic CLOCK-BMAL1 binding to multiple E-box motifs drives circadian *Dbp* transcription and chromatin transitions. *Nat Genet* **38:** 369–374.

Roberts DN, Stewart AJ, Huff JT, Cairns BR. 2003. The RNA polymerase III transcriptome revealed by genome-wide localization and activity-occupancy relationships. *Proc Natl Acad Sci* **100:** 14695–14700.

Roberts DN, Wilson B, Huff JT, Stewart AJ, Cairns BR. 2006. Dephosphorylation and genome-wide association of Maf1 with Pol III-transcribed genes during repression. *Mol Cell* **22:** 633–644.

Rollins J, Veras I, Cabarcas S, Willis I, Schramm L. 2007. Human Maf1 negatively regulates RNA polymerase III transcription via the TFIIB family members Brf1 and Brf2. *Int J Biol Sci* **3:** 292–302.

Upadhya R, Lee J, Willis IM. 2002. Maf1 is an essential mediator of diverse signals that repress RNA polymerase III transcription. *Mol Cell* **10:** 1489–1494.

Vannini A, Ringel R, Kusser AG, Berninghausen O, Kassavetis GA, Cramer P. 2010. Molecular basis of RNA polymerase III transcription repression by Maf1. *Cell* **143:** 59–70.

White RJ. 2004. RNA polymerase III transcription and cancer. *Oncogene* **23:** 3208–3216.

Willis IM, Moir RD. 2007. Integration of nutritional and stress signaling pathways by Maf1. *Trends Biochem Sci* **32:** 51–53.

Received October 11, 2013; accepted in revised form March 31, 2014.

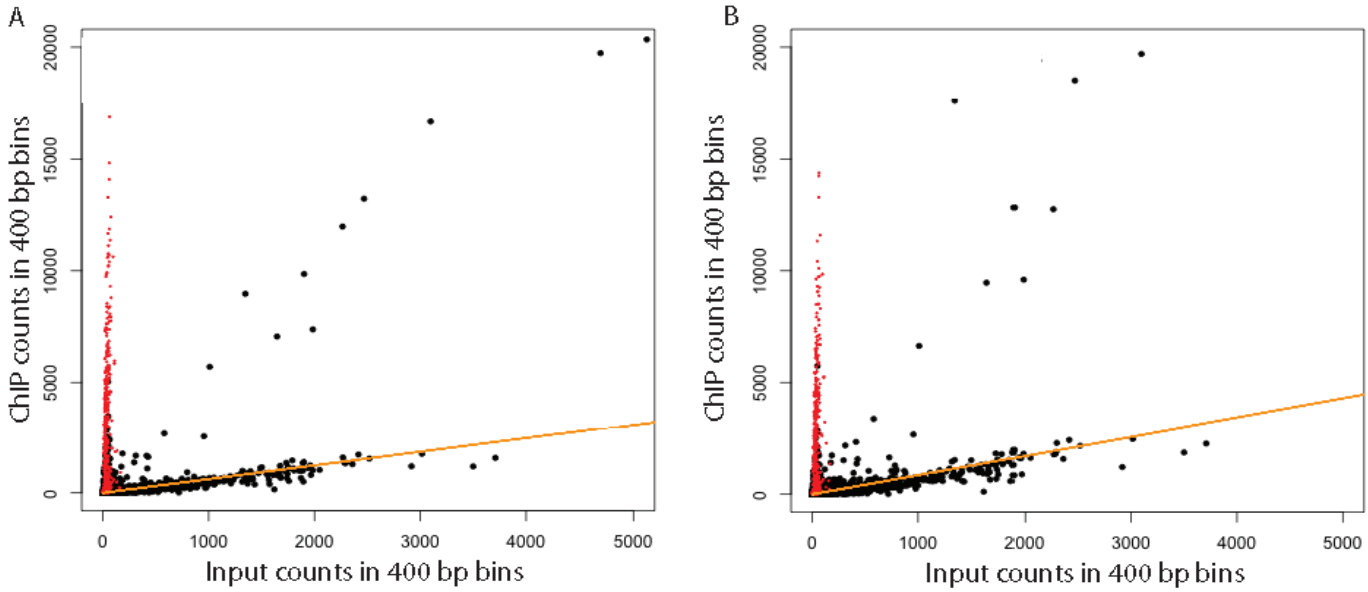

Figure S1. Scatter plots comparing the counts in 400 bp bins for the input 97.5 sample and either the 97.5_S5 ChIP sample (panel A) or the 97.5_S15 ChIP sample (panel B). Bins overlapping with pol III loci (see Table S3 in {Renaud, 2014 #45}) are shown in red. The robust linear regression line (excluding the bins corresponding to pol III loci) is shown in orange.

Supplemental tables S1, S2, can be found online at the address:

http://genome.cshlp.org/content/24/7/1157/suppl/DC1

Chapter IV – Role of Maf1 in Pol 3 transcription and translation in a mouse

Introduction

RNA polymerase 3 (Pol 3) transcribes a small set of non-coding RNA genes (Canella et al., 2010) involved in diverse cellular processes including protein translation, RNA maturation and splicing, and RNA polymerase 2 elongation (Dieci et al., 2007). In yeast, Pol 3 transcription is tightly regulated by nutrient availability and MAF1 has been identified as its main repressor (Boguta et al., 1997; Vannini et al., 2010). Under favorable growth conditions, Maf1 is inactivated by phosphorylation in a TOR complex 1 (TORC1) dependent manner, which results in its nuclear exclusion (Lee et al., 2009; Moir et al., 2006; Zaragoza et al., 1998). Under conditions of nutrient deprivation or stresses like DNA damage, TORC1 is inactivated, MAF1 becomes dephosphorylated and shuttles into the nucleus where it represses Pol 3 transcription (Cai and Wei, 2015; Lee et al., 2009). In mammalian cells, mTORC1 directly phosphorylates MAF1 on three residues (S60, S68, and S75) (Michels et al., 2010). Upon serum deprivation, MAF1 undergoes dephosphorylation (Reina et al., 2006) and represses Pol 3 transcription, but there is no clear evidence that this involves any shuttling between cytoplasmic and nuclear compartments.

tRNAs genes account for almost 2/3 of the Pol III transcriptome in the mouse (Canella et al., 2012; Renaud et al., 2014) and, with the 5S ribosomal RNA genes, are involved in protein translation. tRNAs control ribosomal elongation by bringing a new amino acid into the nascent polypeptidic chain. The production of a mature, fully functional tRNA involves several steps, all of which can be regulated. tRNA precursors are synthetized in the nucleus where they are then trimmed at the 5' and 3' ends by

RNase P and RNase Z, respectively, modified by addition of a CCA sequence and the 3' end, and exported into the cytoplasm where intron-containing tRNA are spliced (Lodish et al., 2000). At several steps during this maturation process, tRNA residues are modified; for example, an adenine in the first position of the anticodon is frequently deaminated to inosine, a modification that occurs in the tRNA precursor (Torres et al., 2015).

The regulation of the various steps in forming a mature tRNA can have consequences on translation. Thus, the ratio of nuclear/cytoplasmic tRNAs is critical as an imbalance in this ratio is followed by a shutdown of translation (Calvo et al., 1999). Moreover, several tRNA modifications impact on translation efficiency. Mice lacking both tRNA methylases DNMT2 and NSUN2 have tRNA methylation defects and a reduced protein translation generating developmental defects (Tuorto et al., 2012). Translation is also regulated by the levels of amino-acylated tRNAs. tRNAs are bound to the appropriate amino acid by several aminoacyl tRNA synthetases. In yeast, elevation of the number of non amino-acylated tRNAs by amino acid deprivation activates GCN2, the primary responder to amino acid deprivation and a kinase of the translation initiation factor eIF2-α (Wek et al., 1995; Zaborske et al., 2009). Phosphorylated eIF2-α blocks recycling of the ternary complex eIF2-α-GTP-tRNAi^{met} and thus inhibits translation (Jackson et al., 2010).

Maf1 indirectly controls tRNAs processing by regulating the rate of Pol 3 transcription. Yeast cells lacking Maf1 have increased levels of precursor tRNAs in the nucleus due to saturation of the yeast exportin Los1 responsible for tRNA trafficking between nucleus and cytoplasm (Karkusiewicz et al., 2011). In the mouse, in addition to its role in controlling Pol 3 transcription, MAF1 also acts for metabolic economy, as mice lacking MAF1 in the entire body are resistant to diet-induced obesity (Bonhoure et al., 2015). Although the mechanism leading to this phenotype is not entirely clear, one contributing factor is likely the higher production of precursors tRNAs in the Maf1 KO mouse that are then degraded. This futile cycle of production / degradation of pre-tRNAs may explain, at least in part, the higher energy expenditure displayed by these mice, and thus their inefficient metabolism. Another contributing factor is factor altered lipid metabolism. As for tRNAs, lipid production and lipophagy are both

increased in the Maf1 KO mice liver, which creates another energy-demanding futile cycle.

In addition to being lean and resistant to high fat diet-induced obesity, Maf1 KO mice are slightly smaller than their wild-type counterparts (Bonhoure et al., 2015). Both phenotypes are puzzling given that knock-down of Maf1 expression with RNAi methods has been reported to lead to opposite effects in the fly (Rideout et al., 2012), the worm (Khanna et al., 2014), and in mouse liver (Palian et al., 2014). Thus, in the fly a decrease in Maf1 level leads to increase larvae volume and a specific deletion in the fat body of the fly larvae increases levels of $tRNAi^{met}$ which in turn increases protein translation. In C.elegans, increased Maf1 levels are followed by reduction of expression of Fasn and Acc1 genes and vice-versa. In mouse liver, Maf1 levels were reduced by targeted siRNA leading to increased levels of Fasn and Acc1 genes and thus increased de novo lipogenesis.

In mammalian cells, mTORC1 is known to regulate the phosphorylation state of MAF1, however, nothing is known about the connection between the feeding status of an animal and MAF1 regulation of Pol 3. In this study, we used wild-type and Maf1 KO mice that were either fasted or refed, i.e. whose metabolism switched from using mostly glucose as a carbon source to using mostly lipids, to examine Pol 3 regulation and the role of MAF1 in such regulation. We show that the removal of MAF1 results in widespread higher Pol III occupancy on pol III genes, and higher pre-tRNA accumulation. The effect is largest under fed conditions, indicating that MAF1 keeps Pol 3 transcription in check even under favorable conditions. We also show that the absence of MAF1 results in defects in translation, which can be explained by a deficiency in tRNA modifications. Thus, complete absence of MAF1 results in much higher synthesis of pre-tRNAs, but most likely in diminished amounts of mature and thus fully functional tRNAs, perhaps because the RNA maturation machinery becomes overwhelmed. This suggests that although reduced MAF1 always results in higher levels of Pol 3 transcription, maximum levels of fully functional tRNAs require precise MAF1 dosage.

Results

Fasting and re-feeding affects Pol 3 occupancy in mouse liver

In mammalian cultured cells, Pol 3 transcription is diminished after serum deprivation or rapamycin treatment (Felton-Edkins et al., 2003; Mauck and Green, 1974; Michels et al., 2010; Scott et al., 2001). To determine how feeding and fasting might affect Pol 3 occupancy in animals, we collected livers from wild-type (WT) mice that had either been fasted (WT_F) or fasted and refed for 4 hours (WT_R). We first monitored gene expression changes using the Affymetrix microarray technology. Gene ontology (GO) analysis (Figure 1A) for both upregulated and downregulated genes with a FDR < 0.05 showed significant differences in several categories, notably the "response to nutrient levels" as well as several metabolic process categories, confirming that liver metabolism is affected under these experimental conditions. Moreover, fasting led to downregulation of TORC1 activity as determined by the decreased phosphorylation of two of its direct targets, RPS6 and 4E-BP1, as well as to decreased activity ERK1/2 as determined by its decreased phosphorylation (Figure 1B).

We measured, as a proxy for Pol 3 transcription activity (Canella et al., 2010), genome-wide Pol 3 occupancy. For each condition, we pooled the livers of three mice and performed replicate chromatin immunoprecipitations with an antibody directed against the POLR3D subunit of Pol 3 followed by high throughput sequencing (ChIP-seq). As an internal reference for sample-to-sample normalization, we included in each immunoprecipitation a spike of human chromatin from a single pool, as previously described (Bonhoure et al., 2014). We calculated scores for a list of loci including annotated Pol 3 genes, whether occupied or not, as well as other Pol 3 occupied loci (see Table S3 in (Renaud et al., 2014)).A cut-off defining genes as "not occupied" or "occupied" was calculated as before (Renaud et al., 2014). As shown in the box plot in Figure 1C, the median of the Pol 3 occupancy scores decreased after fasting. However, loci with high scores under refed conditions (red and orange dots corresponding to top and second quintiles of WT_R scores) generally also had high

scores under fasting conditions, whereas genes in the third, fourth and fifth quintiles generally had lower scores under fasting conditions. The correlation plot in panel 1D illustrates the score changes on a gene per gene basis. Whereas most genes are below the x=y line, reflecting lower scores in the sample from fasted mice as compared to refed mice, genes with high scores tend to cluster along the x=y line. Indeed, the MvA plot in panel 1E confirms that many loci with intermediate scores but very few loci with high scores showed significantly lower occupancy under fasting conditions (red dots). Among the loci with lower occupancy were nearly all 5S genes, some tRNA genes and some SINEs; in contrast, the 4.5S genes as well as all the Pol 3 genes with type 3 promoters, including the occupied selenocysteine tRNA gene, did not show decreased Pol 3 occupancy in fasted liver (see Table S2).

Maf1 KO mice have higher Pol 3 occupancy than WT mice, and the effect is more pronounced in livers from refed mice than liver from fasted mice.

In serum-starved cells, Pol 3 repression is mediated in large part by the Pol 3 repressor MAF1. To determine the role of MAF1 for Pol 3 transcription in mouse liver, we checked Pol 3 occupancy in the livers of WT and Maf1 KO mice(Bonhoure et al., 2014, 2015). As shown in Figure 2A, out of 672 loci examined, there were more loci with scores above the cutoff in liver of refed mice as compared to liver of fasted mice (467 versus 419). In both conditions, these numbers were higher for the liver of Maf1 KO mice as compared to WT but the difference between the two was greater in the refed condition.

The distributions of Pol 3 loci scores for each condition in Figure 2B, revealed greater occupancy in the Maf1 KO mice livers in both refed and fasted state, with a larger increase in the refed condition. This is further illustrated with the MvA plots in Figure 2C.

Under refed condition (Figure 2C, left panel), out of the 467 loci bound by Pol 3 in either WT or Maf1 KO mice or in both, 399 displayed a statistically significant increase in Pol 3 occupancy in the Maf1 KO. These genes correspond to most tRNA

genes (265 out of 285), all but two 5S genes, all 4.5S genes, 8 out of 14 “other Pol 3 genes”, and more than 60% of the SINEs (Table S3). Under 8h fasted condition (Figure 2C, middle panel), 276 loci had a higher occupancy in the Maf1 KO liver than in the WT, and the score differences were smaller than those observed in the refed state (Table S4). Importantly, in Maf1 KO mice, Pol 3 occupancy scores were significantly decreased in 8h fasted relative to refed condition, as illustrated in the right panels of Figure 2D (see also Table S5 for the list of loci), indicating that there are Maf1-independent mechanism to reduce Pol 3 occupancy in response to fasting.

We next focused our analysis on the tRNA genes, which constitute almost 65% of the genes transcribed by Pol 3 (433 out of 672). To determine whether the absence of MAF1 might alter Pol 3 occupancy differentially on different tRNA isotype classes, we compared the cumulative scores for all tRNA genes for each isotype under refed (Figure 2D) and 8h fasted (Figure 2E) conditions. The tRNA isotypes were divided into 22 classes (tRNA^{Met} genes were considered separately from tRNA^{MetInit} genes). In both conditions, the increase in Pol 3 occupancy associated with the Maf1 KO was general. We divided the isotype classes into quantiles according to Pol 3 occupancy in the WT samples, and observed that the various isotypes remained in the same quantile in the Maf1 KO samples, both under refed of 8h fasted condition. However, isotypes in the more occupied quartiles displayed a larger difference in Pol III occupancy in the Maf1 KO samples than less occupied quantiles, an effect especially marked in the refed samples. We finally analyzed Pol 3 occupancy for each tRNA locus in refed or 8h fasted condition respectively in figure 2F and G to check if Maf1 regulation could be specific for some tRNAs. Circular plots represent here the ratio of occupancy in Maf1 KO cells over occupancy in WT. Loci where score was below the cut-off in both WT and Maf1 KO were set with a ratio at 0. In refed condition all the occupied tRNA were showing an increase in Pol 3 occupancy following the KO of Maf1 with a range going from 1.7 to almost 10 fold for the tRNA^{IMet}. 8h fasted condition showed similar pattern but with only 4 tRNAs having a occupancy being statically higher by at least 1.4 fold in the WT. Altogether these results identify MAF1 as a global inhibitor of Pol 3 transcription in mouse liver but also indicate an alternative way, in the absence of MAF1 to repress Pol 3 transcription after fasting.

Maf1 KO mice have higher levels of pre-tRNAs.

To determine the effects of increased Pol 3 occupancy in the Maf1 KO mice, we analyzed by RNA-seq a pool of liver RNA collected from three 16h fasted mice. We attributed sequence tags to either pre-tRNAs or processed tRNAs according to the strategy depicted in Figure 3A. Tags starting or ending precisely at the annotated 5' or 3' ends (which correspond to the processed 5' end 3' ends), or spanning an exon-exon junction, were assigned to processed tRNAs. Tags containing upstream or downstream sequences, or intron sequences, were allocated to precursor tRNAs. As shown in the scatterplots in Figure 3B, total tRNA levels were generally higher in the KO than in the WT (left panel), as were pre-tRNA levels (right panel). In contrast, there appeared to be no systematic increase in processed tRNAs (middle panel), although in this case the relatively low number of tags that could be attributed uniquely to processed tRNAs prevented a firm conclusion. To confirm these results, we performed northern blots with probes specific to processed or precursor tRNAs. As shown in Figures 3C and 3D, levels of mature tRNAs were unchanged in Maf1 KO and wild-type mouse liver in both 16h fasted and refed conditions whereas levels of an isoleucine pre-tRNA were clearly increased in the Maf1 KO. This specific increase in pre-tRNA is also illustrated in Figures 3E and 3D, showing Fluorescent *In Situ* Hybridizations (FISH) of liver sections performed with a probe matching the entire tRNA leu1911 intron (precursor RNA) or a probe spanning the exon-exon junction of the same tRNA (mature). The pre-tRNA signal (red) is mostly nuclear and clearly increased in the Maf1 KO (panel E). In contrast, the processed tRNA signal is mostly cytoplasmic and similar in the WT and Maf1 KO samples (panel F).

The Maf1 KO mice have a decreased translation in liver.

In other systems, down-regulation of Maf1 has been reported to result in an increase in animal size and in translation (Rideout et al., 2012). To assess the general levels of translation in the Maf1 KO mice, we first obtained polysome profiles by sucrose gradient sedimentation (Figure 4A). We repeatedly observed a reduction of the

polysomal fraction for the Maf1 KO mice under refed conditions, suggesting a reduced rate of protein synthesis. To confirm these results, we injected mice with low doses of puromycin, a structural analog of aminoacyl-tRNA and more particularly of tyrosyl-tRNA. Mice were sacrificed 30 minutes later and the incorporation of puromycin into nascent chains of amino acids, which reflects on-going translation (Schmidt et al., 2009), was monitored by western blots performed with antibodies directed against puromycin. As shown in Figure 4B, we observed a decrease in total protein synthesis in the Maf1 KO mice, which incorporated as little as half of the puromycin as compared to wild-type (Figure 4C). The same protein lysates were analyzed by dot blots with similar results (Figure 4D). We confirmed these results by immunohistochemistry of puromycin-injected mice livers, using the same anti-puromycin antibody as in panels B and D (Figure 4E). The cytoplasmic red signal, corresponding to incorporated puromycin, was again clearly decreased in the Maf1 KO mice. If translation is decreased in the Maf1 KO mice, one might expect a smaller amount of total proteins per cell. As shown in Figure 5F, we indeed measured a smaller protein content relative to DNA levels in the Maf1 KO livers. A similar result was obtained with MEFs isolated from WT and Maf1 KO mice (Figure 4G). Moreover, these Maf1 KO MEFs were smaller than the wild-type MEFs (Figure 4H), consistent with decreased translation.

tRNAs from Maf1 KO mice liver have lower level of modifications

The observation that Maf1 KO livers display reduced levels of translation was surprising as the lack of MAF1 was expected to result in higher levels of tRNAs and thus higher levels of translation, as reported in other systems. Our results indicated elevated levels of pre-tRNAs and normal levels of processed tRNAs, providing no simple explanation for a reduced translation. We therefore examined whether the processed tRNAs were fully modified. We used a RT-qPCR method based on the ability of reverse transcriptase to pass through certain modified nucleotides in the presence of high (1 mM), but not low (10 μM) concentration of dNTPs (Figure 5A) (Belin et al., 2009). We first looked at the modification levels of four tRNAs using

primer that do not distinguish between the precursor and processed forms (see Figure S1 for the list of primers) and observed a higher proportion of at least partially unmodified tRNAs in the Maf1 KO samples (Figure 5B). We also used sets of primers specific for the spliced forms of Leu1911 and Tyr27 tRNAs and again observed a modification deficiency (Figure 5C). We conclude that although the levels of mature length tRNAs are similar in WT and Maf1 KO mice, the levels of fully modified, and thus fully mature, tRNAs are lower in the Maf1 KO mice.

Figure 1

A

GO biological process	Adj. Pvalue
Response to nutrient levels	3.69×10^{-13}
Response to topologically incorrect protein	1.66×10^{-08}
Fatty acid metabolic process	$2,39 \times 10^{-08}$
Lipid homeostasis	4.7×10^{-08}
Response to unfolded protein	5.73×10^{-08}
Glucose metabolic process	9.41×10^{-08}
Monosaccharide metabolic process	1.22×10^{-08}
Regulation of cellular ketone metabolic process	1.53×10^{-08}

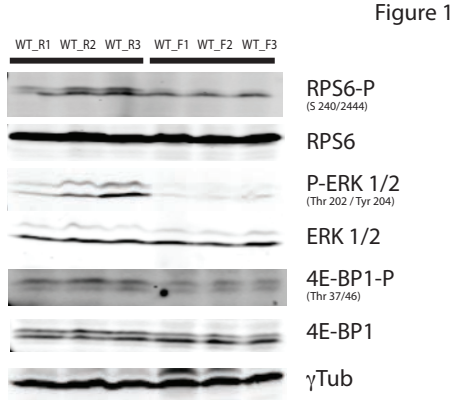

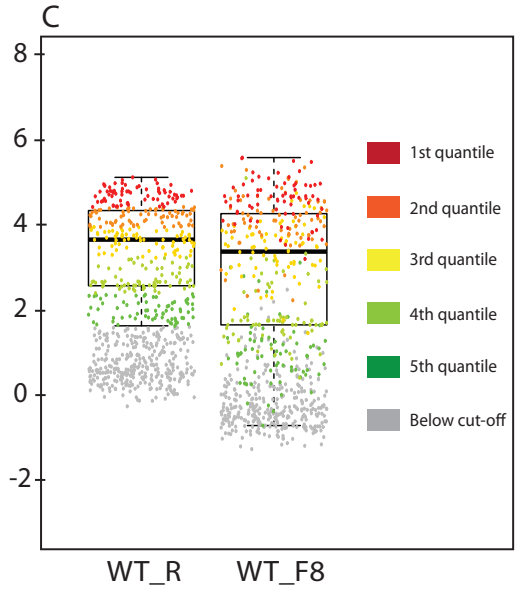

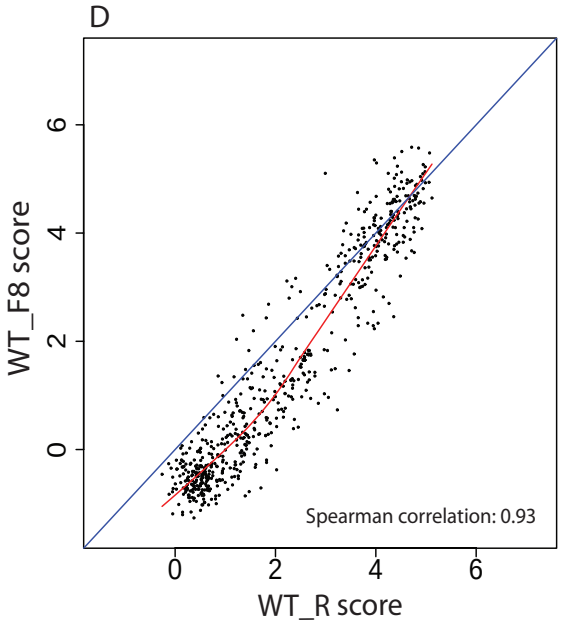

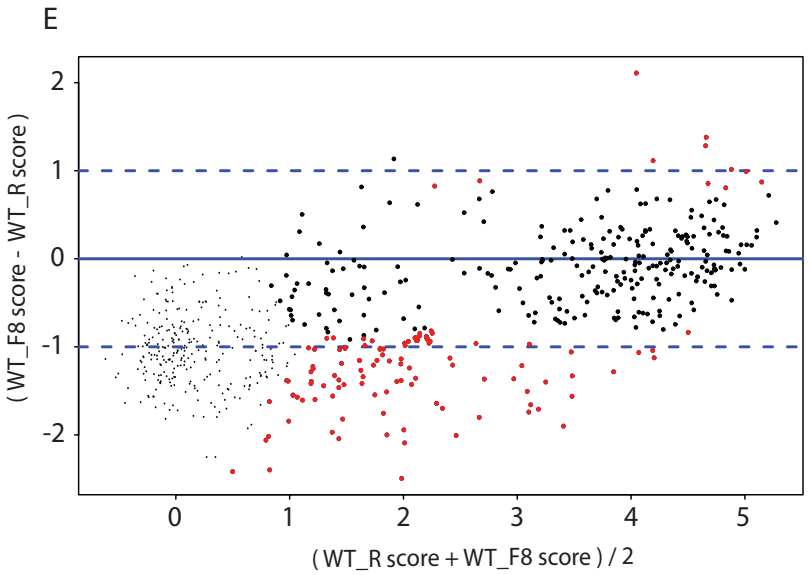

Figure 1. Pol 3 occupancy in mouse liver is lower under fasting conditions than under refed conditions. (A) GO analysis of genes differentially expressed (FDR < 0.05) between 16 h fasted samples and 4 h refed samples from microarray data. For each condition, we performed three microarray hybridizations, each with a pool of RNA originating from 3 different mice (9 mice per condition). (B) Immuno-blots performed with proteins extracted from the liver of three mice fasted or refed as in A. (C) Box plots indicating average Pol 3 occupancy scores for two replicate immunoprecipitations performed with pooled liver samples from three mice. The colored dots correspond to genes in different quantiles as indicated, the grey dots to genes with scores below the cut-off. (D) Scatter plot showing the correlation of Pol 3 occupancy scores for samples from refed (x-axis) or fasted (y-axis) mice. The x=y line is in blue, the regression line is in red. (E) Mva plot showing, for each analyzed locus, the average of the scores in the fasted and refed conditions (x-axis) and the log2 fold change in fasted versus refed conditions (y-axis). Loci with significant changes are indicated in red. See Table S2 for the corresponding scores and limma analysis.

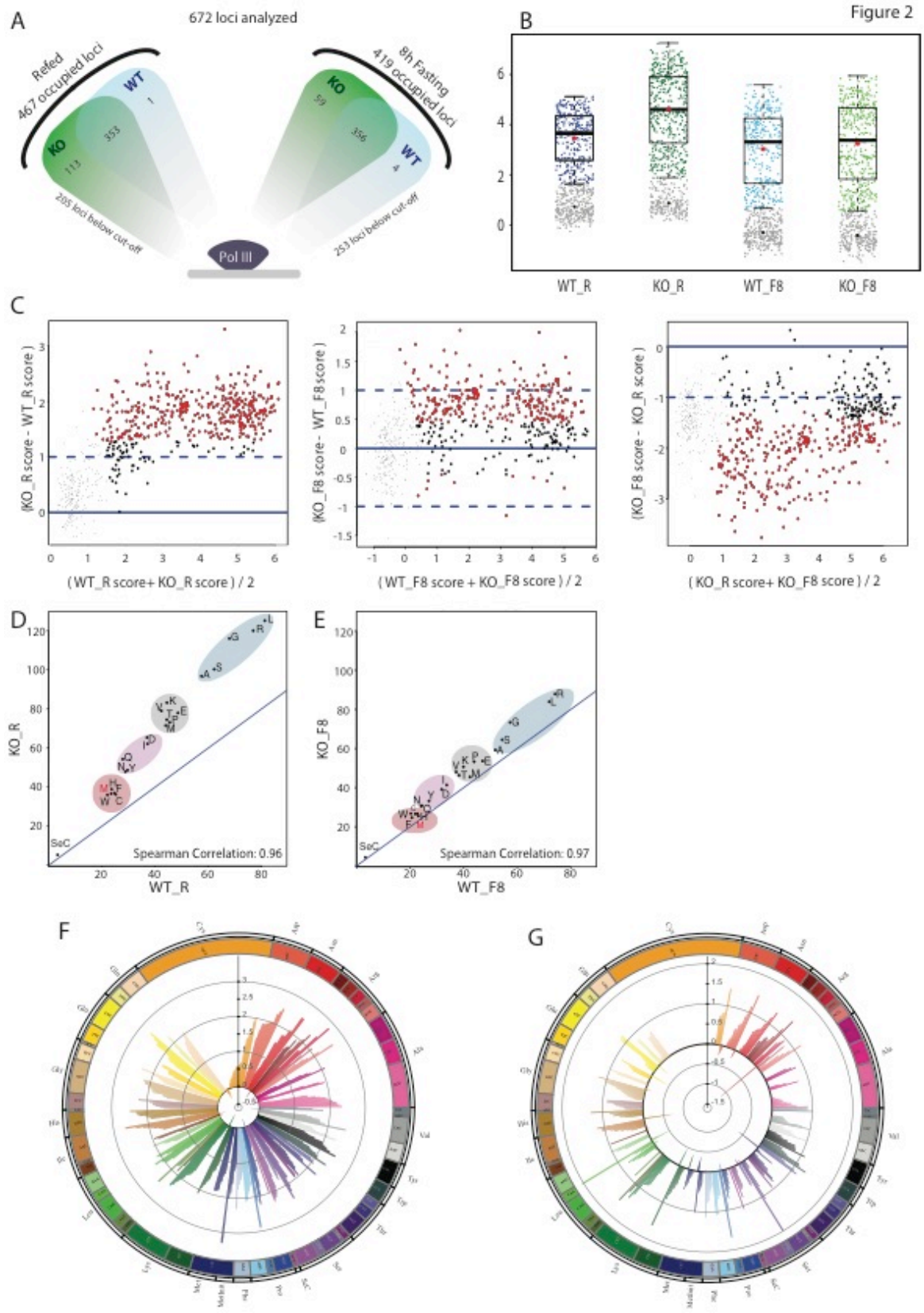
Figure 2
A
672 loci analyzed
Refed
467 occupied loci
WT
1
KO
353
113
205 loci below cut-off
8h Fasting
419 occupied loci
KO
59
356
WT
4
253 loci below cut-off
Pol III
B
WT_R
KO_R
WT_F8
KO_F8
C
(KO_R score - WT_R score)
(WT_R score+ KO_R score) / 2
(KO_F8 score - WT_F8 score)
(WT_F8 score + KO_F8 score) / 2
(KO_F8 score - KO_R score)
(KO_R score+ KO_F8 score) / 2
D
KO_R
WT_R
SeC
Spearman Correlation: 0.96
E
KO_F8
WT_F8
SeC
Spearman Correlation: 0.97
F
G

Figure 2. Maf1 KO mice have altered Pol 3 occupancy in liver under refed and fasted conditions. (A) Number of Pol 3 loci occupied by Pol 3 in ChIP-seq experiments in mouse liver. Numbers are given for loci found occupied by Pol 3 only in WT mice (in blue), only in KO mice (in green) or in both WT and KO mice (merge colour). Results are given for 4h refed animals on the left panel and for 8 h fasted animals on the right. (B) Box plots showing Pol 3 occupancy scores for Pol 3 loci in the liver of wild-type refed or fasted (WT_R and WT_F8 samples) and Maf1 KO refed or fasted (KO_R and KO_F8 samples) mice. The x-axis indicates the sample identity, the y-axis indicates scores. Scores are given as the Log2 (IP/Input). Mice were fasted for 8 h and refed for 4 h. Genes with scores below the cut-off are symbolized by grey dots. (C) MvA plots with the score means on the x-axes and the score differences on the y-axes, as indicated. The small black dots correspond to Pol 3 loci with scores below the cut-off in both samples, the large black dots to Pol 3 with scores showing no significant change, and the red dot to Pol 3 loci with scores showing significant changes as determined by limma (p-value ≤ 0.01). (D) Spearman rank correlations of Pol 3 occupancy total scores for each tRNA isotypes between WT and MAF1 KO mice in a 4 h refed condition. The twenty-one tRNA gene isotypes (tRNASeC gene was left out, $tRNA^{IMet}$ genes were considered separately from $tRNA^{Met}$ genes) were clustered in four different quantiles (blue, grey, pink and orange ovals) according to their Pol 3 occupancy. (E) Spearman rank correlations of Pol 3 occupancy total scores for each tRNA isotypes between WT and MAF1 KO mice in a 8h fasted condition. The tRNA genes were clustered as in E. (F) Circular plot indicating the ratio of Pol 3 occupancy scores between WT and Maf1 KO samples for each annotated tRNA in a 4 h refed condition. (G) Circular plots indicating the ratio of Pol 3 occupancy scores between WT and Maf1 KO samples for each annotated tRNA in a 8 h fasted condition.

Figure 3

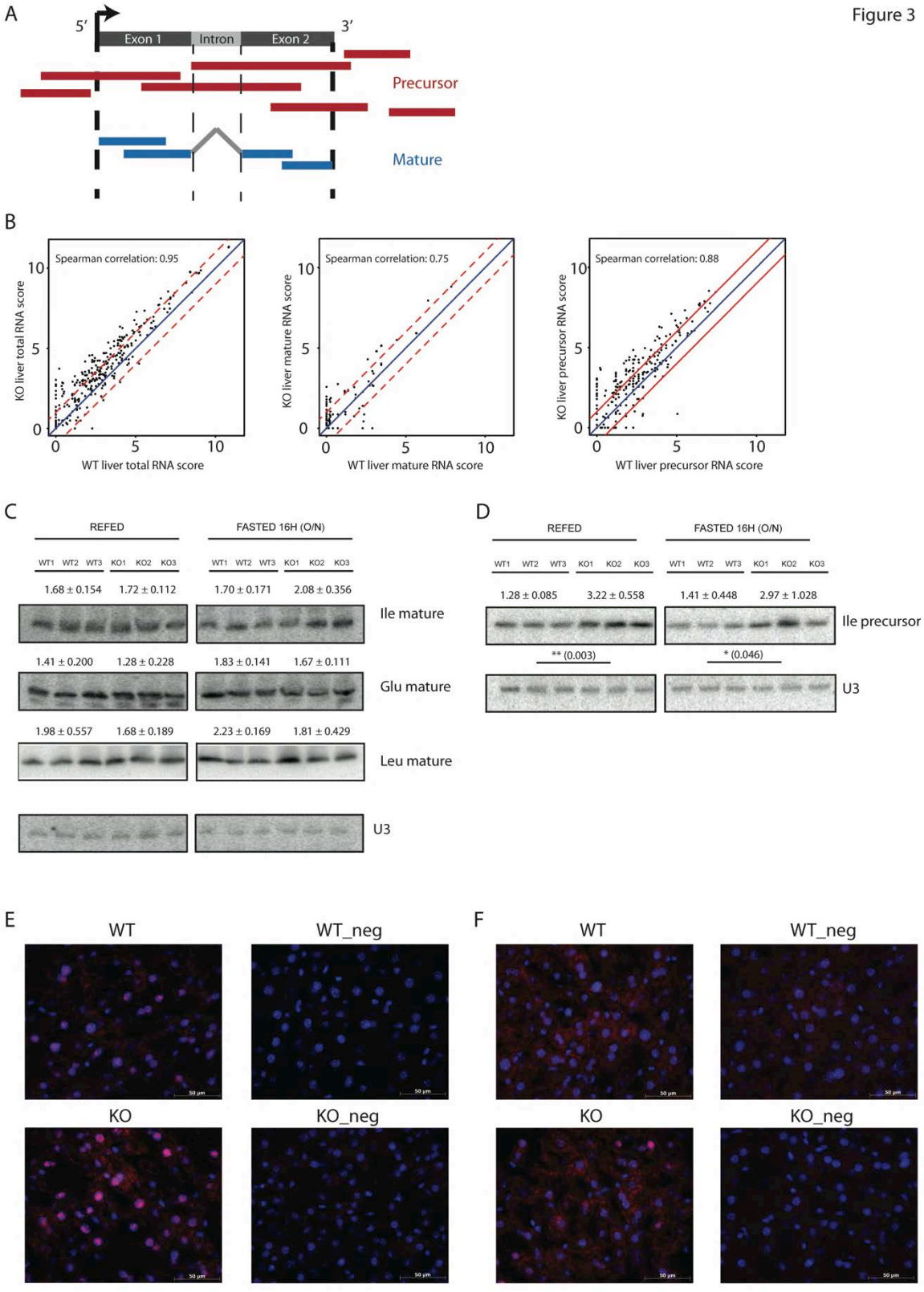
A
5′
Exon 1
Intron
Exon 2
3′
Precursor
Mature
B
Spearman correlation: 0.95
KO liver total RNA score
WT liver total RNA score
Spearman correlation: 0.75
KO liver mature RNA score
WT liver mature RNA score
Spearman correlation: 0.88
KO liver precursor RNA score
WT liver precursor RNA score
C
REFED
FASTED 16H (O/N)
WT1 WT2 WT3 KO1 KO2 KO3
1.68 ± 0.154
1.72 ± 0.112
1.70 ± 0.171
2.08 ± 0.356
Ile mature
1.41 ± 0.200
1.28 ± 0.228
1.83 ± 0.141
1.67 ± 0.111
Glu mature
1.98 ± 0.557
1.68 ± 0.189
2.23 ± 0.169
1.81 ± 0.429
Leu mature
U3
D
REFED
FASTED 16H (O/N)
WT1 WT2 WT3 KO1 KO2 KO3
1.28 ± 0.085
3.22 ± 0.558
1.41 ± 0.448
2.97 ± 1.028
Ile precursor
** (0.003)
* (0.046)
U3
E
WT
WT_neg
KO
KO_neg
F
WT
WT_neg
KO
KO_neg

Figure 3. Maf1 KO mice have higher levels of precursor RNA in liver. (A) Schematic representation of the strategy to assign tags to precursor or mature RNA following RNA-seq experiment. (B) Spearman rank correlation of tRNA RNA-seq scores for liver samples from WT and KO mice fasted for 16 h. The left panel shows the correlation for all tags, the middle panel for the tags attributed to mature tRNAs, and the right panel for the tags attributed to precursor tRNAs. The x=y line is blue, the two fold change lines are red dotted lines. (C) Northern blots analysis of liver mature tRNAs in both 4 h refed and 16 h fasted conditions. The intensity of each band was quantified and the mean values and standard deviations for the 3 WT and the 3 KO samples are indicated on top of each panel. Small nucleolar RNA U3 was used as a loading control. (D) As in C, but for a precursor isoleucine tRNA. The values under each panel correspond to the t.test-associated p.value. (E) Precursor tRNA FISH signal. A specific digoxigenin-conjugated RNA probe covering the intron of the tRNA leu1911 was used and detected with a horseradish peroxidase-conjugated anti-DIG antibody (red signal). Nuclei were stained with DAPI (blue signal). (F) As in E, but with a probe spanning the intron of the tRNA leu1911.

Figure 4

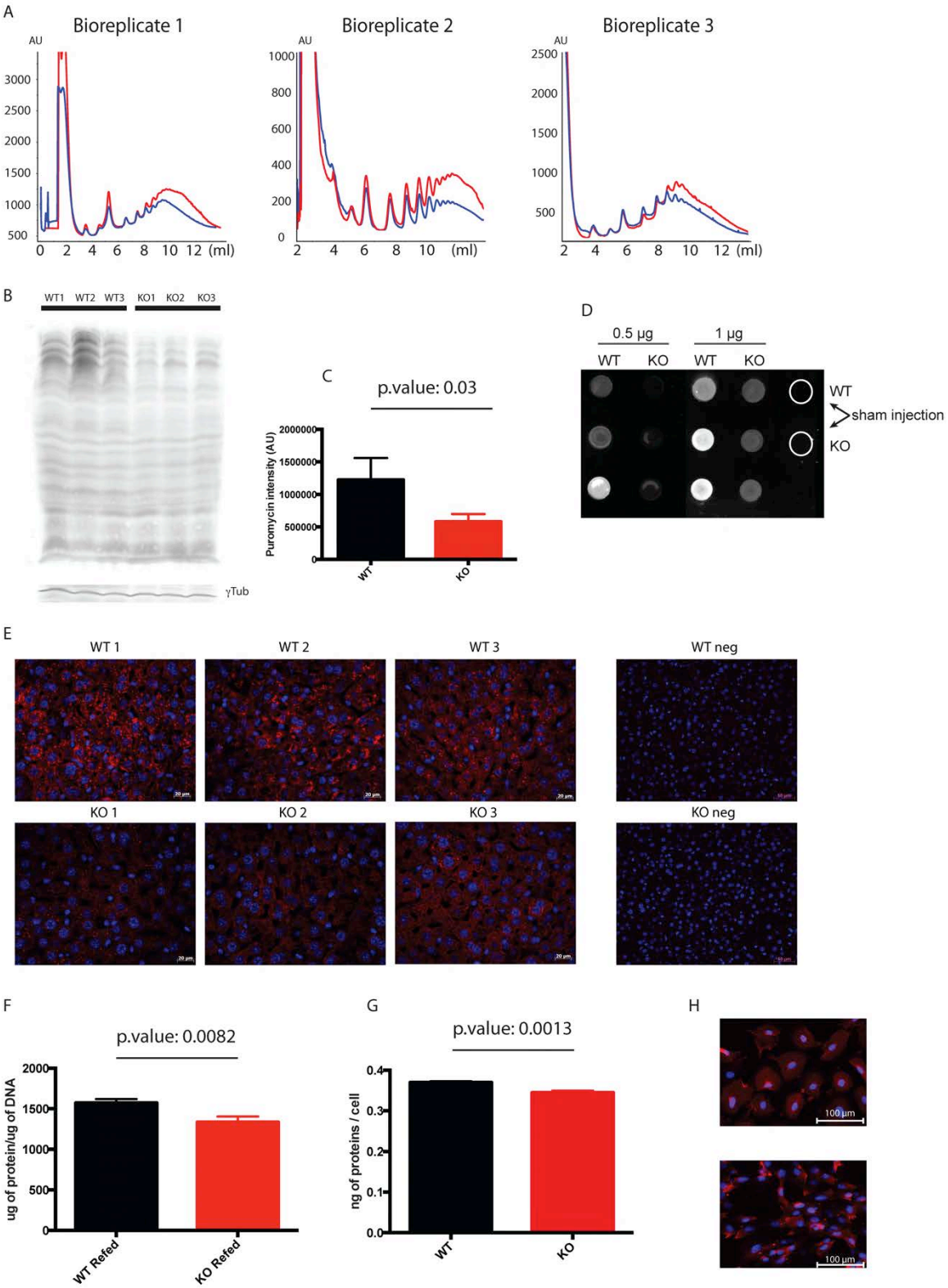
A
Bioreplicate 1
Bioreplicate 2
Bioreplicate 3
AU
(ml)
B
WT1 WT2 WT3 KO1 KO2 KO3
γTub
C
p.value: 0.03
Puromycin intensity (AU)
WT
KO
D
0.5 µg
1 µg
WT
KO
sham injection
E
WT 1
WT 2
WT 3
WT neg
KO 1
KO 2
KO 3
KO neg
F
p.value: 0.0082
ug of protein/ug of DNA
WT Refed
KO Refed
G
p.value: 0.0013
ng of proteins / cell
H
100 µm

Figure 4. (A) Polysome profiles of liver samples from 3 WT (red curves) and 3 Maf1 KO (blue curves) 22-24 week old mice in Refed condition. (B) SUnSET western blot of liver proteins. Mice were injected with 40 nmoles of puromycin per g of body mass, and livers were harvested 30 min later. Puromycin incorporation into newly synthesized proteins was detected with an anti-puromycin antibody. γ-tubulin was used as a loading control. (C) SUnSET western blot lanes quantification. γ -tubulin was used as a loading control. (D) SUnSET Dot-blots of liver proteins. 0.5 μg or 1 μg of total protein from three puromycin-injected WT and Maf1 KO mice was spotted on a nylon membrane and newly synthesized proteins were detected with an anti-puromycin antibody. (E) ISH-SUnSET of liver sections. Livers from puromycin-injected mice were harvested and embedded into paraffin blocks. Paraffin sections were incubated with an anti-puromycin antibody for the detection of newly synthesized proteins (red signal). Nuclei were stained with DAPI (blue signal). The two panels on the right show the negative controls of sham-injected mice. (F) Liver protein levels normalized to DNA content. Protein and DNA from 3 WT (black) and 3 Maf1 KO (red) were extracted from the same liver tissue lysate, quantified, and ratios were plotted. (G) As in F, but for proteins extracted from 3 samples of 1 million WT and 3 samples of 1 million Maf1 KO MEFs. (H) WT and Maf1 KO MEFs were stained with an anti-β-catenin antibody (red signal) and DAPI (blue signal).

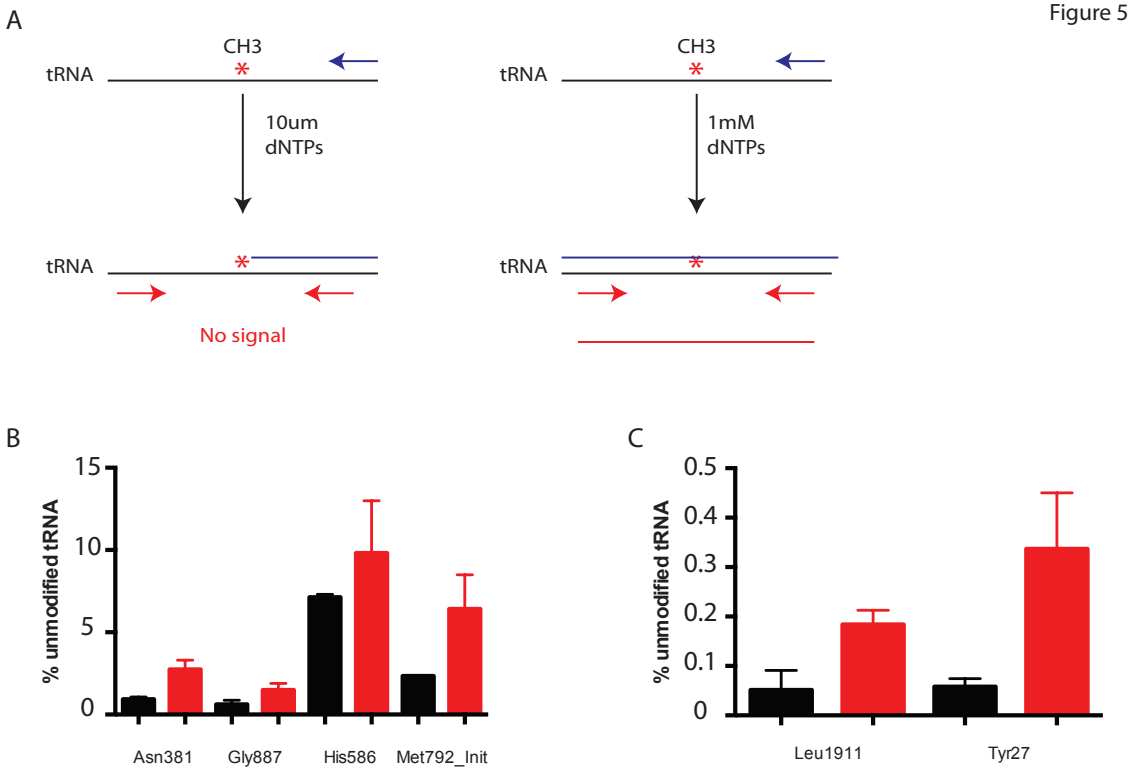

Figure 5. (A) Strategy used to quantify level of methylation on liver tRNAs in WT and Maf1 KO mice in Refed condition. Blue arrow: tRNA-specific primer used for RT. Red arrows: tRNA-specific primers used for PCR. (B) Ratios of unmodified total (precursor + mature) tRNAs in WT (black) and Maf1 KO liver cells. Experiments were performed with high concentration of dNTPs (1 mM) to assess the level of total tRNA and with low concentration (10 μM) to assess the levels of unmodified tRNA. (C) Ratios of unmodified total mature tRNA in WT (black) and Maf1 KO liver cells. Experiments were performed as in B.

Asn_381
GTCTCTGTGGCGCAATCGGTTAGCGCGTTCGGCTGTTAACCGAAAGGTTGGTGGTTCGAGCCCACCCAGGGACG

Gly_887
GCATTGGTGGTTCAGTGGTAGAATTCTCGCCTGCCACGCGGGAGGCCCGGGTTCGATTCCCGGCCAATGCA

His_586
GCCGTGATCGTATAGTGGTTAGTACTCTGCGTTGTGGCCGCAGCAACCTCGGTTCGAATCCGAGTCACGGCA

Met_792
AGCAGAGTGGCGCAGCGGAAGCGTGCTGGGCCCTAACCCAGAGGTCGATGGATCGAAACCATCCTCTGCTA

Leu_1911
GTCAGGATGGCCGAGTGGTCTAAGGCGCCAGACTCAAGgtgacaagccttacctacgggtgTTCTGGTCTCCGAATGGAGG...

Tyr_27
CCTTCGATAGCTCAGCTGGTAGAGCGGAGGACTGTAGctaactccccgttagaagacATCCTTAGGTCGCTGGTTCGACTCC...

Used primers

Asn_381_RT: gtccctgg
Asn_381_Fwd: tctctgtggcgcaatcggttag
Asn_381_Rev: ctgggtgggctcgaaccacc

Gly_887_RT: gcattggcc
Gly_887_Fwd: cattggtggttcagtggt
Gly_887_Rev: tggccgggaatcgaacccgg

His_586_RT: ggcgtgac
His_586_Fwd: ccgtgatcgtatagtggttag
His_586_Rev: tgactcggattcgaaccgag

Met_792_RT: agcagagg
Met_792_Fwd: gcagagtggcgcagcggaag
Met_792_Rev: gaggatggtttcgatccatcg

Leu_1911_RT: cagaactt
Leu_1911_Fwd: tcaggatggccgagtggt
Leu_1911_Rev: agaacttgagtctggcgc

Tyr_27_RT: aggatcta
Tyr_27_Fwd: cttcgatagctcagctgg
Tyr_27_Rev: gatctacagtcctccgct

Figure S1. (A) List of primers used to quantify the level of modification on several tRNAs. The red lines represent where primers used for the reverse transcriptase are mapping on the tRNA sequence and the blue lines represent primers used for the qPCR.

Discussion

We have reported before that mice lacking the Pol 3 repressor MAF1 are lean and resistant to diet-induced obesity, probably in part due to futile synthesis and degradation cycles of both tRNA precursors and lipids. In addition, these mice are slightly smaller, a trait that becomes evident as they reach 24 weeks of age (Bonhoure et al. 2015). In this study, we characterize the effects of the lack of MAF1 for the synthesis of Pol 3 products.

We first show that as mice fast, i.e. as they switch from using mostly glucose as a carbon source to using mostly lipids, there is a decrease in Pol 3 occupancy for the loci that have low or middle Pol 3 occupancy, but not for the loci with the highest occupancy in fed condition, which tend to remain highly occupied after fasting. Thus, out of 354 occupied Pol 3 loci in fed condition, 266 have no significant decrease of Pol 3 occupancy after fasting. Interestingly, this pool of stably occupied genes includes tRNA genes for all amino acid isotypes as well as all the other categories of Pol 3 genes (see Table S1). Thus, after 8h of fasting, Pol 3 occupancy is decreased at a number of specific loci while others remain occupied. This may ensure that some essential functions such as splicing or RNA processing can continue to be carried out, and, in the case of tRNAs, it may reflect adaptation to a new metabolic mode requiring translation of a set of genes with different codon biases (Gingold et al., 2014).

The Maf1 KO mice also showed decreased Pol 3 occupancy after 8h of fasting, indicating that other factors besides MAF1 could repress Pol 3 transcription after nutritional stress. MAF1 is thought to be the major repressor of Pol 3 transcription but several other proteins have been shown to regulate Pol 3 activity including Rb and p53. Moreover, Pol 3 transcription factors can be regulated by phosphorylation; for example, yeast and human BDP1, one of the TFIIIB transcription factor subunits, are inactivated by phosphorylation driven by either Sch9 or CK2 (Hu et al., 2004; Lee et al., 2015). One could imagine these or other unidentified factors contributing to repress Pol 3 occupancy under nutrient stress.

A very striking effect in the Maf1 KO mice was the much higher Pol 3 occupancy observed in the refed conditions. This result was unexpected, as MAF1 is believed to act mostly under stress conditions. This indicates that in fact, MAF1 plays a dampening role on Pol 3 transcription even in the absence of stress. Perhaps MAF1 is needed to keep Pol 3 activity within a pretty narrow range of activity where it provides enough precursors to fulfil the needs of the cell, but not too many to avoid cell transformation by increased protein translation and, at higher levels, incomplete modification of pre-tRNAs (see below).

The much higher Pol 3 occupancy observed in the Maf1 KO mice results in higher levels of precursor tRNAs but not processed, i.e. 5' and 3' trimmed as well as spliced, tRNAs, as determined by RNAseq as well as northern blot and FISH experiments where specific probes for intron of tRNAs were used. A possible interpretation of these results is that the very high levels of precursors overwhelm the processing machinery, of which the nuclear-localized tRNA splicing endonuclease (TSEN) (Peebles et al., 1983) is a major component. Indeed, in Xenopus oocytes, elevated levels of pre-tRNA have been shown to saturate the pre-tRNA splicing machinery (Arts et al., 1998). Unprocessed pre-tRNAs are rejected by the nuclear export machinery (Lund and Dahlberg, 1998), which increases the levels of pre-tRNAs in the nucleus. Consistent with this, we observed that the higher levels of pre-tRNAs in the absence of MAF1 were localized in the nucleus.

In addition to being processed at their 3' and 5' ends and spliced, tRNAs are subjected to chemical modifications that stabilize their structure and allow them to function optimally during translation (Torres et al., 2014). In addition to increased precursor signal in the cytoplasm, we also noticed some nuclear FISH signal from processed tRNAs in the Maf1 KO mouse liver. These may correspond to properly spliced but not completely modified tRNAs, as it has been shown before that partially modified tRNAs can be re-imported in the nucleus to finish their maturation (Kramer and Hopper, 2013). Indeed, our experiments showed a reduced level of tRNA modifications associated with the loss of MAF1. We tested, however, only a small number of tRNAs, and we did not identify the specific modifications affected. We plan to use a method developed by Peter Dedon's group in which tRNAs are first

hydrolyzed to single bases and then analyzed by GC-MS/MS (Dennis et al., 2012). This will reveal which modifications are affected in the MAF1 KO mouse. It will be interesting to check whether the differences are located at position 34, 35, or 36 of the tRNAs corresponding to the anticodon or whether they are found at other key positions. tRNA modifications were shown to protect the tRNAs against angiogenin-driven cleavage. It could be interesting to check if the pool of tRNA-derived fragments is increased in the Maf1 KO mouse.

tRNAs are key molecules for protein translation participating in translation elongation by bringing the new amino acids that are incorporated. Recently, several studies have shown that a defect in tRNA modification is followed by a decrease in protein translation (Damon et al., 2015; Lamichhane et al., 2013; Rojas-Benitez et al., 2015; Tuorto et al., 2012). Thus, the deficiency in tRNA modification in the Maf1 KO mouse might explain one of our key findings, namely that the Maf1 KO mice display reduced protein synthesis in the liver. This result could explain, in turn, the slight decrease in size of the Maf1 KO mice (Bonhoure et al., 2015). Our experiments indicate a reduction of protein synthesis, however, we do not know whether some proteins are more affected than others, or whether the translation reduction is global and quite uniform. An important follow-up study will be to perform ribosome profiling experiments, i.e. to sequence ribosome-protected mRNA fragments, as described in (Ingolia et al., 2009). This might allow the identification of the specific targets that are less translated. As Maf1 KO mice develop a resistance to diet-induced obesity (Bonhoure et al., 2015), one could imagine that specific genes involved in lipid metabolism might be less translated in the Maf1 KO mice.

In summary, MAF1 is a regulator of RNA polymerase 3 transcription in mouse liver both in fasted and refed condition. In fasted condition, MAF1 acts for metabolic economy by decreasing the level of synthetized Pol 3 transcripts. In refed condition the role of MAF1 is probably rather to control Pol 3 activity to prevent overwhelming of both RNA processing and modification machineries. The loss of Maf1 increases the level of ineffective tRNA molecules in the cell leading to a decrease in protein translation.

References

Arts, G.J., Fornerod, M., and Mattaj, I.W. (1998). Identification of a nuclear export receptor for tRNA. Curr. Biol. *8*, 305–314.

Belin, S., Beghin, A., Solano-Gonzàlez, E., Bezin, L., Brunet-Manquat, S., Textoris, J., Prats, A.-C., Mertani, H.C., Dumontet, C., and Diaz, J.-J. (2009). Dysregulation of ribosome biogenesis and translational capacity is associated with tumor progression of human breast cancer cells. PLoS One *4*, e7147.

Boguta, M., Czerska, K., and Zoładek, T. (1997). Mutation in a new gene MAF1 affects tRNA suppressor efficiency in Saccharomyces cerevisiae. Gene *185*, 291–296.

Bonhoure, N., Bounova, G., Bernasconi, D., Praz, V., Lammers, F., Canella, D., Willis, I.M., Herr, W., Hernandez, N., Delorenzi, M., et al. (2014). Quantifying ChIP-seq data: A spiking method providing an internal reference for sample-to-sample normalization. Genome Res. *24*, 1157–1168.

Bonhoure, N., Byrnes, A., Moir, R.D., Hodroj, W., Preitner, F., Praz, V., Marcelin, G., Jr, S.C.C., Martinez-lopez, N., Singh, R., et al. (2015). Loss of the RNA polymerase III repressor MAF1 confers obesity resistance. 934–947.

Cai, Y., and Wei, Y.H. (2015). Distinct regulation of Maf1 for lifespan extension by Protein kinase A. *7*, 133–143.

Calvo, O., Cuesta, R., Anderson, J., Gutiérrez, N., García-Barrio, M.T., Hinnebusch, a G., and Tamame, M. (1999). GCD14p, a repressor of GCN4 translation, cooperates with Gcd10p and Lhp1p in the maturation of initiator methionyl-tRNA in Saccharomyces cerevisiae. Mol. Cell. Biol. *19*, 4167–4181.

Canella, D., Praz, V., Reina, J.H., Cousin, P., and Hernandez, N. (2010). Defining the RNA polymerase III transcriptome: Genome-wide localization of the RNA polymerase III transcription machinery in human cells. Genome Res. *20*, 710–721.

Canella, D., Bernasconi, D., Gilardi, F., LeMartelot, G., Migliavacca, E., Praz, V., Cousin, P., Delorenzi, M., Hernandez, N., Deplancke, B., et al. (2012). A multiplicity of factors contributes to selective RNA polymerase III occupancy of a subset of RNA polymerase III genes in mouse liver. Genome Res. *22*, 666–680.

Damon, J.R., Pincus, D., and Ploegh, H.L. (2015). tRNA thiolation links translation to stress responses in Saccharomyces cerevisiae. Mol. Biol. Cell *26*, 270–282.

Dennis, M.K., Field, A.S., Burai, R., Ramesh, C., Whitney, K., Bologa, C.G., Oprea, T.I., Yamaguchi, Y., Hayashi, S., Sklar, L. a, et al. (2012). NIH Public Access. *127*, 358–366.

Dieci, G., Fiorino, G., Castelnuovo, M., Teichmann, M., and Pagano, A. (2007). The expanding RNA polymerase III transcriptome. Trends Genet. *23*, 614–622.

Felton-Edkins, Z. a., Fairley, J. a., Graham, E.L., Johnston, I.M., White, R.J., and Scott, P.H. (2003). The mitogen-activated protein (MAP) kinase ERK induces tRNA synthesis by phosphorylating TFIIIB. EMBO J. *22*, 2422–2432.

Gingold, H., Tehler, D., Christoffersen, N.R., Nielsen, M.M., Asmar, F., Kooistra, S.M., Christophersen, N.S., Christensen, L.L., Borre, M., Sørensen, K.D., et al. (2014). A Dual Program for Translation Regulation in Cellular Proliferation and Differentiation. Cell *158*, 1281–1292.

Hu, P., Samudre, K., Wu, S., Sun, Y., and Hernandez, N. (2004). CK2 phosphorylation of Bdp1 executes cell cycle-specific RNA polymerase III transcription repression. Mol. Cell *16*, 81–92.

Ingolia, N.T., Ghaemmaghami, S., Newman, J.R.S., and Weissman, J.S. (2009). Genome-wide analysis in vivo of translation with nucleotide resolution using ribosome profiling. Science *324*, 218–223.

Jackson, R.J., Hellen, C.U.T., and Pestova, T. V (2010). The mechanism of eukaryotic translation initiation and principles of its regulation. Nat. Rev. Mol. Cell Biol. *11*, 113–127.

Karkusiewicz, I., Turowski, T.W., Graczyk, D., Towpik, J., Dhungel, N., Hopper, A.K., and Boguta, M. (2011). Maf1 protein, repressor of RNA polymerase III, indirectly affects tRNA processing. J. Biol. Chem. *286*, 39478–39488.

Khanna, A., Johnson, D.L., and Curran, S.P. (2014). Physiological Roles for mafr-1 in Reproduction and Lipid Homeostasis. Cell Rep. *9*, 2180–2191.

Kramer, E.B., and Hopper, A.K. (2013). Retrograde transfer RNA nuclear import provides a new level of tRNA quality control in Saccharomyces cerevisiae. Proc. Natl. Acad. Sci. U. S. A. *110*, 21042–21047.

Lamichhane, T.N., Blewett, N.H., Crawford, A.K., Cherkasova, V. a, Iben, J.R., Begley, T.J., Farabaugh, P.J., and Maraia, R.J. (2013). Lack of tRNA modification isopentenyl-A37 alters mRNA decoding and causes metabolic deficiencies in fission yeast. Mol. Cell. Biol. *33*, 2918–2929.

Lee, J., Moir, R.D., and Willis, I.M. (2015). Differential Phosphorylation of RNA Polymerase III and the Initiation Factor TFIIIB in Saccharomyces cerevisiae. PLoS One *10*, e0127225.

Lee, J.H., Moir, R.D., and Willis, I.M. (2009). Regulation of RNA polymerase III transcription involves SCH9-dependent and SCH9-independent branches of the target of rapamycin (TOR) pathway. J. Biol. Chem. *284*, 12604–12608.

Lodish, H., Berk, A., and Zipursky, S. (2000). Processing of rRNA and tRNA. In Molecular Cell Biology, p. Section 11.6.

Lund, E., and Dahlberg, J.E. (1998). Proofreading and aminoacylation of tRNAs before export from the nucleus. Science *282*, 2082–2085.

Mauck, J.C., and Green, H. (1974). Regulation of pre-transfer RNA synthesis during transition from resting to growing state. Cell *3*, 171–177.

Michels, A. a, Robitaille, A.M., Buczynski-Ruchonnet, D., Hodroj, W., Reina, J.H., Hall, M.N., and Hernandez, N. (2010). mTORC1 directly phosphorylates and regulates human MAF1. Mol. Cell. Biol. *30*, 3749–3757.

Moir, R.D., Lee, J., Haeusler, R. a, Desai, N., Engelke, D.R., and Willis, I.M. (2006). Protein kinase A regulates RNA polymerase III transcription through the nuclear localization of Maf1. Proc. Natl. Acad. Sci. U. S. A. *103*, 15044–15049.

Palian, B.M., Rohira, A.D., Johnson, S. a. S., He, L., Zheng, N., Dubeau, L., Stiles, B.L., and Johnson, D.L. (2014). Maf1 Is a Novel Target of PTEN and PI3K Signaling That Negatively Regulates Oncogenesis and Lipid Metabolism. PLoS Genet. *10*, e1004789.

Peebles, C.L., Gegenheimer, P., and Abelson, J. (1983). Precise excision of intervening sequences from precursor tRNAs by a membrane-associated yeast endonuclease. Cell *32*, 525–536.

Reina, J.H., Azzouz, T.N., and Hernandez, N. (2006). Maf1, a new player in the regulation of human RNA polymerase III transcription. PLoS One *1*.

Renaud, M., Praz, V., Vieu, E., Florens, L., Washburn, M.P., L'Hôte, P., and Hernandez, N. (2014). Gene duplication and neofunctionalization: POLR3G and POLR3GL. Genome Res. *24*, 37–51.

Rideout, E.J., Marshall, L., and Grewal, S.S. (2012). Drosophila RNA polymerase III repressor Maf1 controls body size and developmental timing by modulating tRNAiMet synthesis and systemic insulin signaling. Proc. Natl. Acad. Sci. *109*, 1139–1144.

Rojas-Benitez, D., Thiaville, P.C., de Crecy-Lagard, V., and Glavic, A. (2015). The Levels of a Universally Conserved tRNA Modification Regulate Cell Growth. J. Biol. Chem. jbc.M115.665406.

Schmidt, E.K., Clavarino, G., Ceppi, M., and Pierre, P. (2009). SUnSET, a nonradioactive method to monitor protein synthesis. Nat. Methods *6*, 275–277.

Scott, P.H., Cairns, C. a., Sutcliffe, J.E., Alzuherri, H.M., McLees, a., Winter, a. G., and White, R.J. (2001). Regulation of RNA Polymerase III Transcription during Cell Cycle Entry. J. Biol. Chem. *276*, 1005–1014.

Torres, a. G., Pineyro, D., Rodriguez-Escriba, M., Camacho, N., Reina, O., Saint-Leger, a., Filonava, L., Batlle, E., and Ribas de Pouplana, L. (2015). Inosine modifications in human tRNAs are incorporated at the precursor tRNA level. Nucleic Acids Res. *43*, 5145–5157.

Torres, A.G., Batlle, E., and Ribas de Pouplana, L. (2014). Role of tRNA modifications in human diseases. Trends Mol. Med. *20*, 306–314.

Tuorto, F., Liebers, R., Musch, T., Schaefer, M., Hofmann, S., Kellner, S., Frye, M., Helm, M., Stoecklin, G., and Lyko, F. (2012). RNA cytosine methylation by Dnmt2 and NSun2 promotes tRNA stability and protein synthesis. Nat. Struct. Mol. Biol. *19*, 900–905.

Vannini, A., Ringel, R., Kusser, A.G., Berninghausen, O., Kassavetis, G. a., and Cramer, P. (2010). Molecular basis of RNA polymerase III transcription repression by Maf1. Cell *143*, 59–70.

Wek, S. a, Zhu, S., and Wek, R.C. (1995). The histidyl-tRNA synthetase-related sequence in the eIF-2 alpha protein kinase GCN2 interacts with tRNA and is required for activation in response to starvation for different amino acids. Mol. Cell. Biol. *15*, 4497–4506.

Zaborske, J.M., Narasimhan, J., Jiang, L., Wek, S. a., Dittmar, K. a., Freimoser, F., Pan, T., and Wek, R.C. (2009). Genome-wide analysis of tRNA charging and activation of the eIF2 kinase Gcn2p. J. Biol. Chem. *284*, 25254–25267.

Zaragoza, D., Ghavidel, a, Heitman, J., and Schultz, M.C. (1998). Rapamycin induces the G0 program of transcriptional repression in yeast by interfering with the TOR signaling pathway. Mol. Cell. Biol. *18*, 4463–4470.

Material and Methods

Animals

C57/BL6 male, 12–14-week-old (at time of sacrifice), mice were sacrificed after 16h of fasting (from 4PM to 8AM), 8h of fasting (from 4PM to 12AM) or after 4h of refeeding (fasting followed by full access to food during 4h) as indicated. All animal care and handling was performed according to Swiss law for animal protection.

Spiked Mouse Chromatin Immunoprecipitation

Perfused C57Bl/6 mice liver were homogenized in 4 mL of PBS containing 1% of formaldehyde and left in the same buffer for cross-linking for a total of 10 minutes. Nuclei were isolated as described in (Ripperger and Schibler 2006). Nuclear lysis was performed in 1.2 mL of 50 mM Tris/HCl (pH 8.1), 10 mM EDTA, 1% SDS, 50 µg/mL PMSF, 1 µg/mL Leupeptin. The nuclear lysate was then supplemented with 0.92 mL of 20 mM Tris/HCl (pH 8.1), 150 mM NaCl, 2 mM EDTA, 1% Triton X-100, 0.01% SDS, 50 µg/mL PMSF, 1 µg/mL Leupeptin and sonicated with a Branson SLPe sonicator for 10 cycles of 10 s at 50% amplitude, resulting in an average fragment size between 300 and 1000 bp. After each sonication cycle, the chromatin was kept in an ice-cold bath during 20s. Chromatin samples from three mice were pooled, de-cross-linked, and an aliquot was extracted for DNA quantification. Human HeLa cell chromatin was prepared as described in (Canella et al. 2010) and DNA concentration was assessed.

ChIPs were performed with 30.8 µg of total DNA containing 2.5% of human spike chromatin and 10 µL of serum from a rabbit immunized with a peptide 100% conserved in human and mouse POLR3D (CS681 antibody, C-terminal peptide CSPDFESLLDHKHR) (Chong et al. 2001). This antibody has been used extensively for ChIP-seq experiments, both in human and mouse cells (Canella et al. 2010; Canella et al. 2012; Renaud et al. 2014). The ChIPs were performed as described previously in (Forsberg et al. 2000; Dhami et al. 2010) with a few modifications. Briefly, the chromatin samples were incubated with the antibodies overnight at 4°C. The next day, 20 µL of protein A sepharose beads (CL4B GE Healthcare) were added and the samples were further incubated for 3 h. The beads were next washed once with 20

mM Tris/HCL (pH 8.1), 50 mM NaCl, 2 mM EDTA, 1% Triton X-100, 0.1% SDS, twice with 10 mM Tris/HCL (pH 8.1), 250 mM LiCl, 1 mM EDTA, 1% NP-40, 1% deoxycholic acid, and twice with TE buffer 1X (10 mM Tris/Cl (pH 7.5), 1 mM EDTA). Bound material was then eluted from the beads in 300 µL of elution buffer (100 mM $NaHCO_3$, 1% SDS), treated first with RNase A (final concentration 8 µg/mL) during 6 h at 65°C and then with proteinase K (final concentration 345 µg/mL) overnight at 45°C. The next day, the samples were purified with PCR clean-up kit from Macherey Nagel and eluted in 50 µL of elution buffer.

Ultra-high throughput sequencing.

Ten ng of DNA from each ChIP was next used to prepare sequencing libraries according to the Illumina sample Prep ChIP Seq Kit protocol (Illumina; San Diego, California, USA; Cat. No IP-102-1001), except that size selection of the samples was performed after, rather than before, library amplification. Sequencing libraries were loaded onto one lane of a HiSeq 2000 flow cell and sequenced at 100 cycles. For each condition we sequenced input chromatin sample and corresponding ChIP sample(s).

ChIP-seq analysis

Data analysis was performed as described in Bonhoure et al. (2014).

RNA-seq analysis

Liver tissue from overnight fasted 22-24 week old mice maintained on a breeder chow diet was harvested and freeze-clamped in liquid nitrogen. Total RNA was prepared (Qiagen miRNeasy), treated with DNase 1, and RNA quality was assessed by capillary electrophoresis (Agilent 2100 Bioanalyzer). Library preparation and directional RNA-seq was performed at the Einstein Epigenomics Core Facility. Three biologically independent samples (RNA integrity numbers >7.5, Agilent Bioanalyzer) from wild-type and Maf1 KO mice were sequenced. For analysis of the Pol 3 transcriptome, sequence tags were mapped in three sequential steps. The first mapping was performed with Bowtie on the Mm9 Mouse genome assembly release. The tags left unmapped were then aligned with BLAT on the Pol 3 loci listed in Table S1. As twenty four tRNA genes contain introns, the remaining tags were aligned in a third round with BLAT to sequences corresponding to spliced tRNAs. The results of

the three alignment steps were pooled and the tags aligning in the Pol 3 loci listed in Table S1 were counted. The tags were scaled to the total number of tags aligning in Pol 2 genes, and tags with multiple matches in the genome were given a weight corresponding to the number of matches divided by the number of times they were sequenced. Scores corresponding to the log2 of tags per gene were then calculated. Tags were considered derived from precursor tRNAs when they extended either upstream or downstream of the mature tRNA coding region or overlapped with tags extending upstream or downstream of the tRNA coding region, or for tRNA genes containing an intron, when they contained intron sequences. Sequence tags were considered derived from mature tRNAs when they start or end precisely at the 5' and 3' ends of the annotated tRNA, and for tRNA genes containing an intron, when they spanned the exon-exon junction.

Northern Blot analysis

Liver samples (50-100 mg, flash frozen in liquid N_2) from 16 h fasted or 4 h refed mice were homogenized in Trizol (Thermo Fisher Scientific) and RNA was purified according to the manufacturer's directions. RNA was precipitated twice, quantified, and resolved by denaturing polyacrylamide electrophoresis before electrophoretic transfer to nylon membranes (GE Healthcare Amersham Hybond N^+) and hybridization with [^{32}P]-end labelled oligonucleotide probes at 40°C (Li et al. 2000). tRNA signals detected by phosphoimaging were quantified and normalized to U3 snRNA to compare expression in wild-type and knockout samples. The probe sequences were: $tRNA^{Glu(CTC)}$: 5'-CGCCGAATCCTAACCACTAG-3' ; $tRNA^{Leu(CAA)}$: 5'-CTCCATTCGGAGACCAGAA-3' ; mature-$tRNA^{Ile(TAT)}$: 5'-ACCTCGGCATTATAAGTACC-3' ; pre-$tRNA^{Ile(TAT)}$: 5'-ATCGCTTACGCCTAGCACTG-3' ; U3 snRNA :5'-GGAGGGAAG AACGATCATCA-3'.

Fluorescent *In Situ* hybridization analysis

Liver tissues were fixed in 4% paraformaldehyde during 24 h followed by cryoprotection in 30% sucrose/PBS during 24 h at 4°C. Tissues were embedded in Tissue Tek OCT compound and 10 µm section were cut with a cryostat. Prior to hybridization, sections were digested with 10 µM of proteinase K (ABI AM2546) during 12 min at 37%. Sections were washed with 0.2% glycine/PBS and treated with

0.1M triethanolamine (pH 8) during 10 min and 0.1M triethanolamine / 0.25% acetic anhydride again during 10 min. Double digoxigenin-labelled probe were hybridized overnight at 54°C in hybridization buffer (50% de-ionized formamide, 5X SSC, 5X Denhardt's solution, 0.5 mg/ml of salmon sperm DNA). Sections were washed and incubated with anti-DIG antibody (Roche Cat N. 11 207 733 910) at RT during 30 min. Sections were washed again and incubated with fluorophore (Perkin Elmer NEL744001KT) at RT during 10 min followed by incubation in DAPI diluted 1/10000 in PBS at RT during 15 min. Pictures were taken with the Zeiss Axio imager M1 microscope. The sequences of the probe specific to precursor and mature $tRNA^{Leu(CAA)}$ were 5'-CACCCGTAGGTAAGGCTTGTCAC-3' and 5'-GGAGACCAGAACTTGAGTCT-3', respectively.

Western Blot analysis

Liver samples (50-100 mg, flash frozen in liquid N_2) from 16 h fasted or 4 h refed mice were homogenized with a dounce in RIPA lysis buffer (Millipore 20-188). Proteins were separated on 8-12% gradient SDS-polyacrylamide gels and transferred onto nitrocellulose membranes (GE Healthcare Amersham Protan). Membranes were incubated with antibody directed against RPS6 (Cat N.2217), phosphor-RPS6 (Cat N.2211), ERK (Cat N.9102), phosphor-ERK (Cat N.4370), 4E-BP1 (Cat N.9452), phosphor-4E-BP1 Cat N.9459) from Cell Signaling Technologies, and against γ-Tubulin (B-12) from Santa Cruz Biotechnology. Secondary antibodies were obtained from LI-COR and membranes were scanned with an Odyssey imager.

Polysome Profiling

Liver samples (50-100 mg) from 4h refed mice were directly homogenized with a dounce in Polysome buffer (20mM Tris-HCL pH 7.4, 150mM NaCl, 5mM $MgCl_2$, 1mM DTT, 100 $\mu g.mL^{-1}$ Cycloheximide, 1% Triton, 25 Units mL^{-1} Turbo Dnase1, 0.2 Units mL^{-1} RNasin, 1mg/mL heparin, complete protease inhibitor). A fraction of the homogenate was used to assess RNA concentration and a volume corresponding to 50µg of total RNA was loaded on a 15%-60% sucrose gradient. Samples were centrifuged with a SW-40 rotor at 35000 rpm, 4°C during 4h. Profiles were obtained reading the OD at 260nm with the AKTA purifier 10 from GE Healthcare (Amersham).

SUnSET puromycin labelling.

Twelve week old mice were injected with 40 nmol.g^{-1} of puromycin at 9PM, and livers were collected 30 min later. For western blot analysis, a piece of liver was homogenized with a dounce in RIPA buffer and samples containing equal amounts of DNA were loaded on a 10% SDS-polyacrylamide gel. Proteins were transferred onto nitrocellulose membranes (GE Healthcare Amersham Protan) and the membranes were incubated with an antibody directed against Puromycin (Millipore MABE343). For Dot-Blot analysis, the protein samples normalized according to the DNA content were directly spotted onto the nitrocellulose membrane. Antibody directed against γ-Tubulin (Santa Cruz B-12) was used to control for loading.

For immunostaining experiments, a piece of liver from puromycin-injected mice was fixed in 4% PFA/PBS during 8 h and embedded in paraffin. Sections were rehydrated with incubation in several baths of xylol and EtOH 100%, 95%, 80% and 70%. Sections were next incubated with citrate buffer 0.01M, pH 6, and warmed during 10min. Sections were washed several times with PBS and protein were blocked with 1% NGS during 30min at RT followed by incubation of goat anti-mouse IgG2a antibody (Abcam, Cat N° Ab98694) to prevent unspecific binding. After washing, protein were blocked with NGS and sections were incubated with antibody directed against puromycin (Millipore MABE343) at 4°C overnight. Goat anti-mouse A568 antibody (Thermo Fisher Scientific – Cat N° A11019) was next applied for 30min at RT followed by several washes of PBS. Nuclei were next stained with DAPI (Sigma – Cat N° D9542) at the dilution of 1/5000.

Genomic DNA extraction.

A small piece of liver was homogenized in lysis buffer (50 mM Tris/Cl (pH 8.0), 100 mM EDTA, 0.125% SDS, 0.8 mg/ml proteinase K). Samples were incubated at 55°C overnight and DNA was extracted with 1 mL of phenol/chloroform (50/50) followed by centrifugation at 2000g for 10 min. The aqueous phase was collected and the phenol/chloroform extraction was repeated. DNA was precipitated and concentration was assessed by fluorometry with the Qubit technology from Invitrogen.

Cell immunostaining

MEF cells were extracted from WT and Maf1 KO mice and fixed with 4% PFA during 10min. Cells were washed with PBS and protein were blocked with 1% NGS during 30min at RT. Cells were incubated with antibody against b-catenin (BD Bioscience - Cat N° 610153) at the dilution of 1/50 during 1h. After washing with PBS, cells were incubated with goat anti-mouse A568 antibody (Thermo Fisher Scientific – Cat N° A11019) for 30min. Pictures were taken with the Zeiss Axio imager M1 microscope.

tRNA modifications quantification.

Modifications of tRNA were assessed by qRT-PCR. 100 ng of tRNAs was used for reverse transcription with 200 units of M-MLV reverse transcriptase, 40 units of RNasin Ribonuclease inhibitor (Promega N2515), 1 mM of each reverse primer targeting a sequence downstream of a specific methylation site, 0.1M of DTT and either 10 mM or 1 mM of dNTPs. Quantitative amplification of the resulting cDNA was performed with FastStart SYBR Green Mastermix from Roche (04673492001). The primers are listed in Supplementary Figure 1.

Supplemental tables S1, S2, S3, S4, S5, and S6 can be found online at the address: https://www.dropbox.com/sh/e11awnxku364bru/AAD1u2iwhPGOT7yNoXT0dcLRa?dl=0

Discussion and Perspectives

During my thesis I worked on several projects, all related to the study of Pol 3 transcription and its main repressor MAF1. I mainly worked with a Maf1 KO mouse model, which was designed prior the start of my PhD project in collaboration with Ian Willis, Albert Einstein College of Medicine in New York. The Maf1 KO mouse was first designed to study the effect of Pol 3 transcription in cancer development. Maf1 being a repressor of Pol 3 transcription, we speculated that the Maf1 KO mouse might display elevated Pol 3 products levels. Since increased tRNA levels are linked with cancer development, we thought that the Maf1 KO mouse might be prone to developing tumours. Surprisingly, we never observed any cancer development associated with the Maf1 KO mouse; instead, the mouse developed resistance to high-fat diet-induced obesity. It is important, however, to underscore that we never challenged the mouse with tumorigenic treatments, which might still reveal a propensity to develop cancers. Further experiments using carcinogenic drugs could reveal a tumour suppressor role for MAF1 in mouse. For example, one could determine whether Maf1 KO mice develop hepatocarcinomas with faster kinetics after a single injection of diethylnitrosamine (DEN) (Bakiri and Wagner, 2013). Another commonly used method of inducing tumours is the use of 12-O-tetradecanoylphorbol-13 acetate (TPA) to induce skin tumours (Massoumi et al, 2006), which could also be tested on Maf1 KO and WT mice. Nevertheless, given the lack of any spontaneous tumour, we consider it unlikely that the Maf1 KO mice might display an unsuspected higher propensity to develop tumours when challenged with tumorigenic products.

Although the Maf1 KO mice did not develop cancer, they remained abnormally thin and resistant to high fat-diet-induced obesity. Our experiments revealed defects in lipogenesis and lipolysis as well as a futile cycle of tRNA synthesis and degradation, which may account for part of the phenotype. In addition, we found changes in metabolite profiles, notably polyamine pathway metabolites. Recently, a knockout of the nicotinamide-N-methyltransferase (Nnmt) gene was shown to affect polyamine pathway metabolites and to protect mice against diet-induced obesity (Kraus et al.,

2014). We were, therefore, excited when we observed diminished levels of liver and muscle NNMT. Lower NNMT activity can increase nicotinamide levels, which in turn increases NAD^+ levels, and indeed higher NAD^+ levels were observed in the Nnmt KO mouse. Consistent with this observation, NAD^+ level were upregulated in the muscle of the Maf1 KO mouse. Previous report showed that increased NAD^+ levels are linked with high fat diet-induced obesity resistance and enhanced oxidative metabolism (Cantó et al., 2012). Thus, altered NNMT expression in the Maf1 KO and its impact on the polyamine flux as well as NAD+ metabolism are very likely to contribute to the resistance to high fat diet-induced obesity for the Maf1 KO mouse. The mechanism by which knockout of Maf1 leads to reduced NNMT expression remains, however, unclear.

Additionally to their role in protecting mice against high-fat diet induced obesity via enhanced oxidative metabolism, NAD^+ levels were also reported to control longevity in worms (Mouchiroud et al., 2013). NAD^+ controls the activity of the deacetylase SIRT1, of which one function is to control mitochondrial function (Bai et al., 2011; Cantó et al., 2012). SIRT1 main targets include PGC1α and PPARγ, which control glucose and lipid metabolism, and the transcription factor FOXO1 involved in mitochondrial biogenesis and autophagy. We observed impairment of autophagy and lipid metabolism in the Maf1 KO mouse. Future experiments should focus on SIRT1 activity. The levels of SIRT1 protein as well as the acetylation levels of its main targets should be determined. Further, one could for example measure mRNA levels of FOXO1 transcriptional targets.

Enhanced SIRT1 activity increases mitochondrial, but not cytosolic, translation creating a "mitonuclear imbalance" leading to a mitochondrial unfolded protein response (UPR^{mt}), and promotes longevity in fly (Owusu-Ansah et al., 2013), worms (Yokoyama et al., 2002), and mice (Houtkooper et al., 2013). The Maf1 KO mice have an increased longevity and, under high-fat diet, display enhanced mitochondrial activity without changes in mitochondrial number as determined by indirect measurements of mitochondrial DNA level and mitochondrial oxidative chain (Oxphos) protein levels. Maf1 KO mice display reduced cytoplasmic translation, but mitochondrial translation was not assessed. Further studies should be focus on the analysis of mitonuclear imbalance in these mice, in this case perhaps resulting from

reduced cytoplasmic translation rather than increased mitochondrial translation. Mitochondria should be extracted from the mouse tissues and mitochondrial translation should be assessed using a radioactive marker, as puromycin does not enter the mitochondria. Expression of the proteins ClpP and Hsp60 should also be measured as they were identified as UPR^{mt} markers. To complete the mitochondrial study, protein of the Oxphos pathway could be separated on blue native gels for better measurement. The quality and morphology of mitochondria could be studied by electron microscopy.

The Maf1 KO mouse phenotype could also be due to a direct action of MAF1 on key metabolic genes. Earlier studies identified MAF1 as a protein capable of binding to the promoter of the Tbp and Egr-1 (Johnson et al., 2007) genes and repressing their activity. Later work reported that MAF1 also binds to and represses the promoter of the key metabolic genes Fasn and Acc1 (Palian et al., 2014). Thus, additionally to its role repressing Pol 3, MAF1 could be a repressor of key genes involved in adipogenesis. The results implicating MAF1 in the regulation of Pol 2 promoters were obtained with the ChIP-qPCR method, and I have been unable to reproduce them using a cell line expressing a tagged version of MAF1 (HA tag). I also performed ChIP-seq using liver cell from WT and Maf1 KO mice and an antibody directed against the endogenous protein but binding profiles were similar between the two conditions (Figure 5.1) indicating no convincing evidence of Maf1 binding on DNA for the tested conditions. The regions identified bound by MAF1 in both experiments did not correspond to any Pol 3 loci or known MAF1 targets Pol 2 genes. A possible explanation for this negative result is that MAF1 binding on DNA is extremely transient, and the used conditions are not optimal to detect such transient binding on DNA. Future experiments should use the DamID method, which should reveal MAF1-DNA interaction even if the binding of MAF1 is transient. In this experiment, MAF1 would be fused to a DNA adenine methyltransferase (Dam), which methylates adenine present in the palindromic sequence GATC. If the MAF1-Dam fusion comes into the DNA vicinity, the Dam moiety will methylate position 6 of the adenine on the DNA, an epigenetic mark that should be stable through one generation and that is normally absent in eukaryotic cells. Adenine methylation profiles could thus be used next to clarify the relevance of the previous results indicating MAF1 binding to some

Pol 2 promoters. Ideally the experiment would be performed with mouse adipocytes or hepatocytes, both cell lines expressing Acc1 and Fasn.

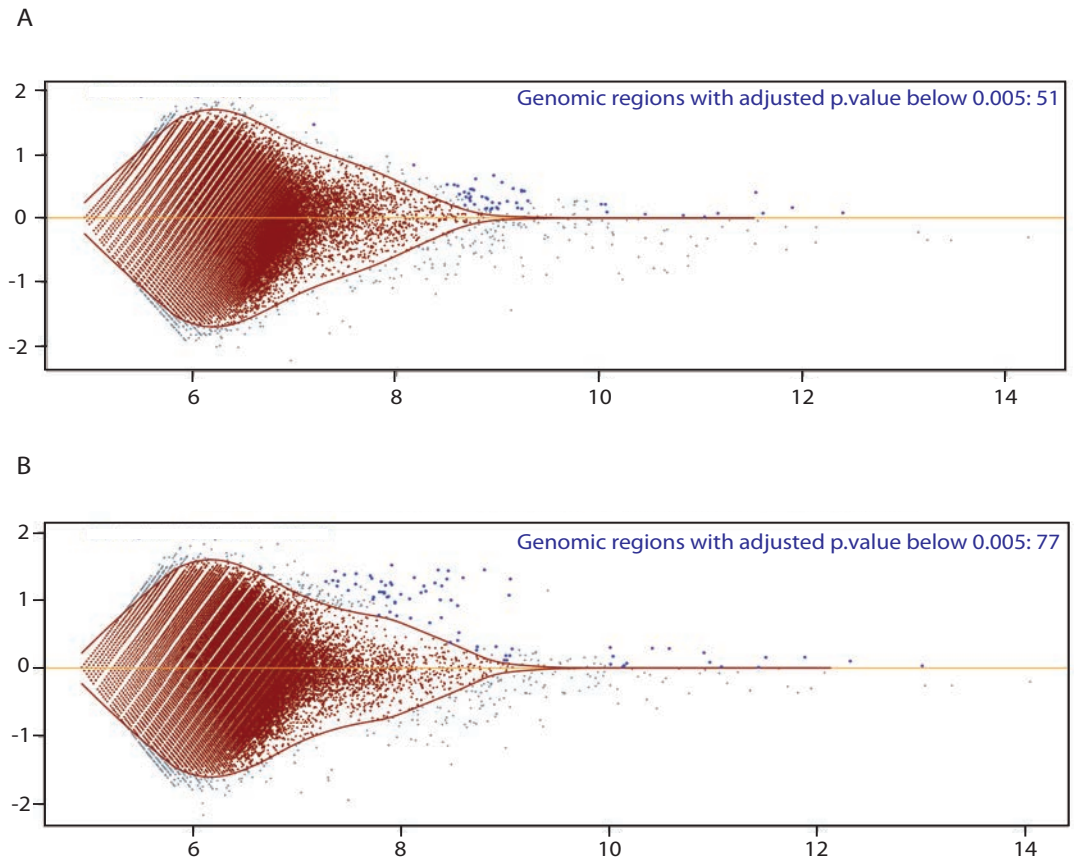

Figure 5.1: Identification of genomic regions bound by MAF1 in liver of WT mice (A) and Maf1 KO mice (B). Each dot represents a 400 nucleotide genomic bin. Red dots correspond to region with background signal, blue dot to regions with a statistically significant MAF1 signal. Other regions with non-significant binding of MAF1 are in grey.

In addition to being lighter, the adult Maf1 KO mice are also statistically smaller compared to their WT counterparts. Protein translation has been linked to both body weight and cell size (Faridi et al., 2003; Rui, 2007; Ruvinsky and Meyuhas, 2006; Tavares et al., 2015). We monitored protein translation in the mouse liver using ribosome sucrose gradient sedimentation profiles and puromycin incorporation and observed that the Maf1 KO mouse displayed a reduced protein translation. To confirm this, we used the ribosome profiling method, in which the ribosome-protected mRNAs are sequenced by high throughput sequencing. The results did not show any

obvious differences for specific mRNA. They also did not reveal obvious global differences in protein translation between WT and KO, perhaps due to the data analysis. If the reduction in translation is global, the differences between the samples will be lost during normalization of the high-throughput data. For future experiments, we should reproduce the ribosome profiling but this time including commercially available spike-in RNA. DNA concentration of the liver extracts (as cell counting is not easy) should be assessed and spike-in RNA should be added in constant proportion relative to DNA content just after the RNAse digestion step. Having spike-in material for normalization will allow detection of global differences between the samples.

The lower level of translation in the liver of Maf1 KO mice was surprising for us as, MAF1 being a repressor of Pol 3 transcription, we had hypothesized that with more produced tRNAs, translation would be enhanced. However, we found that higher Pol 3 occupancy in the Maf1 KO mouse was leading to an enhanced level of precursor tRNAs but not mature tRNAs, the effective molecules involved in translation. Moreover, RT-PCR based experiments on a few mature tRNAs revealed a lower degree of modification in the Maf1 KO mouse. tRNA modification is a critical step in tRNA physiology to maintain a normal level of translation. Our observation suggested that the higher level of precursor tRNAs production in the Maf1 KO mouse is overwhelming the tRNA maturation as well as the tRNA modification machineries. To complete the study, it would be highly interesting to examine the levels of tRNA modifications in greater details. The Dedon group developed a method (Su et al., 2014) where tRNAs are isolated by HPLC, hydrolysed, and single nucleotide modifications are analysed by mass spectrometry.

Such analysis would permit the identification of the tRNA modifications affected in the Maf1 KO mouse, although it would not allow the identification of the specific tRNAs lacking the modification. We might for example find a reduction in tRNA methylation, one of the most studied tRNA modifications whose importance in regulating protein translation has already been demonstrated. Such a finding would give weight to the hypothesis that a tRNA modification defect is causing reduced translation in the Maf1 KO mouse. Another possibility would be to use bisulphite sequencing, which would allow us to map the differences in tRNA methylation and check for their roles in protein translation. Indeed, protocols have been developed in

which cytosines (but not m5C) in RNA are first deaminated and converted to uracil by bisulfite treatment, followed by PCR base amplifications of cDNA and DNA sequencing (Schaefer et al., 2009).

I think future investments on the Maf1 KO mouse project should focus on MAF1 inhibitory drug development. Apart from its resistance to diet-induced obesity, the Maf1 KO mouse does not present any clear symptoms of disease. Altogether, the data suggest that Maf1 could be a potential target for drug development in obesity treatment. Drug development implies the development of an assay amenable to high throughput studies. The project should thus be first oriented towards the design of an *in vitro* system allowing the assessment of MAF1 activity. MAF1 activity is regulated by its phosphorylation state, with the under-phosphorylated form being the active one in Pol 3 repression. One would therefore be interested in developing drugs that either prevent de-phosphorylation of MAF1 or prevent the interaction of dephosphorylated MAF1 with Pol 3. In the first case, one could imagine a compound binding to phosphorylated MAF1 and preventing de-phosphorylation. However, as we have currently no efficient way to obtain correctly phosphorylated MAF1 *in vitro*, this approach might be difficult. It might be easier to identify compounds blocking the interaction of MAF1 and Pol 3. One possible assay would involve cells transfected with a Pol 3 promoter fused to a GFP reporter gene devoid of runs of T residues. A decrease in Maf1 activity due to drug treatment would lead to an increase in Pol 3 activity and so to an increase in GFP expression. Indeed, the expression from a Pol 3 promoter of RNAs that can then be translated has been documented. Gunnery and Mathews have shown expression of the viral trans-activator Tat from a Pol 3 promoter (Gunnery and Mathews, 1995), and Rollins and colleagues have shown expression of luciferase (Rollins et al., 2007).

A probably more sensitive system would be to establish cell lines expressing GFP, either constitutively or from an inducible promoter such as in the Tet-on or Tet-off systems. One would then express a siRNA from a Pol 3 promoter directed against GFP itself or against the Tet repressor fusion protein. In the first use, more active Pol 3 would reduce the GFP signal and in the second it could be designed to increase or decrease it depending on the Tet system used. This type of assay would be important

because it tests the final step, Pol 3 regulation. However, earlier assays might test directly ability of the drug to inhibit MAF1-Pol 3 interaction. Maf1 has been reported to bind to the largest subunit of Pol 3, both in yeast and mammalian cells, and the region of interaction has been narrowed down to the N-terminal part of the protein. However, our group not being experienced in drug development, it would be more efficient to collaborate with a specialized company for the drug design part. This would be a long-term project but new results in Maf1 inhibition could reveal novel insights for obesity treatment.

A second interesting project would be to monitor the level of tRNA modifications and translation of key proteins in several human metabolic diseases. Altered expression of Cdkal1, a tRNA modifying enzyme, has been reported to reduce the level of modification of $tRNA^{lys}$, which causes the development of type 2 diabetes (Wei et al., 2011). However nothing is known about putative links between other modifications and severe metabolic disorders. Using GC-MS/MS and bisulfite sequencing would help to understand the differences in tRNA modifications between samples from healthy and sick patient and ribosome profiling would reveal which mRNA are more or less translated and thus which proteins might be affected. Such studies would further our understanding of the development of metabolic diseases and give us new perspectives to fight them.

References

Bai, P., Cantó, C., Oudart, H., Brunyánszki, A., Cen, Y., Thomas, C., Yamamoto, H., Huber, A., Kiss, B., Houtkooper, R.H., et al. (2011). PARP-1 inhibition increases mitochondrial metabolism through SIRT1 activation. Cell Metab. *13*, 461–468.

Bakiri, L., and Wagner, E.F. (2013). Mouse models for liver cancer. Mol. Oncol. *7*, 206–223.

Cantó, C., Houtkooper, R.H., Pirinen, E., Youn, D.Y., Oosterveer, M.H., Cen, Y., Fernandez-Marcos, P.J., Yamamoto, H., Andreux, P. a., Cettour-Rose, P., et al. (2012). The NAD+ precursor nicotinamide riboside enhances oxidative metabolism and protects against high-fat diet-induced obesity. Cell Metab. *15*, 838–847.

Faridi, J., Fawcett, J., Wang, L., and Roth, R. a (2003). Akt promotes increased mammalian cell size by stimulating protein synthesis and inhibiting protein degradation. Am. J. Physiol. Endocrinol. Metab. *285*, E964–E972.

Gunnery, S., and Mathews, M.B. (1995). Functional mRNA can be generated by RNA polymerase III. Mol. Cell. Biol. *15*, 3597–3607.

Houtkooper, R.H., Mouchiroud, L., Ryu, D., Moullan, N., Katsyuba, E., Knott, G., Williams, R.W., and Auwerx, J. (2013). Mitonuclear protein imbalance as a conserved longevity mechanism. Nature *497*, 451–457.

Johnson, S.S., Zhang, C., Fromm, J., Willis, I.M., and Johnson, D.L. (2007). Mammalian Maf1 Is a Negative Regulator of Transcription by All Three Nuclear RNA Polymerases. Mol. Cell *26*, 367–379.

Kraus, D., Yang, Q., Kong, D., Banks, A.S., Zhang, L., Rodgers, J.T., Pirinen, E., Pulinilkunnil, T.C., Gong, F., Wang, Y., et al. (2014). Nicotinamide N-methyltransferase knockdown protects against diet-induced obesity. Nature *508*, 258–262.

Massoumi, Ramin; Chmielarska, Katarzyna; Hennecke, Katharina; Pfeifer, Alexander; Fässler, R. (2006). Cyld Inhibits Tumor Cell Proliferation by Blocking Bcl-3-Dependent NF-κB Signaling. Cell *125*, 665–677.

Mouchiroud, L., Houtkooper, R.H., Moullan, N., Katsyuba, E., Ryu, D., Cantó, C., Mottis, A., Jo, Y.S., Viswanathan, M., Schoonjans, K., et al. (2013). XThe NAD+/sirtuin pathway modulates longevity through activation of mitochondrial UPR and FOXO signaling. Cell *154*.

Owusu-Ansah, E., Song, W., and Perrimon, N. (2013). XMuscle mitohormesis promotes longevity via systemic repression of insulin signaling. Cell *155*, 699–712.

Palian, B.M., Rohira, A.D., Johnson, S. a. S., He, L., Zheng, N., Dubeau, L., Stiles, B.L., and Johnson, D.L. (2014). Maf1 Is a Novel Target of PTEN and PI3K Signaling That Negatively Regulates Oncogenesis and Lipid Metabolism. PLoS Genet. *10*, e1004789.

Rollins, J., Veras, I., Cabarcas, S., Willis, I., and Schramm, L. (2007). Human Maf1 negatively regulates RNA polymerase III transcription via the TFIIB family members Brf1 and Brf2. Int. J. Biol. Sci. *3*, 292–302.

Rui, L. (2007). A link between protein translation and body weight. J. Clin. Invest. *117*, 310–313.

Ruvinsky, I., and Meyuhas, O. (2006). Ribosomal protein S6 phosphorylation: from protein synthesis to cell size. Trends Biochem. Sci. *31*, 342–348.

Schaefer, M., Pollex, T., Hanna, K., and Lyko, F. (2009). RNA cytosine methylation analysis by bisulfite sequencing. Nucleic Acids Res. *37*.

Su, D., Chan, C.T.Y., Gu, C., Lim, K.S., Chionh, Y.H., McBee, M.E., Russell, B.S., Babu, I.R., Begley, T.J., and Dedon, P.C. (2014). Quantitative analysis of ribonucleoside modifications in tRNA by HPLC-coupled mass spectrometry. Nat. Protoc. *9*, 828–841.

Tavares, M.R., Pavan, I.C.B., Amaral, C.L., Meneguello, L., Luchessi, A.D., and Simabuco, F.M. (2015). The S6K protein family in health and disease. Life Sci. *131*, 1–10.

Wei, F., Suzuki, T., Watanabe, S., Kimura, S., Kaitsuka, T., Fujimura, A., Matsui, H., Atta, M., Michiue, H., Fontecave, M., et al. (2011). Deficit of tRNA Lys modification by Cdkal1 causes the development of type 2 diabetes in mice. J. Clin. Invest. *121*, 3598–3608.

Yokoyama, K., Fukumoto, K., Murakami, T., Harada, S.I., Hosono, R., Wadhwa, R., Mitsui, Y., and Ohkuma, S. (2002). Extended longevity of Caenorhabditis elegans by knocking in extra copies of hsp70F, a homolog of mot-2 (mortalin)/mthsp70/Grp75. FEBS Lett. *516*, 53–57.